Energy Efficient Resource Allocation for Wireless Powered Communication Networks

Haohang Yang

Department of Electronic and Electrical Engineering

University of Sheffield

Supervisor: Prof. Xiaoli Chu

This thesis is submitted for the approval of the

Doctor of Philosophy

October 2021

To my dear parents:

Without your unreserved support and help, I cannot finish this thesis successfully, and I would not be who I am today.

Acknowledgements

First and foremost, I am very grateful to my supervisor Professor Xiaoli Chu for providing me with the opportunity to study at the University of Sheffield. Her guidance and recommendations help me to determine the research direction of this thesis. Her crucial advices and ideas inspire me to create meaningful and novel works. I would like to thank also my co-supervisor Professor Jie Zhang, his experience and knowledge have encouraged me all the time during my PhD life.

I would like to acknowledge the financial support from the European Union's Horizon 2020 Research and Innovation Programme under Grant 734798, in part by the Science and Technology Plan Project of Guangdong Province under Grant 2018A050506015, and in part by JSPS KAKENHI Grant JP16K00117 and KDDI Foundation, and from the European Union's Horizon 2020 research and innovation program under the grant agreement No. 734798, the National Key RD Program of China (2019YFE0113200), National Natural Science Foundation of China (61901317), Fundamental Research Funds for the Central Universities (JB190104), Joint Education Project between China and Central-Eastern European Countries (202005), and the 111 Project (B08038). Also, I am deeply grateful to all the members for their help in Iquadrat and in Harbin Institute of Technology during my secondment in Spain and China, respectively.

I would like to express my gratitude to the collaborators of the work during my PhD studies, Dr. Yinghui Ye, Dr. Kai Liang, and Dr. Long Li. Special thanks to Dr. Yinghui Ye for his insightful advices and comments on my work during the past three years. Also, I would like to extend my sincere thanks to all the colleagues in the Communications Group at the University of Sheffield for their kind help in many aspects of my PhD life.

Above all, I would like to express my gratitude to my parents for their unreserved love, which gives me strong motivation to finish my PhD study. I would like to thank also my family and friends. I would not be who I am today without them.

Abstract

The exponential growth of smart wireless devices has put much pressure on the spectral efficiency and energy efficiency (EE) of the Internet of things (IoT) networks and wireless sensor networks. In order to support energy constrained wireless devices, wireless powered communication networks (WPCN) have been proposed based on different wireless powered transmission (WPT) technologies, e.g., simultaneous wireless information and power transfer (SWIPT), harvest then transmit (HTT) and backscatter communication (BackCom). We note that energy-efficient resource allocation schemes need to be tailored to the different WPT technologies used in WPCNs. In this thesis (including four papers), we classify WPCNs into three types according to the way of information transmission: active transmission, passive transmission and hybrid transmission, and present energy-efficient resource allocation schemes for them in different scenarios of WPCNs.

In active transmission-based WPCNs, a radio frequency (RF) power source, e.g., a base station (BS) or a power beacon (PB), sends an RF signal to a transmitter, which harvests energy from the received RF signal through its energy harvesting (EH) circuit and generates its own RF signal to carry information to a receiver. In Paper I, we consider a SWIPT-enabled device-to-device (D2D) underlaid network, where a D2D receiver decodes information and harvests energy from its associated D2D transmitter simultaneously via its SWIPT circuit, and propose to maximize the sum EE of all D2D links by optimizing the spectrum resource and power allocation, and the power splitting ratio of each D2D device based on a non-linear EH model. We find that the number of SWIPT-enabled D2D links that maximize the sum EE is limited by the EH circuit sensitivity, especially when the D2D communication distance is long.

In passive transmission-based WPCNs, an RF power source sends an RF signal to a backscatter device (BD), which backscatters parts of the incident RF signal to a receiver and harvests energy from the rest of the incident RF signal to support the backscatter circuit. In Paper II, we propose to ensure the max-min EE fairness among the backscatter links by jointly optimizing the PB transmission power and the backscatter reflection coefficients. Our results show that the proposed max-min EE resource allocation scheme is more effective when the throughput requirement of the BDs is lower and the channel power gain difference among different PB-to-BD links is smaller. In Paper III, we propose to maximize the system EE of a symbiotic radio (SR) network that contains a primary link and multiple BDs, each being able to harvest energy while backscattering, by optimizing the primary transmitter (PT) transmission power, the BDs' reflection coefficients and time division multiple access (TDMA) time slot durations for both the parasitic SR (PSR) and commensal SR (CSR) cases. The simulation results show that the system EE is maximized when all BDs only achieve the minimum throughput requirement in the PSR case, while in the CSR case, the system EE is maximized when a best BD that can contribute the most toward the system EE is allocated the maximum allowed time to backscatter its information to the primary receiver (PR), and this best BD is determined by the optimized PT transmission power in the corresponding time slot.

In hybrid transmission-based WPCNs, the wireless devices are equipped with both the RF signal generation circuit and the backscatter circuit to support active transmission and passive transmission, respectively. In paper IV, we maximize the total EE of all the IoT nodes, which are powered by an unmanned aerial vehicle (UAV) and need to send information to a reader, by optimizing the UAV's transmit power and trajectory, the IoT nodes' backscatter reflection coefficients, transmit power for active transmission, and time allocation between backscattering and active transmission. Our results show that the UAV tends to fly toward the IoT nodes with better channel conditions to the reader, and the maximum total EE of the IoT nodes is achieved when the IoT node that is closest to the reader achieves the highest throughput, while other IoT nodes maintaining the minimum throughout requirement.

List of Abbreviations

5G 5th generation

6G 6th generation

AmBC ambient backscatter communication

AWGN additive white Gaussian noise

BackCom backscatter communication

BCD block coordinated decent

BD backscatter device

BS base station

CSR commensal symbiotic radio

CUE cellular user

D2D device-to-device

EE energy efficiency

EH energy harvesting

HTT harvest then transmit

IF information fusion

IoT Internet of things

IRS intelligent reflective surface

KKT Karush-Kuhn-Tucker

LoS line of sight

NOMA non-orthogonal multiple access

PB power beacon

PR primary reader

PSR parasitic symbiotic radio

PT primary transmitter

RB resource block

RF radio frequency

RFID radio frequency identification

SCA successive convex approximation

SCP successive convex programming

SR symbiotic radio

SWIPT simultaneous wireless information and power transfer

TDMA time-division multiple access

UAV unmanned aerial vehicle

WPBC wireless powered backscatter communications

WPCN wireless powered communication networks

WPT wireless powered transmission

Table of contents

Part I

Introduction and Overview

Chapter 1

Introduction

1.1 Background

1.1.1 Wireless Powered Communication Networks

It is predicted that the number of the connected devices could be tens or hundreds of billions in the near future [1, 2]. Also, the requirements of high quality video and widescreen resolutions in these huge amount of devices have put much pressure on the power sources [3], especially for the devices in Internet of things (IoT) networks or sensor networks with limited battery capacity. This challenge encourages us either to look for sustainable power sources or consider wireless powered communication networks (WPCN) for prolonging the lifetime of energy-constrained communication networks [4–7]. Natural sustainable power sources like solar, wind and hydroelectric are considered in [8–10], but the stability and the availability of such natural power sources are much worse than the energy harvested in WPCNs due to the location, climate and time [11]. Despite the power sources stored in the battery, energy harvesting (EH) in WPCNs is employed to capture and convert radio frequency (RF) energy in the ambient environment into electricity power [3][1]. Therefore, the devices in WPCNs could reduce the dependency on batteries and utilize the harvested energy to work for a longer period of time.

[1] Base on the information from PowerCast (www.powercastco.com), three types of RF-to-DC converter chips have been developed including PCC114, PCC110 and PCC210, where the former two chips have the conversion efficiency up to 75% and the latter chip has the highest conversion efficiency up to 95%.

Moreover, the researchers have proposed a passive circuit without equipping a battery, i.e., the passive backscatter circuit [12]. Indeed, the results from [13] indicate that a batteryless backscatter circuit can work continuously with an incident RF power of 18 dBm for EH. For better development of fifth generation (5G) and next-generation sustainable networks, the deployment of WPCNs will remain the main motivation nowadays and in the future.

1.1.2 Active Transmission in WPCNs

Active transmission in WPCNs indicates that a transmitter harvests energy from an RF source, e.g., a base station (BS) or a power beacon (PB), then the transmitter utilizes the harvested energy to transmit information actively to a receiver. Since active transmission in WPCNs generates the RF signal with sufficient energy, on one hand, the high transmission rate and reliability can be guaranteed, on the other hand, it needs to spend time on harvesting energy before transmitting information [14]. The time allocation between EH and information transmission needs to be taken into account. Two active transmission schemes are given in Fig. 1.1 and Fig. 1.2 as harvest then transmit (HTT) scheme and simultaneously wireless information and power transfer (SWIPT) scheme, respectively.

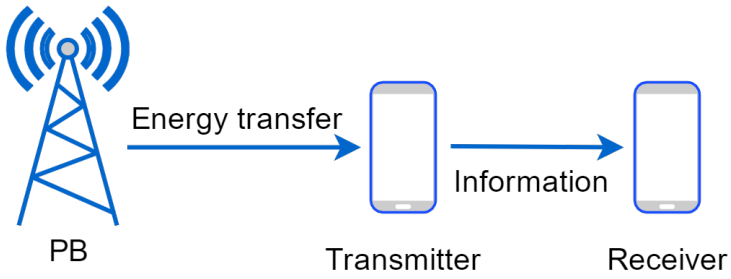

Fig. 1.1 An illustration of a typical HTT scheme.

Fig. 1.1 demonstrates that a PB sends an RF signal to a transmitter, the transmitter converts the RF signal into electricity power via its EH circuit, then the transmitter generates its own RF signal and sends information to a receiver by utilizing the harvested energy. This creates so called HTT scheme [14, 15]. It's worth to mention that the PB in Fig. 1.1 works as a dedicated

RF power source, such power sources can be RF signals from several PBs, TV radio signals, noise power and any other surrounding signals that may be wasted [16].

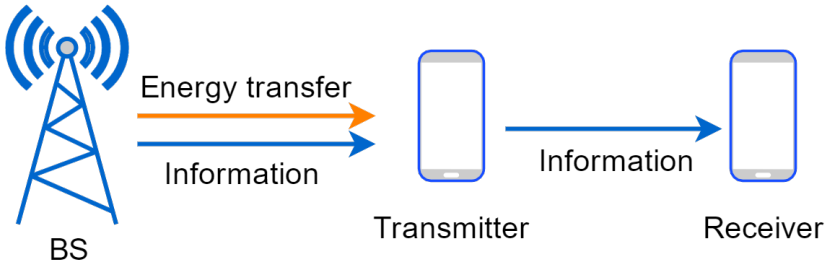

Fig. 1.2 An illustration of a typical SWIPT scheme.

Fig. 1.2 illustrates a typical SWIPT networks, where a BS transmits an RF signal to a transmitter, and the transmitter harvests the energy and decodes the information from the received signal simultaneously through a SWIPT circuit. SWIPT circuit is composed of information decoding component and EH component, and it can be implemented either in a power splitting mode or a time switching mode, where the former mode splits the received signal into two signal streams, one stream is for information decoding and the other stream is for EH, the latter mode splits the time duration, one duration is for information decoding and the other duration is for EH [17–19]. Then the transmitter utilizes the harvested energy to generate its own RF signal for transmitting information to a receiver. In this case, the transmitter works both as an information decoder and an information sender. It is noted that the transmitter in Fig 1.2 can be a relay node which receives and decodes the information from the BS, then forwards the original information to a receiver by utilizing the harvested energy during SWIPT [20, 17]. Also, there exists a simple case only containing a BS/transmitter and a receiver, the receiver decodes the information from the BS/transmitter by utilizing the energy harvested via SWIPT [21].

1.1.3 Passive Transmission in WPCNs

Passive transmission in WPCNs usually refers to backscatter communication (BackCom) as shown in Fig. 1.3, where a PB sends an RF signal to a backscatter transmitter, then the

transmitter modulates its own information on the incident RF signal and reflects one part of the signal to a backscatter receiver by tuning its antenna impedance. The other part of the incident RF signal is harvested for circuit power consumption [12, 22]. Different from active transmission, backscatter circuit is not equipped with any active RF components, thus the backscatter transmitter does not generate RF signals, it simply backscatters the incident signal to the backscatter receiver, which significantly reduces the circuit energy consumption [12, 22].

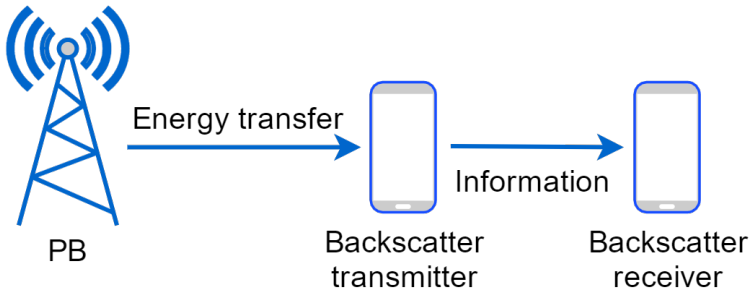

Fig. 1.3 An illustration of a typical BackCom network.

Based on the backscatter circuit design, BackCom is divided into passive BackCom and semi-passive BackCom, where the former design indicates that there is no battery in the backscatter circuit and the latter design refers to a backscatter circuit equipped with an internal power source. The key benefit of passive BackCom is its low cost and small size, thus it is simple to be massively deployed. However, the only power source is from the received RF signal, the effective transmission range of passive BackCom is relatively short. While in semi-passive BackCom, the transmission range is extended due to an internal power source and its reliability is better than passive BackCom. Also, the access delay in semi-passive BackCom is greatly reduced since the backscatter transmitter does not need to wait for harvesting enough energy for circuit operation. Since semi-passive BackCom still backscatters the incident RF signals, the transmission rate is not largely improved due to its passive counterpart [12].

Based on the network deployment, BackCom is classified into three major types: monostatic BackCom, bistatic BackCom and ambient BackCom (AmBC). In the monostatic BackCom,

the RF source, i.e., PB in Fig. 1.3. and the backscatter receiver are placed in the same device, i.e., a tag reader. thus it has the problem of round-trip pathloss. The monostatic BackCom is mostly emplyoed in short-range Radio Frequency Identification (RFID) applications. Fig. 1.3 just shows the bistatic BackCom, where the RF source is separated from the backscatter receiver and is dedicated, e.g., a PB or a BS. This configuration allows flexible adjustment of the locations of the RF source for different purposes, e.g., optimal transmission rate or energy efficiency (EE). Also, its fabrication cost is cheaper than the integrated tag reader in the monostatic BackCom due to less complex circuit design. AmBC is similar to bistatic BackCom, where the RF source and the backscatter receiver are separated. However, the RF source in AmBC is not dedicated, the backscatter transmitter can utilize the RF energy from the ambient source like a TV tower signal, radio signal or the signal from WIFI access point. Since the ambient RF sources are utilized, the energy consumption in AmBC is significantly reduced. Another key advantage of AmBC is that extra frequency spectrum is not needed compared with monostatic BackCom and bistatic BackCom. Such advantages also bring an important challenge, i.e., the RF signal from the ambient source is difficult to be estimated and decoded at the backscatter receiver. Many researchers have been studying to address the above mentioned problems or challenges [22].

1.1.4 Hybrid Transmission in WPCNs

Hybrid transmission is the combination of active transmission and passive transmission, where the active RF component and the backscatter circuit are integrated in the same device, i.e., a hybrid transmitter [14]. In Fig. 1.4, a PB sends an RF signal to a hybrid transmitter, in the first time slot, the hybrid transmitter performs passive transmission to modulate its own information on the incident RF signal and backscatters the signal to a receiver while harvesting energy from the PB. In the second time slot, the hybrid transmitter performs active transmission to generate its own RF signal and transmits information to the receiver by utilizing the harvested energy during BackCom.

Due to the cooperation of active transmission and passive transmission, hybrid transmission in WPCNs can take the advantages of both, that is, it can transmit information via BackCom

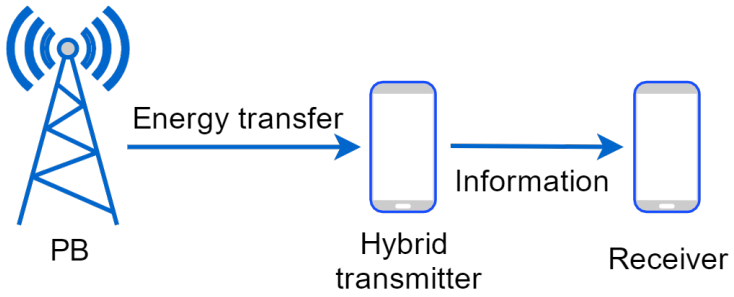

Fig. 1.4 An illustration of a typical hybrid WPCN.

with low energy consumption while harvesting energy from the RF sources and it can send information to a receiver in an active mode with high data rate and reliability when the energy storage is sufficient. Switching between the active transmission mode and passive transmission mode can bring significant system performance improvement, i.e., higher data rate and EE, in WPCNs. This also brings the challenges of optimizing the transitions among EH, active transmission and passive transmission [12, 14].

1.2 Motivation and Objectives

The aim of this thesis is to classify WPCNs into three types based on how the information is transmitted, and we further intend to find energy-efficient resource allocation schemes for the three types of WPCNs in different scenarios, i.e., a SWIPT-enabled device-to-device (D2D) network, an unmanned aerial vehicle (UAV)-enabled network, a symbiotic radio (SR) network and the backscatter networks with multiples users. The analytical and numerical results can shed insights on the deployment of WPCNs. Based on the aforementioned purposes, the following research questions are stated.

- Q1: How to classify WPCNs in terms of how the information is transmitted?
- Q2: How to integrate WPCNs with WPCNs with a SWIPT-enabled D2D network, a UAV-aided network, a SR network and the backscatter networks with multiples users?

- Q3: How to propose energy-efficient resource allocation schemes for WPCNs in the scenarios of a SWIPT-enabled D2D network, a UAV-enabled network, a SR network and the backscatter networks with multiples users?
- Q4: How to optimize the key parameters to improve the EE performance in WPCNs?

In this thesis, Section 1.1.2−1.1.4 in Chapter 1 answer Q1, where WPCNs are classified into active transmission, passive transmission and hybrid transmission based on how the information is transmitted. Q2−Q4 are addressed in Paper I-IV of Part II, respectively, where a SWIPT-enabled D2D WPCN, an unmanned aerial vehicle (UAV)-enabled WPCN, a SR WPCN and a backscatter WPCN with multiple users are established. Energy-efficient resource allocation schemes are proposed in these WPCNs to maximize the EE by optimizing the key parameters, e.g., transmitter's transmission power, backscatter reflection coefficient and time allocation for multiple users.

1.3 Thesis Outline and Organization

The thesis is divided into two parts, Part I contains three chapters and Part II includes four journal papers.

Chapter 1 gives a basic introduction of a SWIPT-enabled WPCN and divide it into three types based on how the information is transmitted, i.e., active transmission, passive transmission and hybrid transmission. The motivation and objectives are also introduced in this chapter.

In Chapter 2, the research works on the three types of transmission in WPCNs are described. The mathematical optimization tools are also introduced to address the proposed research problems, i.e., convex transformation and convex optimization.

Chapter 3 summarizes the contributions of the four journal papers and gives the conclusions with future research directions.

Chapter 2

Literature Review

2.1 Research Works on Active Transmission

The authors in [23] aimed to maximize the spectral efficiency by optimizing the optimal time allocations for the users in a time division multiple access (TDMA) based WPCN and a non-orthogonal multiple access (NOMA) based WPCN, respectively, where the users transmitted information to an access point via HTT protocol. They found that the TDMA based WPCN not only consumed less energy, but also was more spectral efficient than NOMA based WPCN. In [24], the authors maximized the achievable EE of a WPCN by jointly optimizing the time allocation and power control of each user while considering the initial battery energy of the users, the HTT protocol was also considered in this WPCN. The numerical results show that each user could achieve its own maximum EE when the transmission time was sufficiently long. The authors in [25] maximized the sum throughput of the IoT devices in a SWIPT enabled IoT network by jointly optimizing the time, transmit power and spectrum allocation for each IoT device. The simulation results show that their proposed scheme for solving the throughput maximization problem could obtain superior performance in terms of the sum throughout of the IoT devices. In [26], energy efficient resource allocation in SWIPT cooperative wireless networks was studied to maximize the EE of the network by optimizing the power splitting ratio, the relay selection schemes and the power allocations for the users. The numerical results demonstrated that the proposed resource allocation scheme achieved the maximum EE with

low computational complexity, in which the proposed relay selection outperformed the typical relay selection schemes in terms of EE. Other research works on active transmission based WPCNs can be found in [27–30]. However, the above works only consider linear EH model with constant energy conversion efficiency, and the EH circuit sensitivity is ignored.

2.2 Research Works on Passive Transmission

The EE of a UAV-enabled BackCom network was maximized in [31] by jointly optimizing the UAV's trajectory, the backscatter device's (BD) scheduling and the carrier emitters' transmission power. The simulation results show that the proposed communicate-while-fly scheme achieved significant EE gains compared with the hover-and-fly scheme, the state-of-the-art UAV-monostatic BackCom scheme, and the carrier emitter-relay scheme. In [32], the authors aimed to maximize the minimum throughput among all BDs by jointly optimizing the backscatter time and reflection coefficients of the BDs, and the access point's power allocation. The extensive simulation results show that the proposed joint design achieved significant throughput gain as compared to the benchmark schemes. The authors in [33] maximized the throughput of the AmBC system via jointly optimizing the time scheduling, transmit power allocation, and reflection coefficient for the users. The simulation results demonstrated that the proposed method can significantly increase the throughput of the AmBC system with a fast convergence speed. In [34], the authors presented the first attempt to maximize the EE of the users in a NOMA-BackCom network by jointly optimizing the BS transmit power and the reflection coefficients of BDs. Numerical results verified the effectiveness of the proposed scheme in improving the EE by comparing it with the other benchmark schemes. Other research works on passive transmission based WPCNs can be found in [35–38]. However, the above works ignore the situation where the BDs work at the same time and at the same frequency band, and the interference power at the receivers cannot be mitigated.

2.3 Research Works on Hybrid Transmission

The authors in [39] proposed a hybrid BackCom-HTT mode for a cognitive WPCN, where the throughput of the network was maximized by optimizing the time allocation between backscattering and energy harvesting and that between the bistatic backscatter mode and the HTT mode. The numerical results demonstrated the advantage of the proposed hybrid HTT and BackCom mode over the benchmark mode in terms of system throughput. In [40], the authors maximized the EE of all the devices in a hybrid BackCom-HTT network by optimizing the transmit power of the PB and hybrid devices, and the time allocation among EH, the backscatter mode and the HTT mode. The simulation results demonstrated the superiority of the proposed scheme in terms of EE of all the devices. The authors in [41] proposed hybrid backscatter communication for a WPCN and maximized the throughput by performing the optimal time allocation. They proved that the proposed hybrid backscatter communication could increase the transmission range of WPCNs. In [42], the EE of the cognitive radio system in a hybrid AmBC-HTT mode was maximized by optimizing the detection threshold, the degree of trade-off between the cognitive radio system in AmBC mode and HTT mode, and the data transmission time. The extensive results demonstrated the performance gain of the proposed model in terms of EE. However, the above works only consider fixed PB or BS, while the UAV-aided hybrid BackCom-HTT WPCNs can help to further improve the system performance in terms of the throughput and EE.

2.4 Mathematical Optimization

A general optimization problem can be formulated as follows:

$$\begin{aligned} &\max_{\mathbf{x}} f(\mathbf{x}) \\ &\text{s.t. } g_j(\mathbf{x}) \geq 0, j = 1, \cdots, J, \\ &\quad h_l(\mathbf{x}) \leq 0, l = 1, \cdots, L, \\ &\quad y_k(\mathbf{x}) = 0, k = 1, \cdots, K, \end{aligned} \tag{2.1}$$

where $\mathbf{x}$ denotes the n-dimensional vector of optimization variables. $f(\mathbf{x})$ is the objective function of the optimization problem, $g_j(\mathbf{x})$, $h_l(\mathbf{x})$ and $y_k(\mathbf{x})$ represent inequality and equality constraints, respectively. The constraints decide the feasible region of $\mathbf{x}$, which is the set of possible value of $\mathbf{x}$. If the set is empty, the optimization problem will be infeasible. If the optimal objection value $f(\mathbf{x}^*) = +\infty$, then the optimization problem is unbounded. According to the formulation of the objective functions and the constraints, optimization problems are mainly classified in to convex and non-convex problems with continuous, discrete or binary variables.

2.4.1 Convex Transformation

a) Dinkelbach based transformation

Dinkelbach based transformation refers to a nonlinear fractional programming method proposed by W. Dinkelbach in [43]. Basically, it can transform a fraction formula in an optimization problem into a subtraction form, which makes the problem convex or much closer to a convex form. Thus, the Dinkelbach based transformation is suitable to be employed to solve EE based problems since EE is defined as the ratio of the throughput to the energy consumption. Some works related to EE based problems have applied this transformation [44, 45]. For an example, a simple EE maximization problem is formulated as follows:

$$\begin{aligned} &\max_{P,t} \ \ EE = \frac{R(P,t)}{EC(P,t)} \\ &\text{s.t. } \ \text{C1} : R(P,t) \geq R_{min}, \end{aligned} \tag{2.2}$$

where P and t are the optimization variables of a transmitter's transmission power and the transmission time, respectively, R denotes the throughput of the link from a transmitter to a receiver, and EC represents the energy consumption of the transmitter and the receiver. C1 guarantees the minimum required throughput of this link. By employing Dinkelbach based transformation, the maximum EE, denoted by Q^*, can be achieved if and only if the following

equation is satisfied [43],

$$\max_{P,t} \; R(P,t) - Q^* EC(P,t) = R(P^*,t^*) - Q^* EC(P^*,t^*) = 0, \tag{2.3}$$

where P^* and t^* are the optimal transmission power and the optimal transmission time, respectively. Then the optimization problem is equivalently transformed into

$$\begin{aligned} &\max_{P,t} \; R(P,t) - Q^* EC(P,t) \\ &\text{s.t. C1.} \end{aligned} \tag{2.4}$$

By observing (2.4), we can find that if P and t are not coupled, the optimization problem may become a linear problem, which is convex and easy to be solved. If P and t are coupled, the optimization problem will still be non-convex but much more possible to be solved. We further introduce the next two methods for transforming a non-convex problem to a convex problem.

b) Successive convex approximation

The key idea of a successive convex approximation (SCA) method is to find a local tightly convex approximation to an optimization problem with non-convex objective function and constraints [31, 46, 47]. Taking problem (2.1) as an example, by considering $f(\mathbf{x})$ and $g_j(\mathbf{x})$ as non-convex functions, we apply the first-order Taylor expansion to replace $f(\mathbf{x})$ and $g_j(\mathbf{x})$ with their lower bounded functions. Thus, we can solve the original problem by successively maximizing the lower bound of $f(\mathbf{x})$ with the transformed constraints in an iterative manner. During the optimization process, an initial point x_0 is set as a local point for the first iteration. Then, each obtained solution of x_l after lth iteration is used as next local point to construct the successive local approximation, the iterations continue until the convergence is reached. Also, the convergence is guaranteed since the objective function value is non-decreasing after each iteration due to convex optimization and is usually upper bounded by the constraints.

c) Alternating iterative method

Alternating iterative method aims to decompose a non-convex problem into two or more convex sub-problems, which can find locally optimal solutions of an optimization problem

[33, 48]. Specifically, for the Dinkelbach based transformed problem (2.3) with coupled P and t, this problem is still non-convex. We employ alternating iterative method to solve this problem in an iterative manner, where the original problem is decomposed into two convex sub-problems, i.e., optimizing P with fixed t and optimizing t with obtained P. By alternating the optimization of P and t, the optimization process is repeated until it converges. Also, the convergence is guaranteed since the objective function value, i.e., the EE in (2.3), increases with the number of iterations and is upper bounded by constraint C1.

2.4.2 Convex Optimization

After the aforementioned convex transformation, a convex optimization problem is obtained. If the formulation of the problem is very simple, e.g., a linear formulation, an existing CVX tool in Matlab will be suitable to be directly used since it can efficiently solve linear optimization problem in a very short time. However, if the convex problem is more complex than a linear problem, a Lagrange dual method [49] is introduced below to efficiently solve such convex optimization problems and obtain the closed form expressions of the optimal value of the variables, which can also help to gain more insights.

An optimization problem is formulated as

$$\begin{aligned} &\max_{\boldsymbol{x}} f(\boldsymbol{x}) \\ &\text{s.t. } h_i(\boldsymbol{x}) \geq \varepsilon_1, i = 1, \cdots, p, \\ &\quad g_j(\boldsymbol{x}) \leq \varepsilon_2, j = 1, \cdots, q, \end{aligned} \tag{2.5}$$

where (2.5) is a convex optimization problem with non-linear objective function $f(\boldsymbol{x})$ and constraints $h_i(\boldsymbol{x}) \geq 0$ and $g_j(\boldsymbol{x}) \leq 0$. $\boldsymbol{x}$ represents the n-dimensional vector of optimization variables of the problem. By employing the Lagrange dual method, the Lagrange function for (2.5) is given by

$$\mathbb{L}(\boldsymbol{x}, \boldsymbol{\alpha}, \boldsymbol{\beta}) = f(\boldsymbol{x}) + \boldsymbol{\alpha}(h(\boldsymbol{x}) - \varepsilon_1) + \boldsymbol{\beta}(\varepsilon_2 - g(\boldsymbol{x})), \tag{2.6}$$

where $\boldsymbol{\alpha} \geq 0$ and $\boldsymbol{\beta} \geq 0$ are the Lagrange multipliers vectors associated with the constraints, respectively. Then the dual function of (2.5) is denoted by $\mathbb{G}(\boldsymbol{\alpha}, \boldsymbol{\beta}) = \max_{\boldsymbol{x}} \mathbb{L}(\boldsymbol{x})$, and the

Lagrangian dual optimization problem can be formulated as

$$\min_{\boldsymbol{\alpha},\boldsymbol{\beta}} \max_{\boldsymbol{x}} \mathbb{L}. \tag{2.7}$$

For given Lagrange multipliers and based on Karush-Kuhn-Tucker (KKT) conditions, we have

$$\frac{\partial \mathbb{L}}{\partial \boldsymbol{x}} = 0. \tag{2.8}$$

Thus, we can obtain the closed form expression of the optimal solution $\boldsymbol{x}^*$ as well as the maximum objective function value by calculating (2.8).

The above process is repeated until the Lagrange multipliers converge and it satisfies the complementary slackness conditions, i.e., $\alpha(h(\boldsymbol{x})-\varepsilon_1)=0, \boldsymbol{\beta}(\varepsilon_2-g(\boldsymbol{x}))=0$. For obtained $\boldsymbol{x}$ in each iteration, the Lagrange multipliers are updated by using a gradient based method, where

$$\boldsymbol{\alpha}(l+1) = \boldsymbol{\alpha}(l) - s_1(h(\boldsymbol{x})-\varepsilon_1), \tag{2.9}$$

$$\boldsymbol{\beta}(l+1) = \boldsymbol{\beta}(l) - s_2(\varepsilon_2 - g(\boldsymbol{x})), \tag{2.10}$$

where l is the iteration number, s_1 and s_2 represent the step sizes for the associated Lagrange multipliers. The step size is usually selected based on the system parameters' value, and more details about how to choose the values of the step sizes in a gradient method is discussed in [49].

Chapter 3

Contributions of the Thesis

This thesis classifies WPCNs into three types, i.e., active transmission, passive transmission and hybrid transmission, based on how the information is transmitted. Also, the three types of WPCNs in different scenarios are introduced in Chapter 2 with the description of basic system models. Furthermore, energy-efficient resource allocation problems are solved in the aforementioned WPCNs for different scenarios. i.e., a SWIPT-enabled D2D network, a UAV-enabled network, a SR network and the backscatter network with multiple users. The above contents are included in four journal papers in Part II and their main contributions are summarized in Section 3.1.

The author of this dissertation conceives the ideas and works on system model establishment, problem formulation, problem solution, implementation of algorithms, simulation, numerical results analysis, and the writing of Paper I-IV. Dr. Yinghui Ye and I contribute to the network modelling of the five papers. Pro. Xiaoli Chu guided and supervised all the works. All authors discuss the theoretical aspects and review the manuscript.

3.1 Papers Included in the Thesis

Paper I: Resource and Power Allocation in SWIPT Enabled Device-to-Device Communications Based on a Non-Linear Energy Harvesting Model, co-authored with Yinghui Ye,

Xiaoli Chu and Mianxiong Dong. This paper has been published in *IEEE Internet of Things Journal*, Volume: 7, Issue: 11, Page(s): 10813 - 10825, Date of publication: 17 April 2020.

In the first paper, we aim to maximize the sum EE of all D2D links in a SWIPT enabled D2D underlaid cellular network, where the CUEs are allocated with orthogonal RBs and each D2D link share the same spectrum resource with a CUE. Specifically, the D2D links reuse the uplink spectrum resources of the CUEs, where each D2D transmitter causes interference to a BS and each CUE causes interference to a co-channel D2D receiver.

Before maximizing the sum EE of all D2D links, since we consider the EH sensitivity sothat some D2D links cannot perform SWIPT, a pre-matching algorithm is proposed to divide D2D links into SWIPT-enabled D2D links and Non-EH D2D links. Then we formulate the EE maximization problem for each SWIPT-enabled D2D link and propose an iterative algorithm to maximize the EE per D2D link by optimizing the D2D transmission power and the power splitting ratio based on a non-linear EH model, the closed-form expressions of the locally optimal D2D transmission power and power splitting ratio are also derived. After this, the EE preference lists for both SWIPT-enabled D2D links and CUEs are constructed based on the solutions to the per-D2D-link EE maximization problems. Then we propose a one-to-one constraint stable matching algorithm to match each SWIPT-enabled D2D link with a CUE in the same channel for maximizing the sum EE of all SWIPT enabled D2D links. The convergence and computational complexity are also analyzed. The sum EE of Non-EH D2D links is also maximized by using a similar matching based algorithm. Simulation results show that the proposed algorithms converge very fast, and the EE increases with the number of D2D links and greatly decreases with the D2D communication distance. Also, the sum EE achieved by our proposed algorithms is higher than an existing matching based energy-efficient resource allocation scheme and some benchmark schemes. Furthermore, the EH sensitivity considered in this paper significantly affects the number of SWIPT-enabled D2D links especially for maximizing the EE when the D2D communication distance is long.

Paper II: Max-Min Energy-Efficient Resource Allocation for Wireless Powered Backscatter Networks, co-authored with Yinghui Ye and Xiaoli Chu. This paper has been published in

IEEE Wireless Communications Letters, Volume: 9, Issue: 5, May 2020, Page(s): 688 - 692, Date of Publication: 13 January 2020.

In the second paper, we present the first attempt to maximize the minimum link EE among all the co-channel wireless powered passive backscatter links by jointly optimizing the PB transmission power and the backscatter reflection coefficients, where a PB sends the RF signals to the backscatter transmitters and the transmitters modulate their own information on the incident RF signals and backscatter the modulated signals to the backscatter receivers while harvesting energy from the RF signals. Since multiple backscatter links work in the same frequency band and at the same time, each backscatter transmitter causes interference to other backscatter receivers. The mutual interference among the multiple co-channel backscatter links leads to complicated coupling effects between the backscatter reflection coefficients and the PB transmission power, and the complexity significantly increases with the number of backscatter links. For analytical tractability, we solve the formulated problem for the case of two co-channel backscatter links.

We propose an iterative algorithm to decompose the max-min EE problem into two sub-problems conditioned on the convexity of the objective function: one is a convex optimization problem, while the other is non-convex. The convex problem is solved by employing Lagrange dual method and KKT conditions, and the non-convex problem is solved by exploiting the characteristics of the associated constraints. The closed form expressions of the globally optimal PB transmission power and the globally optimal backscatter coefficients are also obtained during the optimization process. Simulation results show that the proposed iterative algorithm converges very fast and the EE gap between the best user and the worst user after max-min resource allocation is much smaller than the EE gap in the system EE maximization scheme. Also, such EE gap is much smaller with higher throughput requirements for the backscatter links. Furthermore, the max-min EE resource allocation is more effective when the throughput requirement of the BDs is lower and the channel power gain difference from the PB to each backscatter transmitter is smaller.

Paper III: Energy Efficiency Maximization for Symbiotic Radio Networks with Multiple Backscatter Devices, co-authored with Yinghui Ye, Kai Liang and Xiaoli Chu. This

paper has been published in *IEEE Open Journal of the Communications Society*, Volume: 2, Page(s): 1431 - 1444, Date of Publication: 21 June 2021.

In the third paper, the system EE is maximized by jointly optimizing the PT transmission power and the BDs' reflection coefficients and TDMA time slot durations for both the PSR and CSR cases in a SR network, where the PT and the PR are designed to support both the primary and BackCom transmissions, multiple BDs take turn to modulate their own information on the incident primary signal and backscatter the modulated signal to the PR by following TDMA, while harvesting energy from the incident primary signal to support their circuit operation.

Due to multiple coupled variables in the objective function and the constraints, the formulated problem is non-convex and is hard to solve directly. To solve the problem, in the PSR case, we first introduce auxiliary variables and utilize the Dinkelbach-based method to transform the original problem from a fraction form into a subtraction form, then employ a BCD method in conjunction with a successive convex programming (SCP) technique to solve the problem. The closed-form expression of the sub-optimal reflection coefficients and PT transmission power is derived by employing the Lagrange dual method. In the case of CSR, as the system EE is a monotonically increasing function of the BDs' reflection coefficients, we first obtain the globally optimal reflection coefficients. Then, employing techniques similar to the PSR case but without using the BCD method, we obtain the sub-optimal solutions of the PT transmission power and the BDs' time slot durations, and derive the closed-form expressions of the sub-optimal PT transmission power. Based on the above obtained solutions, we propose a Dinkelbach based iterative algorithm to solve the formulated problems in the PSR and CSR cases. The convergence and computational complexity of the proposed algorithm are analyzed and verified by simulation. Also, the simulation results show that the proposed algorithm converges very fast and the system EE is maximized when the primary link contributes almost the EE and each BD only achieves the minimum throughput requirement in the PSR case. In the CSR case, the system EE is maximized when a best BD that can contribute the most toward the system EE is allocated the maximum allowed time to backscatter its information to the PR while the other BDs' throughputs being kept at the minimum required level. Furthermore,

this best BD is not fixed and is determined by the optimized PT transmission power in the corresponding time slot.

Paper IV: Energy Efficiency Maximization for UAV-Enabled Hybrid Backscatter-Harvest-then-Transmit Communications, co-authored with Yinghui Ye, Xiaoli Chu and Sumei Sun. This paper has been published in *IEEE Transactions on Wireless Communication*, DOI: 10.1109/TWC.2021.3116509, Date of Publication: 06 October 2021.

In the fourth paper, we formulate a problem to maximize the EE of all the IoT nodes by jointly optimizing the UAV's transmit power and trajectory and the allocation of communication resources, including the backscatter reflection coefficients, the transmit power of IoT nodes during active transmission, and the time allocation between BackCom and active transmission in the UAV-enabled hybrid BackCom-HTT network, where a UAV works as a mobile energy source to provide RF energy for all the ground IoT nodes. The IoT nodes utilize the incident RF signal to communicate with a reader via a hybrid BackCom-HTT scheme, where the IoT nodes first perform BackCom and then perform active transmission.

Since the EE of multiple IoT nodes are jointly maximized, the formulated optimization problem involves many variables that are coupled in the objective function and/or the constraints. Through theoretical analysis, we reveal that letting the UAV transmit with the maximum power maximizes the EE of all the IoT nodes. Leveraging this finding and the generalized fractional programming theory, we first introduce Dinkelbach-based method to transform the original optimization problem into a more tractable but still non-convex problem. Then, we use a BCD method in conjunction with a Lagrange dual method and a SCP technique to solve the problem. The closed-form expressions for the sub-optimal reflection coefficient and active transmit power of each IoT node are derived. Based on the obtained solutions, we propose a Dinkelbach based iterative algorithm to maximize the EE of all the IoT nodes in the UAV-enabled hybrid BackCom-HTT network. The simulation results show that the proposed algorithm has a fast convergence speed, and can achieve a much higher total EE than the benchmark schemes. In addition, the UAV tends to fly to the IoT nodes that are closer to the reader and we observe that the maximum total EE of the IoT nodes is achieved when the IoT node that is closest to the reader achieves a much higher throughput than other IoT nodes and the other IoT nodes only

achieve the minimum throughput requirement. Furthermore, the available time is used up for maximizing the EE of all the IoT nodes.

3.2 Papers not Included in the Thesis

- **Energy Supply Minimization in Wireless Powered Backscatter Communication Networks**, co-authored with Yinghui Ye and Xiaoli Chu. This paper is under preparation and is planned to be submitted to a transaction journal on August, 2021.

References

[1] J. G. Andrews, S. Buzzi, W. Choi, S. V. Hanly, A. Lozano, A. C. K. Soong, and J. C. Zhang, "What will 5g be?" *IEEE Journal on Selected Areas in Communications*, vol. 32, no. 6, pp. 1065–1082, 2014.

[2] A. Osseiran, F. Boccardi, V. Braun, K. Kusume, P. Marsch, M. Maternia, O. Queseth, M. Schellmann, H. Schotten, H. Taoka, H. Tullberg, M. A. Uusitalo, B. Timus, and M. Fallgren, "Scenarios for 5g mobile and wireless communications: the vision of the metis project," *IEEE Communications Magazine*, vol. 52, no. 5, pp. 26–35, 2014.

[3] T. D. Ponnimbaduge Perera, D. N. K. Jayakody, S. K. Sharma, S. Chatzinotas, and J. Li, "Simultaneous wireless information and power transfer (swipt): Recent advances and future challenges," *IEEE Communications Surveys Tutorials*, vol. 20, no. 1, pp. 264–302, 2018.

[4] E. Hossain, M. Rasti, H. Tabassum, and A. Abdelnasser, "Evolution toward 5g multi-tier cellular wireless networks: An interference management perspective," *IEEE Wireless Communications*, vol. 21, no. 3, pp. 118–127, 2014.

[5] V. Raghunathan, S. Ganeriwal, and M. Srivastava, "Emerging techniques for long lived wireless sensor networks," *IEEE Communications Magazine*, vol. 44, no. 4, pp. 108–114, 2006.

[6] K. Pentikousis, "In search of energy-efficient mobile networking," *IEEE Communications Magazine*, vol. 48, no. 1, pp. 95–103, 2010.

[7] T. Chen, Y. Yang, H. Zhang, H. Kim, and K. Horneman, "Network energy saving technologies for green wireless access networks," *IEEE Wireless Communications*, vol. 18, no. 5, pp. 30–38, 2011.

[8] S. Sudevalayam and P. Kulkarni, "Energy harvesting sensor nodes: Survey and implications," *IEEE Communications Surveys Tutorials*, vol. 13, no. 3, pp. 443–461, 2011.

[9] D. Niyato, E. Hossain, M. M. Rashid, and V. K. Bhargava, "Wireless sensor networks with energy harvesting technologies: a game-theoretic approach to optimal energy management," *IEEE Wireless Communications*, vol. 14, no. 4, pp. 90–96, 2007.

[10] L. Hou and S. Tan, "A preliminary study of thermal energy harvesting for industrial wireless sensor networks," in *2016 10th International Conference on Sensing Technology (ICST)*, 2016, pp. 1–5.

[11] Y. Alsaba, S. K. A. Rahim, and C. Y. Leow, "Beamforming in wireless energy harvesting communications systems: A survey," *IEEE Communications Surveys Tutorials*, vol. 20, no. 2, pp. 1329–1360, 2018.

[12] X. Lu, D. Niyato, H. Jiang, D. I. Kim, Y. Xiao, and Z. Han, "Ambient backscatter assisted wireless powered communications," *IEEE Wireless Communications*, vol. 25, no. 2, pp. 170–177, 2018.

[13] S. D. Assimonis, S.-N. Daskalakis, and A. Bletsas, "Sensitive and efficient rf harvesting supply for batteryless backscatter sensor networks," *IEEE Transactions on Microwave Theory and Techniques*, vol. 64, no. 4, pp. 1327–1338, 2016.

[14] S. Gong, J. Xu, D. Niyato, X. Huang, and Z. Han, "Backscatter-aided cooperative relay communications in wireless-powered hybrid radio networks," *IEEE Network*, vol. 33, no. 5, pp. 234–241, 2019.

[15] D. Li, "Backscatter communication via harvest-then-transmit relaying," *IEEE Transactions on Vehicular Technology*, vol. 69, no. 6, pp. 6843–6847, 2020.

[16] X. Lu, P. Wang, D. Niyato, D. I. Kim, and Z. Han, "Wireless networks with rf energy harvesting: A contemporary survey," *IEEE Communications Surveys Tutorials*, vol. 17, no. 2, pp. 757–789, 2015.

[17] H. Liu, K. J. Kim, K. S. Kwak, and H. Vincent Poor, "Power splitting-based swipt with decode-and-forward full-duplex relaying," *IEEE Transactions on Wireless Communications*, vol. 15, no. 11, pp. 7561–7577, 2016.

[18] Y. Xu, C. Shen, Z. Ding, X. Sun, S. Yan, G. Zhu, and Z. Zhong, "Joint beamforming and power-splitting control in downlink cooperative swipt noma systems," *IEEE Transactions on Signal Processing*, vol. 65, no. 18, pp. 4874–4886, 2017.

[19] Y. Xu, G. Li, Y. Yang, M. Liu, and G. Gui, "Robust resource allocation and power splitting in swipt enabled heterogeneous networks: A robust minimax approach," *IEEE Internet of Things Journal*, vol. 6, no. 6, pp. 10 799–10 811, 2019.

[20] Y. Liu, "Joint resource allocation in swipt-based multiantenna decode-and-forward relay networks," *IEEE Transactions on Vehicular Technology*, vol. 66, no. 10, pp. 9192–9200, 2017.

[21] H. Yang, Y. Ye, X. Chu, and M. Dong, "Resource and power allocation in swipt-enabled device-to-device communications based on a nonlinear energy harvesting model," *IEEE Internet of Things Journal*, vol. 7, no. 11, pp. 10 813–10 825, 2020.

[22] N. Van Huynh, D. T. Hoang, X. Lu, D. Niyato, P. Wang, and D. I. Kim, "Ambient backscatter communications: A contemporary survey," *IEEE Communications Surveys Tutorials*, vol. 20, no. 4, pp. 2889–2922, 2018.

[23] Q. Wu, W. Chen, D. W. K. Ng, and R. Schober, "Spectral and energy-efficient wireless powered iot networks: Noma or tdma?" *IEEE Transactions on Vehicular Technology*, vol. 67, no. 7, pp. 6663–6667, 2018.

[24] Q. Wu, M. Tao, D. W. Kwan Ng, W. Chen, and R. Schober, "Energy-efficient resource allocation for wireless powered communication networks," *IEEE Transactions on Wireless Communications*, vol. 15, no. 3, pp. 2312–2327, 2016.

[25] W. Sun, Q. Song, J. Zhao, L. Guo, and A. Jamalipour, "Adaptive resource allocation in swipt-enabled cognitive iot networks," *IEEE Internet of Things Journal*, pp. 1–1, 2021.

[26] S. Guo, X. Zhou, and X. Zhou, "Energy-efficient resource allocation in swipt cooperative wireless networks," *IEEE Systems Journal*, vol. 14, no. 3, pp. 4131–4142, 2020.

[27] S. Bi and R. Zhang, "Placement optimization of energy and information access points in wireless powered communication networks," *IEEE Transactions on Wireless Communications*, vol. 15, no. 3, pp. 2351–2364, 2016.

[28] D. Xu and Q. Li, "Joint power control and time allocation for wireless powered underlay cognitive radio networks," *IEEE Wireless Communications Letters*, vol. 6, no. 3, pp. 294–297, 2017.

[29] Z. Zhou, M. Peng, Z. Zhao, W. Wang, and R. S. Blum, "Wireless-powered cooperative communications: Power-splitting relaying with energy accumulation," *IEEE Journal on Selected Areas in Communications*, vol. 34, no. 4, pp. 969–982, 2016.

[30] K. Liang, L. Zhao, G. Zheng, and H.-H. Chen, "Non-uniform deployment of power beacons in wireless powered communication networks," *IEEE Transactions on Wireless Communications*, vol. 18, no. 3, pp. 1887–1899, 2019.

[31] G. Yang, R. Dai, and Y.-C. Liang, "Energy-efficient uav backscatter communication with joint trajectory design and resource optimization," *IEEE Transactions on Wireless Communications*, vol. 20, no. 2, pp. 926–941, 2021.

[32] G. Yang, D. Yuan, Y.-C. Liang, R. Zhang, and V. C. M. Leung, "Optimal resource allocation in full-duplex ambient backscatter communication networks for wireless-powered iot," *IEEE Internet of Things Journal*, vol. 6, no. 2, pp. 2612–2625, 2019.

[33] S. Xiao, H. Guo, and Y.-C. Liang, "Resource allocation for full-duplex-enabled cognitive backscatter networks," *IEEE Transactions on Wireless Communications*, vol. 18, no. 6, pp. 3222–3235, 2019.

[34] Y. Xu, Z. Qin, G. Gui, H. Gacanin, H. Sari, and F. Adachi, "Energy efficiency maximization in noma enabled backscatter communications with qos guarantee," *IEEE Wireless Communications Letters*, vol. 10, no. 2, pp. 353–357, 2021.

[35] Y.-C. Liang, Q. Zhang, E. G. Larsson, and G. Y. Li, "Symbiotic radio: Cognitive backscattering communications for future wireless networks," *IEEE Transactions on Cognitive Communications and Networking*, vol. 6, no. 4, pp. 1242–1255, 2020.

[36] S. Gong, X. Huang, J. Xu, W. Liu, P. Wang, and D. Niyato, "Backscatter relay communications powered by wireless energy beamforming," *IEEE Transactions on Communications*, vol. 66, no. 7, pp. 3187–3200, 2018.

[37] B. Lyu, Z. Yang, G. Gui, and Y. Feng, "Wireless powered communication networks assisted by backscatter communication," *IEEE Access*, vol. 5, pp. 7254–7262, 2017.

[38] W. Ma, W. Wang, and T. Jiang, "Joint energy harvest and information transfer for energy beamforming in backscatter multiuser networks," *IEEE Transactions on Communications*, vol. 69, no. 2, pp. 1317–1328, 2021.

[39] B. Lyu, H. Guo, Z. Yang, and G. Gui, "Throughput maximization for hybrid backscatter assisted cognitive wireless powered radio networks," *IEEE Internet of Things Journal*, vol. 5, no. 3, pp. 2015–2024, 2018.

[40] L. Shi, R. Q. Hu, J. Gunther, Y. Ye, and H. Zhang, "Energy efficiency for rf-powered backscatter networks using htt protocol," *IEEE Transactions on Vehicular Technology*, vol. 69, no. 11, pp. 13 932–13 936, 2020.

[41] S. H. Kim and D. I. Kim, "Hybrid backscatter communication for wireless-powered heterogeneous networks," *IEEE Transactions on Wireless Communications*, vol. 16, no. 10, pp. 6557–6570, 2017.

[42] R. Kishore, S. Gurugopinath, P. C. Sofotasios, S. Muhaidat, and N. Al-Dhahir, "Opportunistic ambient backscatter communication in rf-powered cognitive radio networks," *IEEE Transactions on Cognitive Communications and Networking*, vol. 5, no. 2, pp. 413–426, 2019.

[43] W. Dinkelbach, "On nonlinear fractional programming," *Management Science*, vol. 13, no. 7, pp. 492–498, March 1967, Available: http://www.jstor.org/stable/2627691.

[44] D. W. K. Ng, E. S. Lo, and R. Schober, "Wireless information and power transfer: Energy efficiency optimization in ofdma systems," *IEEE Transactions on Wireless Communications*, vol. 12, no. 12, pp. 6352–6370, 2013.

[45] ——, "Energy-efficient resource allocation in ofdma systems with large numbers of base station antennas," *IEEE Transactions on Wireless Communications*, vol. 11, no. 9, pp. 3292–3304, 2012.

[46] M. Hua, L. Yang, C. Li, Q. Wu, and A. L. Swindlehurst, "Throughput maximization for uav-aided backscatter communication networks," *IEEE Transactions on Communications*, vol. 68, no. 2, pp. 1254–1270, 2020.

[47] L. Xie, J. Xu, and R. Zhang, "Throughput maximization for uav-enabled wireless powered communication networks," *IEEE Internet of Things Journal*, vol. 6, no. 2, pp. 1690–1703, 2019.

[48] P. Tseng, "Convergence of a Block Coordinate Descent Method for Nondifferentiable Minimization," *Journal of Optimization Theory and Applications*, vol. 109, no. 3, pp. 475–494, June 2001. [Online]. Available: https://ideas.repec.org/a/spr/joptap/v109y2001i3d10.1023_a1017501703105.html

[49] H.-J. Luethi, "Convex Optimization: Stephen Boyd and Lieven Vandenberghe," *Journal of the American Statistical Association*, vol. 100, pp. 1097–1097, September 2005. [Online]. Available: https://ideas.repec.org/a/bes/jnlasa/v100y2005p1097-1097.html

Part II

Papers

Chapter 4

Paper I

Resource and Power Allocation in SWIPT-Enabled Device-to-Device Communications Based on a Non-linear Energy Harvesting Model

Haohang Yang, Yinghui Ye, Xiaoli Chu and Mianxiong Dong

Published in *IEEE Internet of Things Journal, Volume: 7, Issue: 11, Page(s): 10813 - 10825, Date of publication: 17 April 2020.*

Resource and Power Allocation in SWIPT-Enabled Device-to-Device Communications Based on a Nonlinear Energy Harvesting Model

Haohang Yang[1], Yinghui Ye[2], Xiaoli Chu[1], and Mianxiong Dong[3]

[1] Department of Electronic and Electrical Engineering, the University of Sheffield, Sheffield, S1 4ET, United Kingdom

[2] Shaanxi Key Laboratory of Information Communication Network and Security, Xi'an University of Posts & Telecommunications, China

[3] Department of Information and Electronic Engineering, Muroran Institute of Technology, Muroran, Hokkaido, Japan

Abstract

Due to the limited battery capacity in mobile devices, simultaneous wireless information and power transfer (SWIPT) has been proposed as a promising solution to improving the energy efficiency (EE) in Internet of things (IoT) networks, i.e., device-to-device (D2D) networks, by allowing mobile devices to harvest energy from ambient radio frequency (RF) signals. However, the nonlinear behavior of RF energy harvesters has largely been ignored in existing works on SWIPT. In this paper, we propose to maximize the sum EE of all D2D links in a D2D underlaid cellular network by optimizing the resource and power allocation based on a non-linear energy harvesting (EH) model. Toward this end, we first propose a pre-matching algorithm to divide the D2D links into a SWIPT enabled group and a non-EH group that cannot meet the EH circuit sensitivity. We then develop a two-layer iterative algorithm to jointly optimize the D2D transmission power and the power splitting ratio to maximize the EE for each SWIPT enabled D2D link. On this basis, we build the preference lists for both SWIPT enabled D2D links and cellular user equipment (CUEs), and propose a one-to-one constraint stable matching algorithm to maximize the sum EE of all SWIPT enabled D2D links by optimizing the spectrum resource sharing between D2D links and CUEs. The sum EE of non-EH D2D links is maximized through

an iterative power control algorithm and a one-to-one stable matching algorithm. Simulation results show that our proposed algorithms achieve a much higher sum EE than the existing matching based energy-efficient resource allocation scheme for SWIPT enabled D2D networks.

1 Introduction

With the fast development of wireless communication systems, it is predicted that there will be 7 trillion wireless devices worldwide by 2020 [1], imposing significant pressures on increasing the energy efficiency (EE) of Internet of things (IoT) networks [2]-[4]. A large number of IoT applications are emerging in residential areas, hospitals, factories, etc. Several wireless techniques have been proposed to support IoT, such as ZigBee and WiFi. However, most of them work in unlicensed bands and cannot guarantee the quality of service (QoS) for IoT applications [5], [6]. It is expected that future IoT systems will mainly be supported by 5G mobile networks [7].

Meanwhile, device-to-device (D2D) communications are intrinsic to IoT systems. Hence, D2D communications underlaying cellular networks have been considered as a promising technology to support IoT networks [5], [6]. D2D communications, one of the important scenarios in IoT networks, allow two user equipment (UE) in proximity to communicate with each other directly without passing through a base station (BS) by reusing the spectrum resource of cellular links, and hence improve the EE of a cellular network. However, there will be mutual interference between spectrum-sharing D2D links and cellular UE (CUEs), which need to be mitigated through proper resource allocation schemes [8]-[10]. Meanwhile, radio frequency (RF) enabled energy harvesting (EH), which allows UE to harvest energy from ambient RF signals [11], has been proposed to improve the EE of wireless communications. One popular EH technology is the simultaneous wireless information and power transfer (SWIPT), where the receiver is able to harvest energy and process information simultaneously via a power splitting scheme or a time switching scheme [12]-[16]. In addition to WPT, techniques for EH from natural resources have also been developed for IoT networks [17]-[19].

The EE definition is based on the whole D2D link which comprises the energy harvested by the D2D receiver. Also, in the long term, each D2D user statically has the same probability

of being a transmitter or a receiver, and the proposed algorithms will benefit all D2D users in the network. Although there are considerable number of works on the D2D networks with EH, the researches on the SWIPT based D2D are still insufficient due to the following reasons. Some works assume that the energy source is from the unstable natural resource [20], e.g., solar energy. The other works allow the energy harvester to harvest energy from ambient RF signals [21]. SWIPT is not considered in both cases. Note that SWIPT is expected to operate under short distances because it is mainly limited by the received signal power and the minimum required energy for activating the EH circuit, a.k.a., the EH circuit sensitivity (e.g., -20 dBm [22], which is much higher than the thermal noise power), while the information transfer depends on the receive signal to interference plus noise ratio (SINR). The shared short-range nature between D2D communications and SWIPT motivates the combination of them to further improve the EE performance. For long-distance wireless transmissions in IoT networks, EH could employ laser-charging, e.g., UAV-enabled IoT networks with laser charging was studied in [23] and [24].

The resource allocation schemes for conventional D2D communications without SWIPT may not be applicable for SWIPT enabled D2D communications, where the conventionally considered harmful interference could be exploited for EH. The authors in [25] employed game theory to define the utility of SWIPT-enabled D2D links and allocated D2D transmission power by an iterative algorithm. In [11], a stable matching algorithm was proposed to optimize the spectrum resource and power allocation to improve the average EE for SWIPT-enabled D2D communications. In [26], a transmission flow mechanism was developed to evaluate the impact of different network parameters on the harvested energy and the outage capacity in a SWIPT-based D2D cooperative network. The authors in [27] proposed a scheme that selects between full duration (FD) and partial duration (PD) SWIPT schemes to maximize the data rate of a SWIPT-enabled D2D link. In [28], a power control scheme was proposed to maximize the D2D rate without degrading the performance of CUEs in a downlink SWIPT network.

However, the above works have assumed a simplified linear EH model, where the amount of harvested energy is linearly proportional to the received power, which is not the case in a practical EH system due to the non-linearity of the diodes, inductors, and capacitors [29].

Moreover, the energy conversion efficiency was assumed a fixed value in [11], [21], [22], [25], [26], while the power splitting ratio was assumed as a fixed value in [11], [25]-[27], thus missing the opportunity to optimize it for improving the EE of a SWIPT enabled D2D underlaid network.

In this paper, we aim to maximize the sum EE of all D2D links in a SWIPT enabled D2D underlaid cellular network, where D2D links reuse uplink resources and a piecewise linear EH model[1] is considered for SWIPT. Our main contributions are summarized as follows.

- Considering the impact of EH circuit sensitivity, we propose a pre-matching algorithm to identify the D2D links that can perform SWIPT under the constraints of EH circuit sensitivity and minimum throughput requirement. Based on the pre-matching results, we maximize the EE of each SWIPT enabled D2D link.

- We propose a one-to-one constraint stable matching algorithm to maximize the sum EE of SWIPT enabled D2D links by optimizing the spectrum resource sharing between D2D links and uplink CUEs. This matching algorithm ensures that each SWIPT enabled D2D link is matched to a CUE.

- In the one-to-one constraint stable matching algorithm, the preference lists for both D2D links and CUEs are constructed based on the solutions to the per-D2D-link EE maximization problems, which jointly optimize the D2D transmission power and power splitting ratio based on a piecewise linear EH model for each SWIPT enabled D2D link. Since the two variables are coupled in the objective function, making it difficult to solve, we propose a two-layer energy efficient iterative algorithm (TLEEIA) to solve it by applying the block coordinated decent (BCD) method.

- The sum EE of non-EH D2D links is maximized by devising an iterative power control algorithm and a stable matching algorithm but with a lower complexity than that for SWIPT enabled D2D links.

[1]There are many non-linear EH models reported in the literature. The piecewise linear EH model is one of the most analytically tractable models while ensuring a good accuracy [30].

- We perform extensive simulations to evaluate the EE performance of our proposed algorithms in comparison with a baseline scheme which employs our proposed algorithms based on a linear EH model, the matching based energy-efficient resource allocation scheme in [11], and two heuristic algorithms including proposed matching with maximum D2D transmission power scheme and random matching with maximum D2D transmission power scheme. The impacts of some system parameters, e.g., the number of D2D links or CUEs and the D2D communication range, on the sum EE of D2D links are also examined. Furthermore, we find that the EH sensitivity significantly affect the number of SWIPT-enabled D2D links especially when the D2D communication distance is long.

The rest of the paper is organized as follows. The system model of a D2D communication underlaid cellular network is built in Section 2. In Section 3, the detailed EE optimization process for each SWIPT enabled D2D link is introduced. In Section 4, a one-to-one constraint stable matching algorithm is proposed to solve the resource allocation problem so as to maximize the sum EE of SWIPT enabled D2D links, the sum EE maximization of non-EH D2D links is also derived in this section. In Section 5, the simulation results are presented. Section 6 concludes the paper.

2 System Model

2.1 Network Model

As shown in Fig. 1, a BS[2] is located at the center of a signal cell that covers CUEs and D2D users. Each D2D link i consists of transmitter i (TX i) and receiver i (RX i), and they communicate with each other directly by sharing the spectrum resource with a CUE in an underlaid mode [3]. We assume that there are M orthogonal resource blocks (RBs) allocated to M

[2]The BS obtains all the necessary channel state information (CSI) by collecting feedbacks from the CUEs and D2D devices. In LTE/LTE-A networks, each user (which can be a CUE or a BS assisted D2D device) is scheduled to periodically send measurement reports (including CSI) to the serving BS [31], while the acquisition and reporting of CSI between D2D/cellular transmitters and D2D receivers could employ the techniques proposed in [31], [32].

[3]Our proposed system will not introduce extra system overhead, the CSI estimation required in our proposed system is the same as that required in D2D networks without EH. As the optimization problem is solved at the

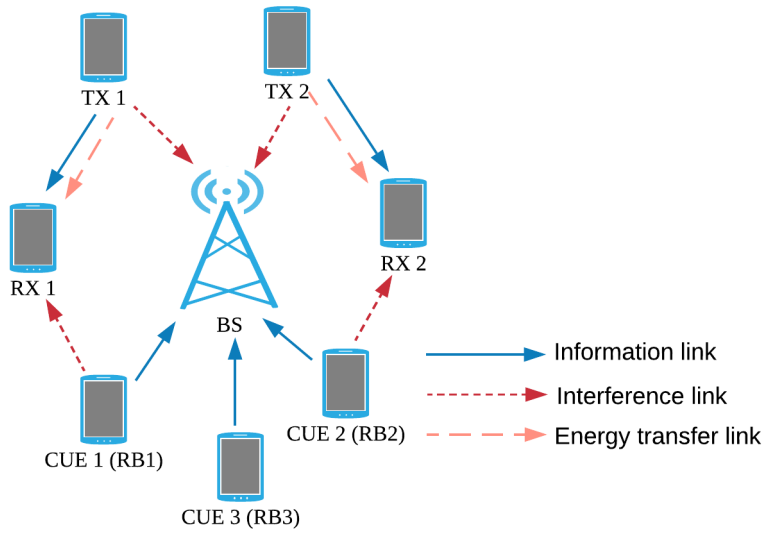

Fig. 1 SWIPT enabled D2D networks.

CUEs and shared by N D2D links. For simplicity, we denote all CUEs and all D2D links by the sets $\hat{C}$={1, 2, ...,k, ..., M} and $\hat{D}$ ={1, 2, ..., i, ..., N}, respectively. We suppose that $N \leq M$ and that a D2D link can only share the RB of one CUE and the RB of a CUE can only be reused by at most one D2D link[4]. For simplicity, the entire time block is normalized to 1. A flat fading channel is considered, where the distance dependent pathloss and Rayleigh fading are used to model the large-scale fading and the small-scale fading, respectively. It is also assumed that the channel state remains static within each resource block. There is no intra-cell interference among CUEs by employing orthogonal frequency division multiple access (OFDMA) [36], [37]. Besides, QoS in this paper is measured by the signal-to-interference-plus-noise ratio (SINR).

We assume that D2D peer discovery and link establishment have been completed. As a D2D pair reuses an uplink RB of a CUE, the D2D receiver receives interference from the co-channel CUE while the D2D transmitter causing interference to the BS. We assume that each D2D device is equipped with a RF EH circuit and an information decoding unit. Due

BS for all the D2D links within its coverage, solving the optimization problem does not consume power at the D2D devices. In addition, the D2D receiver is able to harvest energy from the signals transmitted by the D2D transmitter and the co-channel CUE [21], [33].

[4]Multiple co-channel D2D links may experience strong mutual interference that needs to be mitigated by an advanced interference mitigation scheme. For analytical tractability, we assume that one RB is reused by at most one D2D link [11], [34], [35]. The case with multiple co-channel D2D links will be studied in our future work.

to the EH circuit sensitivity and D2D link QoS requirement, some D2D links cannot perform SWIPT. Thus, we will propose a pre-matching algorithm to divide all D2D links into non-EH D2D links and SWIPT enabled D2D links in section 3.

2.2 Non-EH D2D Links

As discussed in Section 2.1, in the D2D underlaid cellular network, the interference to the BS comes from a co-channel D2D transmitter and only a co-channel CUE causes interference to a D2D receiver. Thus, when sharing the same RB, the SINR of cellular link k[5] and non-EH D2D link i are given by

$$\mathrm{SINR}_k^C = \frac{P_k^C h_k^C}{P_i^D h_i^B + N_0 + N_1} = \frac{P_k^C d_k^{C-\alpha} h_k^{'C}}{P_i^D d_i^B h_i^{'B} + N_0 + N_1}, \tag{1}$$

$$\mathrm{SINR}_i^D = \frac{P_i^D h_i^D}{P_k^C h_{k,i} + N_0 + N_1} = \frac{P_i^D d_i^{D-\alpha} h_i^{'D}}{P_k^C d_{k,i}{}^{-\alpha} h_{k,i}^{'} + N_0 + N_1}, \tag{2}$$

where P_k^C and P_i^D are the transmission power[6] of CUE k and D2D transmitter i, respectively, h_k^C and h_i^D represent the channel responses of cellular uplink k and D2D link i, respectively, d_k^C is the distance from CUE k to the BS and d_i^D represents the distance between the TX and RX of D2D link i. Similarly, h_i^B and $h_{k,i}$ are the channel responses of interference link from D2D link i to BS and the interference link from CUE k to D2D link i, respectively, d_i^B and $d_{k,i}$ are the distance of the interference links above, $h_k^{'C}$, $h_i^{'D}$, $h_i^{'B}$, $h_{k,i}^{'}$ are the Rayleigh channel coefficients accordingly, α is the free space pathloss exponent, N_0 is the additive white gaussian noise (AWGN) power, and N_1 is the noise power due to RF band to base band conversion.

Then the throughputs of cellular link k and D2D link i are respectively given by

$$T_k^{'C} = \log_2(1 + \mathrm{SINR}_k^C), \tag{3}$$

[5]Since most notations in this paper are related to CUE k, but the optimization problem focuses mainly on maximizing the EE for D2D links, for notational simplicity, we will omit subscript k from notations where appropriate.

[6]For analytical tractability, we assume that all CUEs transmit at the maximum power level [11], [38]. The impact of CUE transmission power on the sum EE of D2D links will be evaluated through simulation in Section 6.4

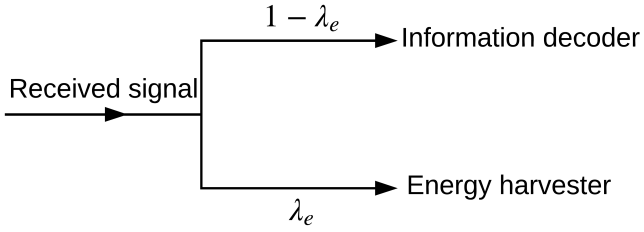

Fig. 2 Power splitting unit.

$$T_i^{'D} = \log_2(1+\mathrm{SINR}_i^D). \tag{4}$$

2.3 SWIPT Enabled D2D Links

SWIPT can be implemented in either a power splitting mode or a time switching mode. We consider the power splitting mode in this paper since it has been proved to be more efficient in both throughput and EE [39]. As shown in Fig. 2, the power splitting unit splits the received radio signal into two signal streams. One stream is for information decoding and the other is for EH, where λ_e denotes the power splitting ratio, which determines the portion of the received signal used for EH. A D2D receiver can harvest energy from the signals transmitted by its paired D2D transmitter and the interference from the co-channel CUE and the surrounding thermal noise.

For SWIPT enabled D2D link i, the throughput is given by

$$T_i^D = \log_2\left(1+\frac{(1-\lambda_i^e)P_i^D h_i^D}{(1-\lambda_i^e)(P_k^C h_{k,i}+N_0)+N_1}\right), \tag{5}$$

where the useful information signal, the interference and the noise are scaled by the factor of $(1-\lambda_i^e)$.

The received power for EH at D2D receiver i when sharing the RB with CUE k is given by

$$P_i^R = \lambda_i^e(P_i^D h_i^D + P_k^C h_{k,i} + N_0). \tag{6}$$

We employ the piecewise linear EH model proposed in [24][7], which fits over real measurement data. Accordingly, the amount of power harvested by D2D receiver i is given as

$$EH_i^D = \begin{cases} 0, & P_i^R \in [P_{th}^0, P_{th}^1]; \\ k_j P_i^R + b_j, & P_i^R \in [P_{th}^j, P_{th}^{j+1}], j \in 1, ..., L-1; \\ P_{max}^{EH}, & P_i^R \in [P_{th}^L, P_{th}^{L+1}], \end{cases} \tag{7}$$

where $\mathbf{P_{th}} = \{P_{th}^j | 1 \leq j \leq L+1\}$ is the set of thresholds on P_i^R for $L+1$ linear segments; k_j and b_j are the coefficient and the intercept of the linear function in the j-th segment, respectively, P_{th}^1 denotes the minimum received power requirement for activating the RF EH circuit, and P_{max}^{EH} represents the maximum power the RF EH circuit can harvest. It has been shown in [40], [43] that the piecewise linear EH model captures the harvested power more accurately than the linear EH model, the accuracy of the piecewise linear EH model improves with more segments, and a 4-piecewise linear EH model offers a good trade off between accuracy and computational complexity.

The total energy consumption of D2D link i is given as

$$EC_i^D = P_i^D + 2\mathrm{P_{cir}} - EH_i^D, \tag{8}$$

where $\mathrm{P_{cir}}$ is the circuit power consumption for a D2D transmitter (or a D2D receiver) including the power consumption of mixer, frequency synthesizer, etc.

[7]The accuracy of piecewise linear EH model increases with the number of linear segments, [40] proves that the sigmoid function based non-linear EH model in [41] and the piecewise linear EH model are more accurate than the linear EH model for practical RF-DC circuits. Also, the 4-piecewise linear EH model and the sigmoid function have similar accuracy, while the 4-piecewise linear EH model has a lower mean square error than the sigmoid function does. The sigmoid function is difficult to be transformed into a convex form, while the piecewise linear EH model is convex with higher computational complexity. Furthermore, the authors in [42] propose a simple non-linear EH model, which is convex and has low computational complexity. However, this EH model is less accurate than the other two EH models and does not consider EH circuit sensitivity. Therefore, the piecewise linear EH model is used for more tractability and high accuracy.

3 Per-D2D-Link Energy Efficiency Maximization for SWIPT Enabled D2D Links

In this section, we first propose a pre-matching algorithm to separate SWIPT enabled D2D links and non-EH D2D links, then we maximize the EE of each potential SWIPT enabled D2D link based on the pre-matching results.

3.1 Pre-Matching Algorithm

Considering the EH circuit sensitivity, we divide the D2D links into two groups: one group denoted by Eha^D for SWIPT enabled D2D links (which can activate the EH circuit at the receiver while meeting the minimum D2D throughput requirement) and the other denoted by Inf^D for non-EH D2D links (which cannot perform SWIPT). We propose a pre-matching algorithm in Algorithm 1 to obtain the two groups. For any D2D link i, the partner selection set S_i^D is initialized as $\hat{C}$. If when reusing the RB of CUE k, and transmitting at the maximum transmission power $\mathrm{P_{max}}$, D2D link i cannot meet the EH circuit sensitivity and/or the D2D throughput requirement, then CUE k is removed from S_i^D. This step is repeated for each CUE in the set $\hat{C}$ and the partner selection sets S_i^D for D2D link i are obtained, the minimum power splitting ratio for meeting the EH circuit sensitivity requirement of D2D link i is calculated as

$$\lambda_{min}^{e,i} = \frac{P_{th}^{1}}{\mathrm{P_{max}} h_i^D + P_k^C h_{k,i} + N_0}, \tag{9}$$

As $\lambda_{i,min}^{e}$ cannot exceed 1, we can obtain the maximum throughput of D2D link i when satisfying the EH circuit sensitivity requirement as

$$T_{i,max}^{D} = \log_2 \left(1 + \frac{\mathrm{P_{max}} h_i^D}{P_k^C h_{k,i} + N_0 + \frac{N_1}{1-\lambda_{i,min}^{e}}} \right). \tag{10}$$

Algorithm 1: Pre-matching algorithm

1: **Input:** $\hat{D}, \hat{C}, P_k^C, P_{th}^{1}, \mathrm{P_{max}}, \mathrm{T_{min}^{D}}$.

2: **Output:** S_i^D, Inf^D, Eha^D.

3: **Initialize:** $S_i^D = \hat{C}$, $Inf^D = \emptyset$, $Eha^D = \emptyset$.

4: **for** $i \in \hat{D}$ **do**

5: **for** $k \in \hat{C}$ **do**

6: obtain $\lambda_{i,min}^e$ using (9), obtain $T_{i,max}^D$ using (10).

7: **if** $\lambda_{i,min}^e > 1$ or $T_{i,max}^D \leq \mathrm{T}_{\min}^{\mathrm{D}}$ **then**

8: $S_i^D \setminus k$.

9: **end if**

10: **end for**

11: **if** $S_i^D = \emptyset$ **then**

12: $Inf^D \cap i$.

13: **else** $S_i^D \neq \emptyset$, $Eha^D \cap i$.

14: **end if**

15: **end for**

The above procedures will be performed for each D2D link to obtain their partner selection set. At the end of Algorithm 1, if the partner selection set for a D2D link is empty, then this D2D link is grouped into the set Inf^D; otherwise, it is grouped into the set Eha^D.

3.2 Per-D2D-Link EE Problem Formulation

The partner selection set (returned by Algorithm 1) for an SWIPT enabled D2D link may contain more than one CUE, while a CUE may appear in more than one partner selection sets. In order to optimize the matching between SWIPT enabled D2D links and CUEs so that the

sum EE of SWIPT enabled D2D links is maximized, we first maximize the EE for each SWIPT enabled D2D link i in Eha^D. The EE is defined as the ratio of throughput T_i^D to the total power consumption EC_i^D [10].

The EE of D2D link i in Eha^D when reusing the RB allocated to CUE k in S_i^D is given by

$$EE_i^D = \frac{T_i^D}{EC_i^D} = \frac{\log_2\left(1+\frac{P_i^D h_i^D}{(P_k^C h_{k,i}+N_0)+\frac{N_1}{(1-\lambda_i^e)}}\right)}{P_i^D + 2\mathrm{P_{cir}} - EH_i^D}. \tag{11}$$

Accordingly, the EE maximization problem of SWIPT enabled D2D link i is formulated as

$$\begin{aligned}
\mathbf{P1}: \max_{\{P_i^D,\lambda_e^i,i\in Eha^D\}} \; & EE_i^D \\
\text{s.t. } & \mathrm{C1}: 0 < P_i^D \le \mathrm{P_{max}}, \\
& \mathrm{C2}: 0 \le \lambda_i^e \le 1, \\
& \mathrm{C3}: T_i^D \ge \mathrm{T_{min}^D}, \\
& \mathrm{C4}: T_k^C \ge \mathrm{T_{min}^C}, \\
& \mathrm{C5}: P_{th}^j \le P_i^R \le P_{th}^{j+1}, j \in 0,...,L,
\end{aligned} \tag{12}$$

where C1 denotes the maximum transmission power for all D2D transmitters; C2 sets the range of power splitting ratio; C3 and C4 set the minimum throughput requirement for D2D links and cellular links, respectively; C5 indicates that the energy harvester of D2D receiver i works in the j-th linear segment in the piecewise linear EH model.

In order to solve **P1**, we propose a TLEEIA, which includes an outer-loop algorithm given in **Algorithm 2** and an inner-loop iterative algorithm given in **Algorithm 3**. In **Algorithm 3**, the maximum number of segments, N_{max}, in the piecewise linear EH model that P_i^R belongs to is obtained by calculating $P_{i,max}^R = P_{max}h_i^D + P_k^C h_{k,i} + N_0$ and comparing the calculated value with the piecewise linear EH model in (7), where $P_{i,max}^R$ is the maximum received power of D2D RX i. Then, **Algorithm 3** continues to calculate the optimal values of $\{P_{i,1}^D,...,P_{i,j}^D,...,P_{i,N_{max}}^D\}$, $\{\lambda_{i,1}^e,...,\lambda_{i,j}^e,...,\lambda_{i,N_{max}}^e\}$ and $\{EE_{i,1}^D,...,EE_{i,j}^D,...,EE_{i,N_{max}}^D\}$ that maximize the EE of SWIPT enabled D2D link i when it is matched with every possible CUE in the j-th segment. In **Algorithm 2**, the optimal segment that maximizes the EE of SWIPT enabled D2D link i when

matched with every possible CUE is determined by $j^* = \arg\max_j \{EE^D_{i,1}, ..., EE^D_{i,j}, ..., EE^D_{i,N_{max}}\}$, and the corresponding optimal λ_i^{e*}, $P_i^{D^*}$ and $EE_i^{D^*}$ are obtained.

Algorithm 2: TLEEIA−Outer loop algorithm

1: **Input:** $Eha^D, S_i^D, \lambda_{i,j}^e, P_{i,j}^D, EE_{i,j}^D$.

2: **Output:** $P_i^{D^*}$, λ_i^{e*}, $EE_i^{D^*}$.

3: **for** $i \in Eha^D$ **do**

4: **for** $k \in S_i^D$ **do**

5: **for** $j = 1 : N_{max}$ **do**

6: $j^* = \arg\max_j \{EE^D_{i,1}, ..., EE^D_{i,j}, ..., EE^D_{i,N_{max}}\}$.

7: Obtain $P_i^{D^*} = P^D_{i,j^*}$, $\lambda_i^{e*} = \lambda^e_{i,j^*}$, $EE_i^{D^*} = EE^D_{i,j^*}$.

8: **end for**

9: **end for**

10: **end for**

3.3 Inner-Loop Iterative Algorithm

Since **P1** is a non-convex fractional programming problem and difficult to solve, we transform it into a non-fractional problem by employing nonlinear fractional programming [44], given by

$$\begin{aligned} \mathbf{P2}: \max_{\{P_i^D, \lambda_i^e\}} \; & T_i^D - Q_i^{D^*} EC_i^D, i \in Eha^D \\ \text{s.t.} \; & \text{C1} - \text{C5} \end{aligned} \tag{13}$$

where $Q_i^{D^*} = EE_i^{D^*}$. Based on [43], we have the following theorem for solving **P2**.

Theorem 1. *The optimal Q_i^{D*} can be achieved if and only if $T_i^{D*} - Q_i^{D*} EC_i^{D*} = 0$,* where $Q_i^{D*} = \max\limits_{\{P_{i,D}{}^*\}} EE_i^D = \frac{T_i^{D*}}{EC_i^{D*}}$, which is the maximum EE of D2D link *i*, and P_i^{D*}, T_i^{D*} and EC_i^{D*} are the corresponding optimal values when D2D link *i* reuses the RB of CUE *k*.

According to Theorem 1, we can address the original non-convex problem by solving **P2**. Q_i^D is regarded as the negative weight of EC_i^D and we set the initial value of Q_i^D as a small positive value.

We employ Lagrange dual decomposition and Karush-Kuhn-Tucker (KKT) conditions to solve **P2**. The Lagrange function is given by

$$\begin{aligned} L(P_i^D, \lambda_i^e, \alpha, \beta, \gamma, \delta, \varepsilon) = T_i^D - Q_i^{D*} EC_i^D - \alpha(P_i^D - \mathrm{P_{max}}) - \beta(\lambda_i^e - 1) \\ + \gamma(T_i^D - \mathrm{T_{min}^D}) + \delta(T_i^C - \mathrm{T_{min}^C}) + \varepsilon(P_i^R - P_{th}^1), \end{aligned} \tag{14}$$

where α, β, γ, δ and ζ are the Lagrange multipliers for C1-C5, respectively. Then the Lagrange dual optimization problem is obtained as

$$\begin{aligned} &\mathbf{P3}: \\ &\min_{\{\alpha,\beta,\gamma,\delta,\varepsilon \geq 0\}} \quad \max_{\{P_i^D, \lambda_i^e\}} L(P_i^D, \lambda_i^e, \alpha, \beta, \gamma, \delta, \varepsilon), i \in Eha^D \\ &\text{s.t. C5} \end{aligned} \tag{15}$$

To solve P3, we have the following proposition.

Proposition 1. **P3** is convex with respect to λ_i^e when we fix P_i^D and it is also convex with respect to P_i^D when we fix λ_i^e.

Proof. Please see Appendix A. ■

Based on Proposition 1, we can find the locally optimal λ_i^e for a given P_i^D and the locally optimal P_i^D for the optimized λ_i^e by applying the BCD method.[8] Then we use KKT conditions to obtain the expression of λ_i^e for a fixed P_i^D by solving the following equation.

$$\frac{\partial L(P_i^D, \lambda_i^e, \alpha, \beta, \gamma, \delta, \varepsilon)}{\partial \lambda_i^e} = 0. \tag{16}$$

[8] Although the convergence of the BCD method cannot be analyzed theoretically [45], it can converge typically in a few iterations for a moderate number of users as shown in the simulation results.

Theorem 2. *By solving (16) for λ_i^e, the optimal value of λ_i^e in **P3** is given as*

$$\lambda_i^{e*} = \left\{ \frac{-a_2 \pm \sqrt{a_2^2 - 4a_1a_3}}{2a_1} \right\}^+, \tag{17}$$

where $\{X\}^+ = \max\{0, X\}$, $a_1 = K(GH + H^2)$, $a_2 = K(G+2H)N_1$, $a_3 = KN_1^2 - J$, $G = P_i^D h_i^D$, $H = P_k^C h_{k,i} + N_0$, $K = \beta + (Q_i^{D*} + \varepsilon)k_j(G+H)$, *and* $J = GN_1 log_2^e(1+\gamma)$.

Proof. Please see Appendix B. ■

Similarly, when λ_i^e is fixed, the optimal value of P_i^D can be obtained by solving the following equation.

$$\frac{\partial L(P_i^D, \lambda_i^e, \alpha, \beta, \gamma, \delta, \varepsilon)}{\partial\, P_i^D} = 0. \tag{18}$$

Theorem 3. *By solving (18) for P_i^D, the optimal value of P_i^D can be obtained in a closed form as*

$$P_i^{D*} = \max\{0, P_1\}, \tag{19}$$

$$\text{with } \mathrm{P}_1 = \begin{cases} X_N + \sqrt[3]{\frac{-y_N + \sqrt{y_N^2 - g^2}}{2a_1}} + \sqrt[3]{\frac{-y_N - \sqrt{y_N^2 - g^2}}{2a_1}}, & y_N^2 > g^2 \\ X_N - \theta, X_N + 2\theta, & y_N^2 = g^2 \\ X_N + 2\theta\cos(\phi - \frac{2\pi n}{3}), \quad [n = 0,1,2]. & y_N^2 < g^2 \end{cases} \tag{20}$$

where $b_1 = m_3 h_i^D h_{i,B}^2$, $b_2 = (2m_3m_5 + m_3m_6)h_i^D h_i^B - (m_1 - m_2m_3)h_{i,B}^2$, $b_3 = (m_3m_5^2 + m_3m_5m_6 + m_4)h_i^D - (2m_1m_5 + m_1m_6 - 2m_2m_3m_5 - m_2m_3m_6)h_{i,B}$, $b_4 = m_2m_4 + m_2m_3m_5^2 + m_2m_3m_5m_6 - m_1m_5^2 - m_1m_5m_6$. $X_N = \frac{-m_2}{3m_1}$, $y_N = \frac{2b_2^3}{27b_1^2} - \frac{b_2b_3}{3b_1} + b_4$, $g = 2b_1\sqrt{\frac{b_2^2 - 3b_1b_3}{9b_1^2}}^3$, $\phi = \frac{1}{3} arc\cos\frac{-y_N}{g}$, $\theta^2 = \frac{m_2^2 - 3m_1m_3}{9m_1^2}$, $m_1 = (1+\gamma)h_i^D log_2^e$, $m_2 = P_k^C h_{k,i} + N_0 + \frac{N_1}{1-\lambda_i^e}$, $m_3 = Q_i^D(1 + (1-\lambda_i^e)\eta h_i^D - k_j h_i^D) + \alpha - \varepsilon\lambda_i^e k_j h_i^D$, $m_4 = P_k^C h_k^C h_i^B log_2^e \delta$, $m_5 = N_0 + N_1$, $m_6 = P_k^C h_k^C$, and the sign of θ is the same as that of $\sqrt[3]{\frac{y_n}{2b_1}}$.

Proof. Please see Appendix C. ■

Then we use the gradient method to update the values of the Lagrange multipliers as follows:

$$\alpha = \{\alpha + s_1(P_i^D - \mathrm{P_{max}})\}^+, \tag{21}$$

$$\beta = \{\beta + s_2(\lambda_i^e - 1)\}^+, \tag{22}$$

$$\gamma = \{\gamma - s_3(T_i^D - \mathrm{T_{min}^D})\}^+, \tag{23}$$

$$\delta = \{\delta - s_4(T_k^C - \mathrm{T_{min}^C})\}^+, \tag{24}$$

$$\varepsilon = \{\varepsilon - s_5(P_i^R - P_{th}^1)\}^+, \tag{25}$$

where s_1, s_2, s_3, s_4 and s_5 are the step sizes of the associated constraints and they need to be properly initialized for guaranteeing the convergence and optimality. The step size is usually based on the objective function and simulation parameters, we set the step size for updating the five Lagrange multipliers as 10^{-5} in this paper.

We propose an inner-loop iterative algorithm in Algorithm 3 to obtain the optimal value of $\lambda_{i,j}^e$, $P_{i,j}^D$ and $EE_{i,j}^D$ for each SWIPT-enabled D2D link in the j-th segment of the linear piecewise EH model. In Algorithm 3, t is the number of iteration step; I denotes the maximum allowed number of iteration. The iteration terminates when the difference between the value of achieved EE and that of EE in previous step is smaller than ψ or I is achieved.

Algorithm 3: TLEEIA−Inner loop iterative algorithm

1: **Input:** Eha^D, S_i^D.

2: **Output:** $\lambda_{i,j}^e, P_{i,j}^D, EE_{i,j}^D$.

3: **Initialize:** $Q_i^{D*}(t) = Q_i^{D*}(0), P_i^D(t) = P_i^D(0), I, \psi, t = 0$.

4: Obtain $P_{i,R}^{max}$ and decide the maximum number of segments: N_{max}.

5: **for** $i \in Eha^D$ **do**

6: **for** $k \in S_i^D$ **do**

7: **for** $j = 1 : N_{max}$ **do**

8: We use the initialization value $P_i^D(0)$ to obtain $\lambda_i^e(t)$ by calculating (17).

9: **while** $t < I$ **do**

10: We use the achieved value of $\lambda_i^e(t)$ to obtain $P_i^D(t+1)$ by calculating (20).

11: We use the calculated value of $P_i^D(t+1)$ to obtain $\lambda_i^e(t+1)$ by calculating (17).

12: **if** $T_i^D[\lambda_i^e(t+1), P_i^D(t+1)] - Q_i^{D*}(t) EC_i^D[\lambda_i^e(t+1), P_i^D(t+1)] > \psi$ **then**

13: $Q_i^{D*}(t+1) = T_i^D[\lambda_i^e(t+1), P_i^D(t+1)] / EC_i^D[\lambda_i^e(t+1), P_i^D(t+1)]$.

14: **Update** Lagrange multipliers using (21)-(25).

15: **else** $P_{i,j}^D = P_i^D(t+1)$, $\lambda_{i,j}^e = \lambda_i^e(t+1)$, $EE_{i,D}^j = Q_i^{D*}(t)$.

16: **Continue**

17: **end if**

18: $t = t + 1$.

19: **end while**

20: **end for**

21: **end for**

22: **end for**

4 Sum Energy Efficiency Maximization

In this section, we propose a one-to-one constraint stable matching algorithm to maximize the sum EE of SWIPT enabled D2D links, where the preference lists for both D2D links and CUEs will be constructed based on the results of Algorithm 2. The sum EE of non-EH D2D links will be maximized in a similar but simpler way at the end of this section.

4.1 Preference Lists

In order to find the most appropriate CUE for each SWIPT enabled D2D link to share RB with such that the sum EE of all SWIPT enabled D2D links is maximized, which is also referred to as the partner selection problem, we need to build a preference list for each SWIPT enabled D2D link and each CUE based on the results of Algorithms 2.

Each SWIPT enabled D2D link would prefer to share the RB of a CUE that maximizes its EE. The preference list of D2D link i, denoted by $\Omega_i^D = \{\Omega_i^1, \Omega_i^2, ..., \Omega_i^k\}$, where $i \in Eha^D$, is obtained by sorting all the CUEs in S_i^D in the descending order of the EE that D2D link i can achieve when sharing their RBs. Each CUE would prefer to share its RB with a D2D link that causes the least interference to its uplink to the BS. The preference list of CUE k, denoted by $\Omega_k^C = \{\Omega_k^1, \Omega_k^2, ..., \Omega_k^i\}$, where $k \in S_i^D$, is constructed by sorting all the D2D links in Eha^D in the ascending order of the interference power that they cause to the BS when sharing the RB with CUE k. Therefore, we can establish the preference lists for all SWIPT enabled D2D links and the CUEs in S_i^D.

If all the SWIPT enabled D2D links can find their partners, the matching will be called perfect stable matching. However, sometimes due to the bad channel condition or the long D2D communication distance, some of the D2D links can only select few or even one CUE to match with for meeting the constraints especially for EH circuit sensitivity. Thus, such D2D links may have limited CUEs in their preference lists so as in the partner selection set S_i^D. Also, the limited CUEs may match with other D2D links they prefer based on Ω_k^C, this results in such D2D links to be unmatched. Considering the user fairness and the EE performance, we cannot

let such D2D links fail to perform SWIPT. Thus, a one-to-one constraint stable matching is proposed in the next subsection to ensure all SWIPT enabled D2D links can find their partners.

4.2 One-to-One Constraint Stable Matching Algorithm

The BS collects all the preference lists constructed as described above and runs a one-to-one constraint stable matching algorithm to ensure that each SWIPT enabled D2D link is matched to an appropriate CUE. Since stable matching tends to favor the group that proposes to the other group [46], the algorithm lets the D2D links start proposing to the CUEs first. In each loop, the D2D links in Eh_a^D propose to their most preferred CUE one by one. If CUE k ($k \in S_i^D$) receives only one proposal, then it will select the proposing D2D link as its partner. When CUE k receives more than one proposals, if there is a proposing D2D link with only one CUE in its preference list, then CUE k will select this D2D link and reject all the others; if all the proposing D2D links have more than one CUEs on their preference lists, then CUE k will select the most preferred D2D link among the proposing D2D links according to its own preference list Ω_k^C and reject all the others.

During each loop, a D2D link will be removed from (or added to) Eha^D if it is matched to (or refused by) a CUE. At the end of each loop, all SWIPT enabled D2D links will delete their most preferred CUE from their preference lists. In the next loop, each unmatched D2D link in Eha^D will propose to the most preferred CUE one by one in their updated preference list. The one-to-one constraint stable matching algorithm will terminate until all SWIPT enabled D2D links have been matched to a CUE. Finally, the unmatched CUEs are gathered in Φ^R.

Algorithm 4: Constraint stable matching algorithm

1: **Input:** $Eha^D, \hat{C}, \Omega_i^D, \Omega_k^C$.

2: **Output:** Φ, Φ^R.

3: **Initialize:** $\Phi = \emptyset$.

4: **while** $Eha^D \neq \emptyset$ **do**

5: **for** $i \in Eha^D$ **do**

6: D2D link i proposes to its most preferred CUE based on Ω_i^D.

7: **for** $k \in S_i^D$ **do**

8: **if** CUE k receives only one proposal from D2D link i and currently has no partner **then**

9: CUE k and D2D link i are matched, $Eha^D \setminus i$, $\Phi = (i,k)$.

10: **end if**

11: **if** CUE k receives another proposal from D2D link $i^{'}$ **then**

12: CUE k will check Ω_i^D and $\Omega_{i^{'}}^D$.

13: **if** D2D link i or $i^{'}$ has no more preference **then**

14: CUE k will match with D2D link i or $i^{'}$, the matched D2D link will be removed from Eha^D, the unmatched D2D link will be added into Eha^D.

15: **end if**

16: **if** Both D2D links have other preferences **then**

17: CUE k will match with more preferred D2D link based on Ω_k^C, the matched D2D link will be removed from Eha^D, the unmatched D2D link will be added into Eha^D.

18: **end if**

19: **end if**

20: **end for**

21: **end for**

22: All D2D links in Eha^D delete their most preferred CUE in Ω_i^D.

23: **end while**

24: All unmatched CUEs are gathered in Φ^R.

4.3 Sum EE Maximization for Non-EH D2D Links

The non-EH D2D links have been grouped in Inf^D by the pre-matching algorithm in section 3.1. Also, the constraint stable matching algorithm is firstly performed for SWIPT-enabled D2D links for obtaining higher sum EE, and each SWIPT-enabled D2D link is matched with a appropriate CUE. Then we propose an iterative power control algorithm and a one-to-one stable matching algorithm to maximize the sum EE of non-EH D2D links by matching them with the CUEs that have not been matched with any SWIPT enabled D2D link. The difference from Algorithm 4 is that there are no constraints regarding the EH circuit sensitivity or the power splitting ratio. The optimal transmission power of non-EH D2D links i ($i \in Inf^D$) when reusing the RB of CUE k ($k \in \Phi^R$) is given by

$$P_i^{D*} = \left\{ \frac{(1+\beta')\log_2^{\mathrm{e}}}{\alpha' + Q_i^{D*}} - \frac{P_k^C h_{k,i} + N_0 + N_1}{h_i^D} \right\}^+ . \tag{26}$$

Proof. Please see Appendix D. ■

5 Computational Complexity Analysis

The complexity of the pre-matching algorithm in **Algorithm 1** is mainly determined by the number of D2D links and CUEs. Therefore, the computational complexity of **Algorithm 1** is $\mathcal{O}(MN)$, where M and N are the numbers of CUEs and D2D links, respectively.

The TLEEIA algorithm employs an inner-loop algorithm (i.e., Algorithm 3) and an outer-loop algorithm (i.e., Algorithm 2) to solve **P1**. There are three main steps to solve **P1**. In Step 1, we compute the maximum number of segments that P_i^R may belong to, denoted by N_{max}. In Step 2, we solve the optimization problem **P3** for given i. By solving **P3**, we obtain N_{max} power allocation and resource allocation policies, denoted by $\{P_{i,1}^D, ..., P_{i,j}^D, ..., P_{i,N_{max}}^D\}$ and $\{\lambda_{i,1}^e, ..., \lambda_{i,j}^e, ..., \lambda_{i,N_{max}}^e\}$, respectively, and compute the corresponding EE denoted by

$\{EE^D_{i,1},...,EE^D_{i,j},...,EE^D_{i,N_{max}}\}$. In Step 3, the optimal solution of **P1** is determined by $\max_j\{EE^D_{i,1}, ...,EE^D_{i,j},...,EE^D_{i,N_{max}}\}$ and is denoted by $P_i^{D^*}$, λ_i^{e*}, $EE_i{}^{D^*}$. The inner-loop iterative algorithm in **Algorithm 3** solves Step 2. If the 'while' loop of **Algorithm 3** needs Δ_1 iterations to converge, the subgradient method used in **Algorithm 3** needs Δ_2 iterations to converge, and the BCD method used in **Algorithm 3** needs Δ_3 iterations to converge, then the update of P_i^D and λ_i^e need $\mathcal{O}(\Delta_3)$ operations, and the updates of each Lagrange multiplier calls $\mathcal{O}(\Delta_2)$ operations, while there are 5 Lagrange multipliers in **Algorithm 3**. Thus, the computational complexity of **Algorithm 3** is $\mathcal{O}(M'N'\Delta_1 5\Delta_2\Delta_3)$, where N' and M' are the numbers of SWIPT enabled D2D links and CUEs possible to match, respectively. The outer-loop algorithm in **Algorithm 2** solves Step 3, where the computation times are N_{max}. Therefore, the computational complexity of the TLEEIA algorithm is $N_{max}\mathcal{O}(M'N'\Delta_1 5\Delta_2\Delta_3)$ [11], [47].

For the one-to-one constraint stable matching in **Algorithm 4**, due to the fact that every SWIPT enabled D2D link has only one opportunity to propose to CUEs in its preference list, the computational complexity of **Algorithm 4** is $\mathcal{O}(M'N')$ [11]. The computational complexity of the stable matching algorithm in Appendix D for non-EH D2D links is $\mathcal{O}(M''N'')$, where M'' and N'' denote the numbers of remaining CUEs and non-EH D2D links, respectively. In short-range D2D communications, since the numbers of non-EH D2D links and remaining CUEs are typically smaller than those of SWIPT enabled D2D links and CUEs possible to match, respectively, the stable matching algorithm has a lower complexity than the one-to-one constraint stable matching in **Algorithm 4**[9].

6 Simulation Results

This section shows the simulation results of the proposed algorithms based on the piecewise linear EH model in comparison with a baseline which employs our proposed algorithms based on a linear EH model, the matching based energy-efficient resource allocation scheme in [11], and two heuristic algorithms including proposed matching with maximum D2D transmission power scheme and random matching with maximum D2D transmission power scheme. The EE

[9]The proposed algorithms are operated by the BS, without increasing the overhead for CSI acquisition or reporting as compared with the existing BS assisted D2D communications underlaying cellular network.

is analyzed with respect to some key parameters including the number of D2D links or CUEs and the D2D communication distance.

6.1 Parameters Initialization

The simulation parameters are listed in Table 1. Without loss of generality, we assume the same number of D2D links as the number of CUEs.

Table 1 Simulation Parameters

Simulation parameter	Value
Cell radius R	200 m
Number of D2D links N	10∼30
Number of CUEs M	10∼50
D2D communication distance range r	10∼60 m
Pathloss exponent α	3 [48]
Receiver power segment $[P_{th}^0, P_{th}^1, P_{th}^2, P_{th}^3]$	[10, 57368, 230.06, 100] uw
Coefficient $[k_0, k_1, k_2, k_3, k_4]$	[0, 0.3899, 0.6967, 0.1427]
Intercept $[b_0, b_1, b_2, b_3, b_4]$	[0,-1.6613,-19.1737,108.2778]
Maximum harvestable power P_{max}^{EH}	250 uw
Max transmission power for any user P_{max}	23 dBm
CUE transmission power P_k^C	23dBm
Noise power N_0, N_1	-100 dBm [11], [13], [28]
Circuit power consumption P_{cir}	20 dBm
Throughput requirement for D2D link T_{min}^D	2 bit/s/Hz
Throughput requirement for cellular link T_{min}^C	1 bit/s/Hz

6.2 Pre-Matching Fail Rate

Fig. 3 shows the pre-matching fail rate (PMFR) versus the number of D2D links or CUEs and D2D communication distance. PMFR is defined as the ratio of the number of non-EH D2D links to the total number of D2D links as a result of the pre-matching algorithm. As we can see from Fig. 4, the PMFR reduces from 12% to 7.8% with users increasing from 10 to 70. Based on the proposed one-to-one constraint matching algorithm, more CUEs increase the

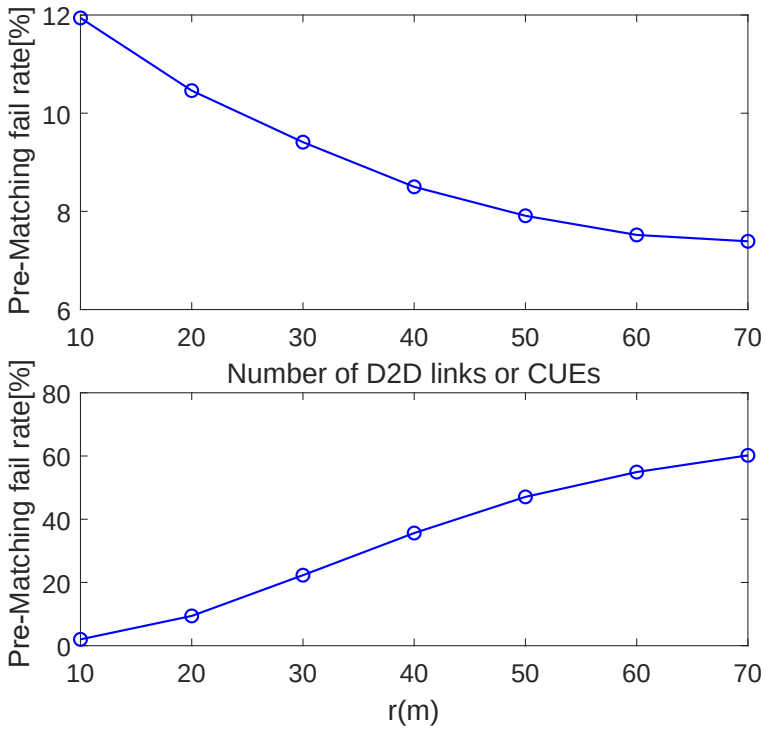

Fig. 3 PMFR versus the number of D2D links (or CUEs) and D2D communication distance.

preference list elements for each D2D link. Therefore, each D2D link has more CUEs to be matched with, which reduces the PMFR. Furthermore, the PMFR increases sharply from 2% to 61% with larger D2D communication distance range from 10m to 70m. When the D2D communication range increases, D2D transmitters need to improve their transmission power to meet the EH constraints, once the required transmission power exceeds P_{max}, such D2D links cannot perform SWIPT which increases the number of Non-EH D2D links, and we have higher PMFR. This also indicates that the PMFR is much sensitive to the D2D communication distance due to the large pathloss and rayleigh fading.

6.3 Convergence of Algorithm 3

Fig. 4 shows the EE per link versus the iteration step for different values of three individual D2D links. The EE of these three links converges very quickly to a unique value at 3rd step, and we find that the EE always converges at 3rd or 4th step for all other D2D links. It proves that

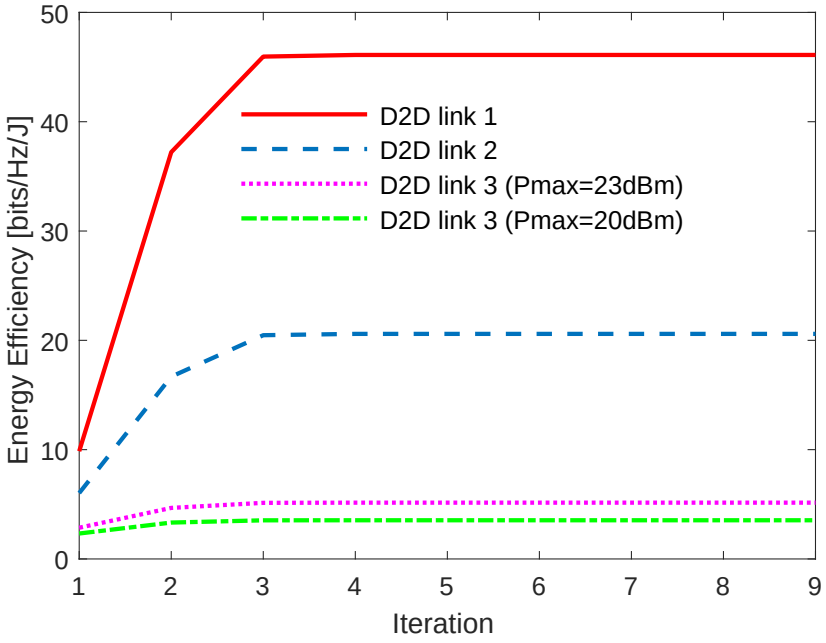

Fig. 4 Convergence of Algorithm 3.

this iterative algorithm is very efficient for solving the optimization problem. Also, different D2D links have different optimal EE based on the channel condition. By observing the EE of D2D link 3 with different maximum D2D transmission power limitation, the EE of D2D link 3 increases with higher maximum transmission power. Since the optimal value of P_i^D of some D2D links exceeds P_{max} , if we allow higher P_{max}, such D2D links can achieve higher EE.

6.4 Sum EE

In this subsection, we compare the sum EE of all D2D links versus the number of D2D links or CUEs, and D2D communication range for different algorithms. In Fig. 5 and Fig. 6, the "optimal solution" is obtained through exhaust search, and the stable matching based resource allocation algorithm of [11] (which does not consider the EE of non-EH D2D links or the optimization of power splitting ratio) is included in comparison with our proposed algorithms under the system model as described from Section 2 to 4. The piecewise linear EH model baseline is obtained by substituting the optimal P_i^D and λ_i^e under the linear EH model into the piecewise linear EH model. Two heuristic algorithms including constraint matching with

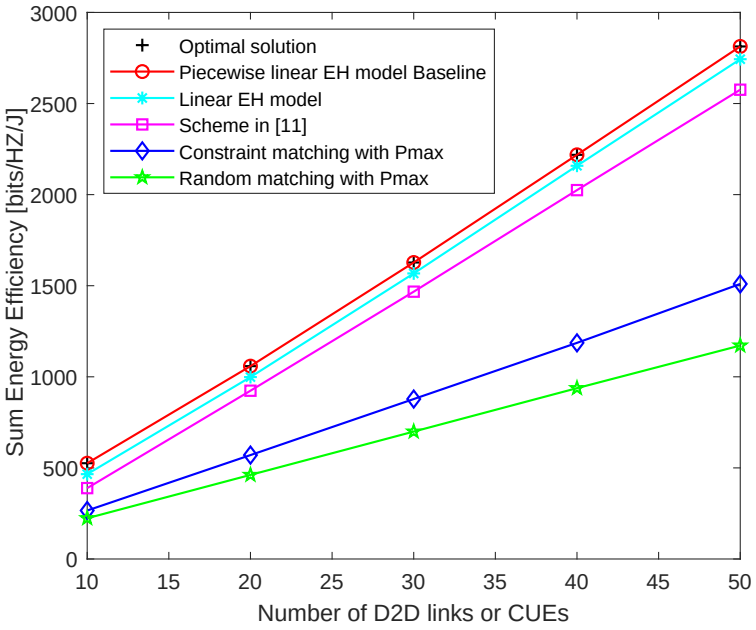

Fig. 5 Sum EE versus the number of D2D links or CUEs ($r = 20m$).

P_{max} and random matching with P_{max} are also proposed to make comparison with our proposed algorithms in EE performance. We do not consider random power allocation in this paper since the required transmission power may exceed the maximum allowed power when the channel condition is bad. If we assume random power allocation, many D2D links will not realize SWIPT which will definitely degrade the EE performance.

Fig. 5 shows the sum EE of all D2D links versus the number of D2D links or CUEs for different algorithms. As more users contribute more EE, for a fixed number of available RBs, the EE increases significantly with more D2D links and lower PMFR in Fig. 3. We can find that our proposed algorithms based on the piecewise linear EH model achieve the highest EE compared with other cases. Also, the gap between the optimal solution and piecewise linear EH model can be definitely ignored. The difference between the EE performance of piecewise linear EH model and baseline indicates that the linear EH model leads to resource allocation mismatches and suffers from EE performance degradation in the piecewise linear EH model. By observing the increasing gap between piecewise linear EH model and [11], we can find that more CUEs and our proposed constraint stable matching makes it much more possible for D2D

links to be matched as SWIPT enabled D2D links and provides more EE. In Fig. 5, the sum-EE improvement of our proposed algorithms is mainly brought by the joint optimization of the D2D transmission power and the power splitting ratio of D2D receivers. We note that the sum EE gap between [11] and our proposed algorithms is not large. This is because the considered D2D communication distance (i.e., 20 m) is short, and the resultant PMFR of our proposed algorithm is low, thus the number of SWIPT enabled D2D links in our proposed system is close to that in [11].

For the constraint matching with P_{max} and random matching with P_{max} algorithms, the power consumption issues have been totally ignored and they focus on improving the throughput of D2D links to increase EE, but this improvement cannot compensate for the loss of EE due to higher energy consumption. By the way, the random matching with maximum power algorithm shows the worst EE performance, this is easy to understand that D2D links can achieve higher EE when they find better CUEs to be their partners. In this paper, we assume that each D2D link shares a resource Block with a CUE, and the number of CUEs and resource blocks is the same. Thus, the number of D2D links cannot exceed the number of resource blocks and is assumed as the same as the number of CUEs in the simulations. The sum EE will increase with the number of D2D links until all the resource blocks are allocated.

Fig. 6 shows the sum EE of D2D links versus D2D communication range r for different algorithms. Our proposed algorithms based on the piecewise linear EH model also achieve the highest EE compared with other cases. The difference between the piecewise linear EH model and the baseline also proves that the linear EH model causes resource allocation mismatches and EE performance degradation. With the increasing of D2D communication range and much lower PMFR in Fig. 3, the EE decreases sharply for all the algorithms while our proposed algorithms based on the piecewise linear EH model still shows the best EE performance, and random matching with maximum power algorithm is still the worst case. The reason for such reduction is that longer D2D communication distance requires D2D transmitter to improve the transmission power for meeting C3 and C5, then much more energy consumption is caused. Also, the throughput of D2D links reduces due to higher pathloss. Therefore, the EE decreases with longer D2D communication distance.

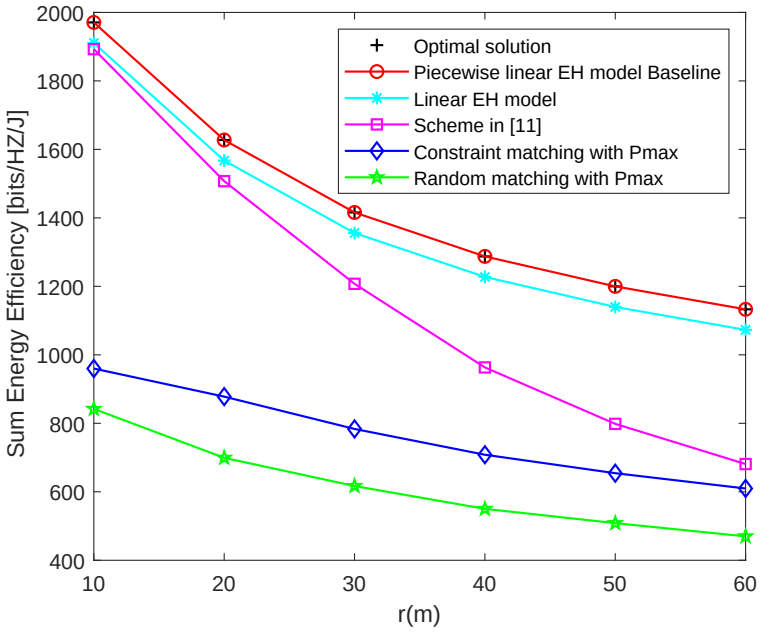

Fig. 6 Sum EE versus D2D communication distance ($N = M = 30$).

Comparing the EE performance in [11] with piecewise linear EH model, when the distance is small, e.g., below 20m, the EE performance is quite close because the PMFR is very low with short distance, D2D links can always find their partners even we consider the practical energy harvesting model. However, there still exists small difference due to the joint optimization of D2D transmission power and power splitting ratio. When the distance becomes larger, more D2D links will fail to communicate in [11] due to high PMFR, which results in significantly degradation of EE, but it is still higher than another two heuristic algorithms within 60m. When the distance exceeds 60m, the EE obtained through the scheme in [11] will be lower that the heuristic algorithms due to huge reduction of the number of SWIPT enabled D2D links. In Fig. 6, as the D2D communication distance increases, leading to a higher PMFR, the sum-EE gain of our proposed algorithm over the algorithm in [11] increases significantly. This gain is achieved by our proposed pre-matching and constraint stable matching algorithms in conjunction with the joint optimisation of the D2D transmission power and the power splitting ratio, especially when the D2D communication distance is long. Furthermore, we find that the EE performance of the two heuristic algorithms are relatively stable, this is because that

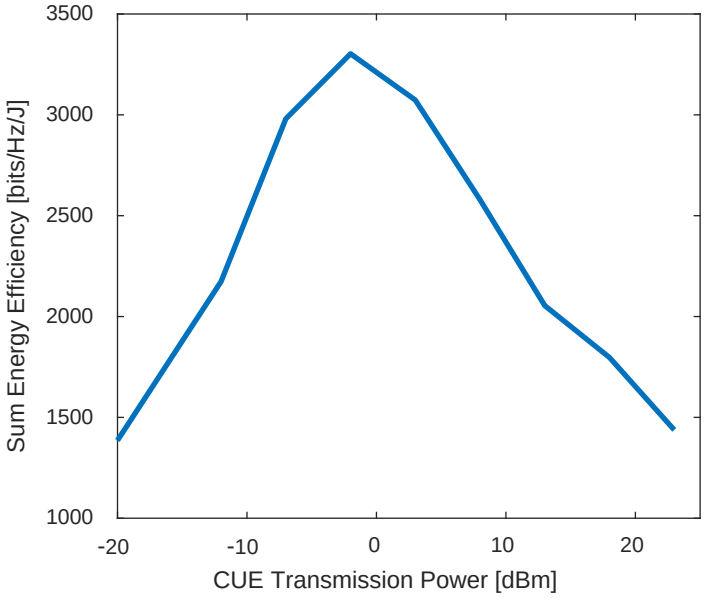

Fig. 7 Sum EE versus CUE transmission power ($N = M = 30$, $r = 25$m).

maximum D2D transmission power is already assumed in these two algorithms, total energy consumption remains unchanged and lower throughput is the main reason for the reduction of EE performance. Comparing these two heuristic algorithms, constraint stable matching still shows better EE performance.

Fig. 7 plots the sum EE of D2D links in our proposed system versus the CUE transmission power. We can see that the sum EE of D2D links first increases with the CUE transmission power. This is because a higher CUE transmission power can provide more energy for D2D receivers to harvest and make it more likely for the CUE to meet the QoS requirement, resulting in a higher probability for it to be matched with a D2D link. When the CUE transmission power increases beyond a certain value (around -2dBm in Fig. 7), the sum EE of D2D links starts to decrease. This is because the EE improvement brought by the higher harvested energy cannot compensate for the loss of EE caused by the increased interference power from co-channel CUEs.

7 Conclusion

In this paper, we have maximized the sum EE of all D2D links by optimizing the allocation of spectrum resource and transmission power in SWIPT enabled D2D underlaid cellular networks based on a piecewise linear EH model. Specifically, we firstly propose a pre-matching algorithm to divide D2D links into a SWIPT enable group and a non-EH group considering the EH circuit sensitivity and D2D transmission rate requirements. We then propose a one-to-one constraint stable matching algorithm to maximize the sum EE of SWIPT enabled D2D links, where the preference lists of CUEs and SWIPT enabled D2D links are built based on the results of the joint optimizations of the transmission power and power splitting ratio that maximize the EE of each SWIPT enabled D2D link. The sum EE of the non-EH D2D links is maximized following a similar approach. Simulation results show that the sum EE is much higher with short D2D communication distance and more users, and our proposed algorithms achieve a much higher sum EE of D2D links than the existing work. In our future work, we will study the joint optimization of CUE transmission power, D2D transmission power and the power splitting ratio to maximize the sum EE.

Appendix A

Proof of Proposition 1

In order to find the convexity of the optimization problem (29), we first derive the second-order derivative of Lagrange function $L(P_i^D, \lambda_i^e, \alpha, \beta, \gamma, \delta, \varepsilon)$ with respect to λ_i^e as shown below. For simplicity, we denote this Lagrange function as L, P_i^D is regarded as a fixed value.

$$\begin{aligned}\frac{\partial L^2}{\partial {\lambda_i^e}^2} = &\frac{-P_i^D h_i^D N_1 log_2^e V((P_i^D h_i^D + V)(1-\lambda_i^e)+N_1)}{(V(1-\lambda_e^i)+N_1)^2((P_i^D h_i^D + V)(1-\lambda_i^e)+N_1)^2} \\ &+ \frac{-P_i^D h_i^D N_1 log_2^e (V(1-\lambda_i^e)+N_1)(P_i^D h_i^D + V)}{(V(1-\lambda_i^e)+N_1)^2((P_i^D h_i^D + V)(1-\lambda_i^e)+N_1)^2} < 0,\end{aligned} \tag{A.1}$$

where $V = P_k^C h_{k,i} + N_0$, all the variables and constants in (A.1) is greater than 0, so the optimization problem is convex with respect to λ_i^e when we fix P_i^D.

Then we fix λ_i^e and derive the second-order derivative of L with respect to P_i^D as

$$\begin{aligned}\frac{\partial L^2}{\partial {P_i^D}^2} = & \frac{-(1+C)h_{i,D}^2 log_2^e}{(P_i^D h_i^D + P_{k,C} h_{k,i} + N_0 + \frac{N_1}{1-\lambda_i^e})^2} \\ & - \frac{(P_k^C h_k^C h_i^B log_2^e)W}{U(P_i^D h_i^B + N_0 + N_1 + P_k^C h_k^C)^2} < 0,\end{aligned} \tag{A.2}$$

where $U = (P_i^D h_i^B + N_0 + N_1)^2$, $W = [(2P_i^D 2h_i^B + 2N_0 + 2N_1)h_i^B + P_k^C h_k^C h_i^B]$, all the variables and constants in (A.2) is greater than 0, so the optimization problem is convex with respect to P_i^D when we fix λ_i^e. Combing (A.1) and (A.2), Proposition 1 is proven.

Appendix B

Proof of Theorem 2

We first let the first-order derivation of L with respect to λ_i^e be 0, which is formulated in (16). Then we transform (16) into a standard quadratic equation as

$$a_1 {\lambda_i^e}^2 + a_2 \lambda_i^e + a_3 = 0, \tag{B.1}$$

Then we obtain the solution of (B.1) based on the two cases as
Case i. If $a_2^2 - 4a_1a_3 = 0$, there exist two equal real roots and we obtain

$$\lambda_e^{i*} = \frac{-a_2 + \sqrt{a_2^2 - 4a_1a_3}}{2a_1} = \frac{-a_2 - \sqrt{a_2^2 - 4a_1a_3}}{2a_1}, \tag{B.2}$$

Case ii. If $a_2^2 - 4a_1a_3 > 0$, there exist two real roots and we obtain

$$\lambda_e^{i*} = \frac{-a_2 \pm \sqrt{a_2^2 - 4a_1a_3}}{2a_1}, \tag{B.3}$$

Combining Case i and Case ii, Theorem 2 is proven.

Appendix C

Proof of Theorem 3

We first let the first-order derivation of L with respect to $P_{i,D}$ be 0, which is formulated in (18). Then we transform (18) into a standard cubic equation as

$$b_1 {P_i^D}^3 + b_2 {P_i^D}^2 + b_3 P_i^D + b_4 = 0, \tag{C.1}$$

According to [49], we can calculate the solution of (C.1) based on three cases as

Case i. If $y_N^2 > g^2$, there exists a real root and we obtain

$$P_{i,D}{}^* = X_N + \sqrt[3]{\frac{-y_N + \sqrt{y_N^2 - g^2}}{2b_1}} + \sqrt[3]{\frac{-y_N - \sqrt{y_N^2 - g^2}}{2b_1}}, \tag{C.2}$$

Case ii. If $y_N^2 = g^2$, there exist two real roots and we obtain

$$P_i^{D*} = X_N - \theta, X_N + 2\theta, \tag{C.3}$$

Case iii. If $y_N^2 < g^2$, there exist three roots and we obtain

$$P_i^{D*} = X_N + 2\theta \cos(\phi - \frac{2\pi n}{3}), \quad [n = 0, 1, 2]. \tag{C.4}$$

Combining Case i, Case ii and Case iii, Theorem 3 is proven.

Appendix D

EE Maximization for Non-EH D2D Links

Similar to the optimization process of SWIPT enabled D2D links, we first formulate the EE optimization problem for each non-EH D2D links as

$$\max_{\{P_i^D, i \in Inf^D\}} EE_i^D = \frac{\log_2\left(1 + \frac{P_i^D h_i^D}{P_k^C h_{k,i} + N_0 + N_1}\right)}{P_i^D + 2\mathrm{P_{cir}}}. \tag{D.1}$$

Subject to

$$0 < P_i^D \leq P_{max}, \tag{D.2}$$

$$T_i^D \geq T_{min}^D. \tag{D.3}$$

Then we employ the same nonlinear fractional programming and Lagrange dual decomposition to transform the problem in (D.1) into a similar Lagrange dual optimization problem which is obtained by

$$\begin{aligned} \min_{\{\alpha',\beta',\gamma'\geq 0\}} \quad & \max_{\{P_i^D, i\in Inf^D\}} L'(P_i^D, \alpha', \beta') \\ & = T_i^D - Q_i^{D*} EC_i^D - \alpha'(P_i^D - \mathrm{P_{max}}) + \beta'(T_i^D - \mathrm{T_{min}^D}), \end{aligned} \tag{D.4}$$

where α' and β' are the Lagrange multipliers associated with (D.2)−(D.3), respectively. It is obvious to find that the optimization problem in (D.1) is convex with respect to $P_{i,D}$, we can easily obtain the expression of the optimal $P_{i,D}$ by using KKT conditions as

$$P_i^{D*} = \left\{ \frac{(1+\beta')\log_2^{\mathrm{e}}}{\alpha' + Q_i^{D*}} - \frac{P_k^C h_{k,i} + N_0 + N_1}{h_i^D} \right\}^+, \tag{D.5}$$

The optimal P_i^D can be achieved easily by iterating (D.5) and updating the Lagrange multipliers until the EE of D2D link i converges to an unique value.

After the iteration, we employ a simpler one-to-one stable matching among the non-EH D2D links and remaining CUEs in Φ^R. The preference lists establishment standards are the same for both non-EH D2D links and remaining CUEs, and the matching process is still the same as we introduced above except the condition in line 11 of Algorithm 4. We do not consider the constraint in line 12 of Algorithm 4 because the requirements for non-EH D2D links are easy to meet and the preference lists of such D2D links are always full, on the other words, non-EH D2D links can always match with any of the remaining CUEs while guaranteeing the throughput requirement of the matched CUE. The sum EE of non-EH D2D links can be maximized through this simple stable matching algorithm.

References

[1] K. Doppler, C. B. Ribeiro and J. Kneckt, “Advances in D2D communications: energy efficient service and device discovery radio," in *Proc. 2011 2nd International Conference on Wireless Communication, Vehicular Technology, Information Theory and Aerospace & Electronic Systems Technology (Wireless VITAE)*, Chennai, 2011, pp. 1-6.

[2] R. Q. Hu and Y. Qian, “An energy efficient and spectrum efficient wireless heterogeneous network framework for 5G systems," *IEEE Communications Magazine*, vol. 52, no. 5, pp. 94-101, May. 2014.

[3] Z. Chang, T. Ristaniemi and Z. Niu, “Radio Resource Allocation for Collaborative OFDMA Relay Networks with Imperfect Channel State Information," *IEEE Transactions on Wireless Communications*, vol. 13, no. 5, pp. 2824-2835, May. 2014.

[4] Y. Cai, Y. Ni, J. Zhang, S. Zhao and H. Zhu, “Energy efficiency and spectrum efficiency in underlay device-to-device communications enabled cellular networks," *China Communications*, vol. 16, no. 4, pp. 16-34, Apr. 2019.

[5] X. Liu and N. Ansari, “Green relay assisted D2D communications with dual batteries in heterogeneous cellular networks for IoT," *IEEE Internet of Things Journal*, vol. 4, no. 5, pp. 1707-1715, Oct. 2017.

[6] Y. Li, K. Chi, H. Chen, Z. Wang and Y. Zhu, "Narrowband Internet of things systems with opportunistic D2D communication," *IEEE Internet of Things Journal*, vol. 5, no. 3, pp. 1474-1484, Jun. 2018.

[7] L. Chettri and R. Bera, “A comprehensive survey on Internet of Things (IoT) toward 5G wireless systems," *IEEE Internet of Things Journal*, vol. 7, no. 1, pp. 16-32, Jan. 2020.

[8] H. Tang and Z. Ding, “Mixed mode transmission and resource allocation for D2D communication," *IEEE Transactions on Wireless Communications*, vol. 15, no. 1, pp. 162-175, Jan. 2016.

[9] R. Yin, C. Zhong, G. Yu, Z. Zhang, K. K. Wong and X. Chen, “Joint spectrum and power allocation for D2D communications underlaying cellular networks," *IEEE Transactions on Vehicular Technology*, vol. 65, no. 4, pp. 2182-2195, Apr. 2016.

[10] H. H. Esmat, M. M. Elmesalawy and I. I. Ibrahim, “Adaptive resource sharing algorithm for device-to-device communications underlaying cellular networks," *IEEE Communications Letters*, vol. 20, no. 3, pp. 530-533, Mar. 2016.

[11] Z. Zhou, C. Gao, C. Xu, T. Chen, D. Zhang and S. Mumtaz, “Energy-efficient stable matching for resource allocation in energy harvesting-based device-to-device communications," *IEEE Access*, vol. 5, pp. 15184-15196, 2017.

[12] H. Liu, K. J. Kim, K. S. Kwak and H. Vincent Poor, “Power splitting-based SWIPT with decode-and-forward full-duplex relaying," *IEEE Transactions on Wireless Communications*, vol. 15, no. 11, pp. 7561-7577, Nov. 2016.

[13] Y. Xu et al., “Joint beamforming and power-splitting control in downlink cooperative SWIPT NOMA systems," *IEEE Transactions on Signal Processing*, vol. 65, no. 18, pp. 4874-4886, Sept.15, 2017.

[14] D. K. Verma, R. Y. Chang and F. Chien, “Energy-assisted decode-and-forward for energy harvesting cooperative cognitive networks," *IEEE Transactions on Cognitive Communications and Networking*, vol. 3, no. 3, pp. 328-342, Sept. 2017.

[15] J. Tang, A. Shojaeifard, D. K. C. So, K. Wong and N. Zhao, “Energy efficiency optimization for CoMP-SWIPT heterogeneous networks," *IEEE Transactions on Communications*, vol. 66, no. 12, pp. 6368-6383, Dec. 2018.

[16] Y. Xu, G. Li, Y. Yang, M. Liu and G. Gui, “Robust resource allocation and power splitting in SWIPT enabled heterogeneous networks: a robust minimax approach," *IEEE Internet of Things Journal*, vol. 6, no. 6, pp. 10799-10811, Dec. 2019.

[17] O. B. Akan, O. Cetinkaya, C. Koca and M. Ozger, “Internet of hybrid energy harvesting things," *IEEE Internet of Things Journal*, vol. 5, no. 2, pp. 736-746, Apr. 2018.

[18] F. Deng, X. Yue, X. Fan, S. Guan, Y. Xu and J. Chen, “Multisource energy harvesting system for a wireless sensor network node in the field environment," *IEEE Internet of Things Journal*, vol. 6, no. 1, pp. 918-927, Feb. 2019.

[19] F. Deng, H. Qiu, J. Chen, L. Wang and B. Wang, “Wearable thermoelectric power generators combined with flexible super capacitor for low-power human diagnosis devices," *IEEE Transactions on Industrial Electronics*, vol. 64, no. 2, pp. 1477-1485, Feb. 2017.

[20] Z. Kuang, G. Liu, G. Li and X. Deng, “Energy efficient resource allocation algorithm in energy harvesting-based D2D heterogeneous networks," *IEEE Internet of Things Journal*, vol. 6, no. 1, pp. 557-567, Feb. 2019.

[21] A. H. Sakr and E. Hossain, “Cognitive and energy harvesting-based D2D communication in cellular networks: stochastic geometry modeling and analysis," *IEEE Transactions on Communications*, vol. 63, no. 5, pp. 1867-1880, May. 2015.

[22] Y. Chen, K. T. Sabnis and R. A. Abd-Alhameed, “New formula for conversion efficiency of RF EH and its wireless applications," *IEEE Transactions on Vehicular Technology*, vol. 65, no. 11, pp. 9410-9414, Nov. 2016.

[23] Y. Huo, X. Dong, T. Lu, W. Xu and M. Yuen, “Distributed and multilayer UAV networks for next-generation wireless communication and power transfer: a feasibility study," *IEEE Internet of Things Journal*, vol. 6, no. 4, pp. 7103-7115, Aug. 2019.

[24] M. Zhao, Q. Shi and M. Zhao, “Efficiency maximization for UAV-enabled mobile relaying systems with laser charging," *IEEE Transactions on Wireless Communications,* doi: 10.1109/TWC.2020.2971987.

[25] J. Huang, C. Xing and C. Wang, “Simultaneous wireless information and power transfer: Technologies, applications, and research challenges," *IEEE Communications Magazine*, vol. 55, no. 11, pp. 26-32, Sept. 2017.

[26] R. I. Ansari, S. A. Hassan and C. Chrysostomou, “A SWIPT-based device-to-device cooperative network," in *Proc. 2017 24th International Conference on Telecommunications (ICT)*, Limassol, 2017, pp. 1-5.

[27] D. Lim, J. Kang, C. Chun and H. Kim, “Joint transmit power and time-switching control for device-to-device communications in SWIPT cellular networks," *IEEE Communications Letters*, vol. 23, no. 2, pp. 322-325, Feb. 2019.

[28] D. Lim, J. Kang and H. Kim, “Adaptive power control for D2D communications in downlink SWIPT networks with partial CSI," *IEEE Wireless Communications Letters*, vol. 8, no. 5, pp. 1333-1336, Oct. 2019.

[29] L. Shi, Y. Ye, R. Q. Hu and H. Zhang, “Energy efficiency maximization for SWIPT enabled two-way DF relaying," *IEEE Signal Processing Letters*, vol. 26, no. 5, pp. 755-759, May. 2019.

[30] G. Lu, L. Shi and Y. Ye, “Maximum throughput of TS/PS scheme in an AF relaying network with non-linear energy harvester," *IEEE Access*, vol. 6, pp. 26617-26625, 2018.

[31] P. Sun, K. G. Shin, H. Zhang and L. He, “Transmit power control for D2D-underlaid cellular networks based on statistical features," *IEEE Transactions on Vehicular Technology*, vol. 66, no. 5, pp. 4110-4119, May. 2017.

[32] D. Burghal and A. F. Molisch, “Efficient channel state information acquisition for device-to-device networks," *IEEE Transactions on Wireless Communications*, vol. 15, no. 2, pp. 965-979, Feb. 2016.

[33] H. H. Yang, J. Lee and T. Q. S. Quek, “Heterogeneous Cellular Network With Energy Harvesting-Based D2D Communication," *IEEE Transactions on Wireless Communications*, vol. 15, no. 2, pp. 1406-1419, Feb. 2016.

[34] J. Hu, W. Heng, X. Li and J. Wu, “Energy-efficient resource reuse scheme for D2D communications underlaying cellular networks," *IEEE Communications Letters*, vol. 21, no. 9, pp. 2097-2100, Sept. 2017.

[35] S. Dominic and L. Jacob, “Distributed resource allocation for D2D communications underlaying cellular networks in time-varying environment," *IEEE Communications Letters*, vol. 22, no. 2, pp. 388-391, Feb. 2018.

[36] M. Robat Mili, P. Tehrani and M. Bennis, “Energy-efficient power allocation in OFDMA D2D communication by multi objective optimization," *IEEE Wireless Communications Letters*, vol. 5, no. 6, pp. 668-671, Dec. 2016.

[37] A. Abrardo and M. Moretti, “Distributed power allocation for D2D communications underlaying/overlaying OFDMA cellular networks," *IEEE Transactions on Wireless Communications*, vol. 16, no. 3, pp. 1466-1479, Mar. 2017.

[38] Y. Yuan, T. Yang, H. Feng and B. Hu, “An iterative matching-stackelberg game model for channel-power allocation in D2D underlaid cellular networks," *IEEE Transactions on Wireless Communications*, vol. 17, no. 11, pp. 7456-7471, Nov. 2018.

[39] K. Xiong, Y. Zhang, Y. Chen and X. Di, “Power splitting based SWIPT in network-coded two-way networks with data rate fairness: an information-theoretic perspective," *China Communications*, vol. 13, no. 12, pp. 107-119, Dec. 2016.

[40] L. Shi, L. Zhao, K. Liang, X. Chu, G. Wu, and H. H. Chen, “Profit maximization in wireless powered communications with improved non-linear energy conversion and storage efficiencies," in *Proc. IEEE International Conference on Communications.*, May. 2017, pp. 1–6.

[41] E. Boshkovska, D. W. K. Ng, N. Zlatanov, A. Koelpin and R. Schober, “Robust Resource Allocation for MIMO Wireless Powered Communication Networks Based on a Non-Linear EH Model,”*IEEE Transactions on Communications*, vol. 65, no. 5, pp. 1984-1999, May 2017, doi: 10.1109/TCOMM.2017.2664860.

[42] Y. Chen, N. Zhao and M. Alouini, “Wireless Energy Harvesting Using Signals From Multiple Fading Channels”, *IEEE Transactions on Communications*, vol. 65, no. 11, pp. 5027-5039, Nov. 2017, doi: 10.1109/TCOMM.2017.2734665.

[43] E. Boshkovska, D. W. K. Ng, N. Zlatanov, and R. Schober, “Practical non-linear energy harvesting model and resource allocation for SWIPT systems," *IEEE Communications Letters.*, vol. 19, no. 12, pp. 2082–2085, Dec. 2015.

[44] W. Dinkelbach, “On nonlinear fractional programming,” *Management Science.*, vol. 13, no. 7, pp. 492-498, Mar. 1967.

[45] D. T. Ngo, S. Khakurel, and T. Le-Ngoc, “Joint subchannel assignment and power allocation for OFDMA femtocell networks,” *IEEE Transactions on Wireless Communications.*, vol. 13, no. 1, pp. 342–355, Jan. 2014.

[46] Gale, D.; Shapley, L. S. (1962). “College admissions and the stability of marriage," *American Mathematical Monthly*. 69: 9–14.

[47] H. Zhang, C. Jiang, N. C. Beaulieu, X. Chu, X. Wen and M. Tao, “Resource allocation in spectrum-sharing OFDMA femtocells with heterogeneous services," *IEEE Transactions on Communications*, vol. 62, no. 7, pp. 2366-2377, Jul. 2014.

[48] K. Haneda et al., “Indoor 5G 3GPP-like channel models for office and shopping mall environments," in *Proc. 2016 IEEE International Conference on Communications Workshops (ICC)*, Kuala Lumpur, 2016, pp. 694-699.

[49] Y. Ye, R. Q. Hu, G. Lu and L. Shi, “Enhance latency-constrained computation in MEC networks using uplink NOMA," *IEEE Transactions on Communications*, doi: 10.1109/TCOMM.2020.2969666.

Chapter 5

Paper II

Max-Min Energy-Efficient Resource Allocation for Wireless Powered Backscatter Networks

Haohang Yang, Yinghui Ye and Xiaoli Chu

Published in *IEEE Wireless Communications Letters, Volume: 9, Issue: 5, May 2020, Page(s): 688 - 692, Date of Publication: 13 January 2020.*

Max-Min Energy-Efficient Resource Allocation for Wireless Powered Backscatter Networks

Haohang Yang[1], Yinghui Ye[2] and Xiaoli Chu[1]

[1] Department of Electronic and Electrical Engineering, the University of Sheffield, Sheffield, S1 4ET, United Kingdom

[2] Shaanxi Key Laboratory of Information Communication Network and Security, Xi'an University of Posts & Telecommunications, China

Abstract

In this letter, we present the first attempt to solve an energy efficiency (EE) based max-min fairness problem for a wireless powered backscatter network where a power beacon (PB), which is a dedicated radio frequency (RF) power resource, and multiple backscatter devices work in the same frequency band. Each backscatter transmitter harvests energy from the signal transmitted by the PB, modulates its own information on the received signal, and backscatters the modulated signal to its associated receiver. We propose to ensure max-min fairness among the backscatter links by jointly optimizing the PB transmission power and the backscatter reflection coefficients. For analytical tractability, we solve the optimization problem for the case of two co-channel backscatter links by employing Lagrange dual decomposition when it is convex, and analyzing the monotonicity of the constraints when it is non-convex. Based on the obtained closed-form expressions of the optimal PB transmission power and the optimal backscatter reflection coefficients, we propose an iterative algorithm for max-min EE resource allocation. Simulation results show that the proposed iterative algorithm converges very fast and achieves a much fairer EE performance among backscatter links than maximizing the system EE of the network.

1 Introduction

Wireless powered backscatter communication has been considered as a promising technology to prolong the network lifetime of Internet of Things (IoT) systems [1]. In recent years, throughput

maximization [2], signal detection [3] and hardware implementation [4] have been investigated for wireless powered backscatter communications, but the energy efficiency (EE) problem has not been sufficiently studied. The authors in [5] maximized the EE of a backscatter link by jointly optimizing the reflection coefficient and the power beacon (PB) transmission power. The EE maximization problem was studied for radio frequency (RF) powered cognitive backscatter communications [6]. However, both [5] and [6] considered only a single backscatter link and their results cannot be readily applied to multiple co-channel wireless powered backscatter links. Moreover, when multiple backscatter transmitters share the transmission power from a PB, it is necessary to ensure the fairness among the co-channel backscatter links.

In this letter, we consider a wireless powered backscatter network, where a PB and multiple backscatter links work in the same frequency band, and propose to maximize the minimum link EE among all the wireless powered backscatter links by jointly optimizing the PB transmission power and the backscatter reflection coefficients. The mutual interference between the multiple co-channel backscatter links and the interference from the PB to the backscatter receivers leads to complicated coupling effects between the backscatter reflection coefficients and the PB transmission power, resulting in a much higher complexity than that of EE maximization for one single backscatter link. The complexity of the max-min EE problem increases with the number of co-channel links, and allowing more backscatter links to access the same channel may cause severe co-channel interference and increase the system complexity, which should be avoided because backscatter circuitry design needs to be kept simple [1]. For analytical tractability, we solve the problem for the case of two co-channel backscatter links. At the end, we obtain closed-form expressions for the optimal PB transmission power and the backscatter reflection coefficients. More specifically, the max-min EE problem is decomposed into two sub-problems conditioned on the convexity of the objective function: one is a convex optimization problem, while the other is non-convex. The convex problem is solved by employing Lagrange dual decomposition and KKT conditions, and the non-convex problem is solved by exploiting the characteristics of the associated constraints. Considering the low complexity and low cost requirements of backscatter devices [1], based on the obtained optimal solution, we propose an iterative algorithm that allows each backscatter transmitter to independently make optimal

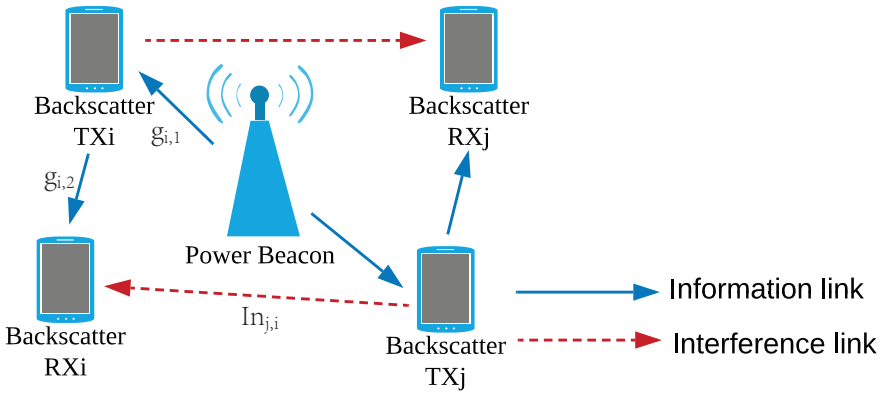

Fig. 1 Wireless powered backscatter networks.

resource allocation decisions that maximize their EE while guaranteeing the fairness among the backscatter links.

2 System model

As illustrated in Fig.1, we consider a wireless powered backscatter network[1] with a PB and M co-channel backscatter links, which are denoted by the set $\hat{D} = \{1, 2, \cdots, i, \cdots, M\}$. Backscatter link i consists of one backscatter transmitter i and one receiver i. Each node is equipped with a single antenna. We assume the availability of perfect channel state information (CSI) at each backscatter node [5]. In each time block T, the PB broadcasts a RF signal while each backscatter transmitter harvests energy from the received RF signal to support its circuit operation and modulates and reflects the received RF signal to carry its information to the associated receiver by properly setting a reflection coefficient.

[1]Note that different from the energy harvesting sensor or relay nodes in wireless powered communication networks (WPCN) or simultaneous wireless information and power transfer (SWIPT) networks that can set their own transmission power levels, the backscatter nodes directly modulate and reflect the incident RF signals transmitted by the PB. Furthermore, multiple variables including the PB transmission power and the reflection coefficients of co-channel backscatter links need to be jointly optimized in backscatter networks, while in WPCN or SWIPT networks, only the transmission power and the transmission time duration or power splitting ratio of sensor or relay nodes are optimized [7], [8].

In addition to the information carrying signal from backscatter transmitter i, receiver i also receives the co-channel interference from the other backscatter transmitters and the PB, and the received power at receiver i is given by $\sqrt{P_a g_{i,1} Z_i g_{i,2}} s(n) c_i(n) + \sqrt{P_a g_{i,3}} s(n) + \sum_{j=1, j\neq i}^{M} \sqrt{P_a g_{j,1} Z_j In_{j,i}} s(n) c_j(n) + N_0$, where P_a is the transmission power of the PB; $Z_i \in [0,1]$, is the reflection coefficient of backscatter transmitter i; N_0 represents the additive white Gaussian noise (AWGN) power; $s(n)$, $c(n)$ denote the signal transmitted and backscattered from the PB and backscatter transmitter i, respectively, and n is the index of the symbols; $g_{i,1}$ and $g_{i,2}$ denote the channel power gains from the PB to transmitter i and from backscatter transmitter i to receiver i, respectively; $In_{j,i}$ represents the channel power gain from backscatter transmitter j to receiver i, and $g_{i,3}$ denotes the channel power gain from the PB to receiver i. Since the PB serves as a RF energy source only, the transmitted signal from the PB $s(n)$ is predefined and is known by all the backscatter receivers, thus receiver i can remove the interference from the PB, i.e., $P_a g_{i,3}$ [5]. Accordingly, the SINR at receiver i is written as

$$\mathrm{SINR}_i = \frac{P_a g_{i,1} Z_i g_{i,2}}{N_0 + \sum_{j=1, j\neq i}^{M} P_a g_{j,1} Z_j In_{j,i}}. \tag{1}$$

The throughput[2] (bits/s) of backscatter link i is given by

$$R_i = T \log_2(1 + \mathrm{SINR}_i). \tag{2}$$

The energy harvested by backscatter transmitter i is

$$EH_i = P_a g_{i,1} (1 - Z_i) \eta T, \tag{3}$$

where $\eta \in [0,1]$ is the energy conversion efficiency[3], for simplicity, the time block T is normalized to one, and we ignore the energy harvested from the thermal noise since it is very small [2], [5]. The backscatter transmitters are batteryless and cannot store the harvested

[2] As the backscatter modulation order increases, the backscattered signals approximately follow a Gaussian distribution and hence we use Shannon expression to calculate the throughput [9]-[12].

[3] The main contribution of this chapter and Paper III, Paper IV do not focus on the EH model. Also, we can still use the non-linear EH models in these chapters and solve the same optimization problems formulated, we employ linear EH model for simplicity and less computational complexity.

energy. We assume that the energy harvested by transmitter i is used only for and is sufficient to support its circuit operation [5], i.e., $EH_i \geq PC_t$, where PC_t denotes the transmitter circuit power consumption and is assumed to be the same for all backscatter transmitters.

The power consumption for link i is composed of the RF transmission power P_a of the PB (which covers the backscatter transmitter circuit power consumption), the circuit power consumption at the PB and receiver i are denoted by PC_{pb} and PC_i, respectively. We assume that the circuit power consumption of each receiver is the same, and the total circuit power consumption of each backscatter link i is $PC_r = PC_{pb} + PC_i$. Thus, the EE of backscatter link i is given by

$$EE_i = \frac{R_i}{P_a + PC_r}. \tag{4}$$

3 Max-Min EE Resource Allocation

3.1 Problem Formulation

We propose to maximize the minimum link EE among all co-channel backscatter links in order to improve the EE of the backscatter network while guaranteeing fairness among co-channel backscatter links. Accordingly, the optimization problem is formulated as

$$\begin{aligned} \mathbf{P1}: \max_{\{P_a, Z_i\}} \quad & \min_{\{i \in \hat{D}\}} EE_i \\ \text{s.t.} \quad & \text{C1}: 0 < P_a \leq P_{\max}, \\ & \text{C2}: 0 \leq Z_i \leq 1, i \in \hat{D}, \\ & \text{C3}: R_i \geq R_{\min}, i \in \hat{D}, \\ & \text{C4}: EH_i \geq PC_t, i \in \hat{D}, \end{aligned} \tag{5}$$

where C1 sets the maximum allowed transmission power P_{max} for the PB transmission power P_a; C2 sets the range of backscatter reflection coefficients; C3 sets the minimum throughput requirement $R_{\min}$ for backscatter links; and C4 ensures that the harvested energy of a backscatter transmitter is sufficient to cover its circuit power consumption. **P1** is a non-convex fractional

optimization problem and is mathematically difficult to solve due to the coupling between variables P_a and Z_i in (1), (3), and (4).

From (1)−(4) we can see that EE_i increases with Z_i, while EH_i decreases with Z_i. Thus, the maximum EE_i is achieved when $EH_i = PC_t$. By solving $P_a g_{i,1}(1-Z_i)\eta = PC_t$ for Z_i, we have

$$Z_i = 1 - \frac{PC_t}{P_a g_{i,1}\eta}. \tag{6}$$

By substituting (6) into (5), **P1** reduces to an optimization problem with respect to P_a only, which can be further transformed into a more tractable form following Lemma 1.

Lemma 1 [13]: After substituting (6) into (5), the optimal solution to **P1** can be obtained if and only if $\max\limits_{\{P_a\}} \min\limits_{\{i\in\hat{D}\}} R_i - Q^*(P_a + PC_r) = \min\limits_{\{i\in\hat{D}\}} R_i^* - Q^*(P_a^* + PC_r) = 0$, where Q^* is the max-min EE, R_i^* and P_a^* are the optimal throughput of backscatter link i and the optimal PB transmission power, respectively.

Based on (6) and Lemma 1, **P1** is converted to

$$\begin{aligned} \mathbf{P2}: \max_{\{P_a\}} \min_{\{i\in\hat{D}\}} \quad & -Q^*(P_a + PC_r) + \log_2\left(1 + \frac{P_a g_{i,1} g_{i,2} - \frac{PC_t g_{i,2}}{\eta}}{P_a \sum_{j=1,j\neq i}^{M} g_{j,1} In_{j,i} - \sum_{j=1,j\neq i}^{M} \frac{PC_t In_{j,i}}{\eta} + N_0}\right) \\ & \text{s.t. C1, C5}: P_a \geq PC_t / g_{i,1}\eta, i \in \hat{D}, \\ & \text{C6}: \log_2\left(1 + \frac{P_a g_{i,1} g_{i,2} - \frac{PC_t g_{i,2}}{\eta}}{P_a \sum_{j=1,j\neq i}^{M} g_{j,1} In_{j,i} - \sum_{j=1,j\neq i}^{M} \frac{PC_t In_{j,i}}{\eta} + N_0}\right) \geq R_{\min}. \end{aligned} \tag{7}$$

By introducing a slack variable Y, **P2** can be expressed as

$$\begin{aligned} & \mathbf{P3}: \max_{\{P_a, Y\}} Y \\ & \text{s.t.} \quad \text{C1}, \text{C5}, \text{C6}, \\ & \text{C7}: \log_2\left(1 + \frac{P_a g_{i,1} g_{i,2} - \frac{PC_t g_{i,2}}{\eta}}{P_a \sum_{j=1,j\neq i}^{M} g_{j,1} In_{j,i} - \sum_{j=1,j\neq i}^{M} \frac{PC_t In_{j,i}}{\eta} + N_0}\right) - Q^*(P_a + PC_r) \geq Y, i \in \hat{D}. \end{aligned} \tag{8}$$

3.2 Convexity Analysis of P3

For notational simplicity, we rewrite C7 as

$$f_i(x) = \log_2\left(1+\frac{A_i x - B_i}{C_i x - D_i}\right) - Q^*(x+PC_r) - Y \geq 0, i \in \hat{D}, \tag{9}$$

where $x = P_a$, $A_i = g_{i,1}g_{i,2}$, $B_i = \frac{PC_t g_{i,2}}{\eta}$, $C_i = \sum_{j=1,j\neq i}^{M} g_{j,1} In_{j,i}$, $D_i = \sum_{j=1,j\neq i}^{M} \frac{PC_t In_{j,i}}{\eta} - N_0$, and $A_i, B_i, C_i \geq 0$.

Taking the first-order derivative of $f_i(x)$ with respect to x, $i \in \hat{D}$ we obtain

$$f_i'(x) = \frac{(B_iC_i - A_iD_i)\log_2 \mathrm{e}}{(C_ix - D_i + A_ix - B_i)(C_ix - D_i)} - Q^*. \tag{10}$$

The second-order derivative of $f_i(x)$ is obtained as

$$\begin{aligned} f_i''(x) = & \frac{-(B_iC_i - A_iD_i)\log_2 \mathrm{e}}{(C_ix - D_i + A_ix - B_i)(C_ix - D_i)} \\ & \times \frac{(C_i + A_i)(C_ix - D_i) + (C_ix - D_i + A_ix - B_i)C_i}{(C_ix - D_i + A_ix - B_i)(C_ix - D_i)}. \end{aligned} \tag{11}$$

Based on (6) and C2, $i \in \hat{D}$, we have $A_ix - B_i \geq 0$ and $C_ix - D_i \geq 0$. If $B_iC_i - A_iD_i > 0$, then $f_i''(x) < 0$ and **P3** is convex; otherwise, $f_i''(x) \geq 0$ and **P3** is non-convex. We will solve **P3** for these two cases, respectively. However, **P3** is still intractable mainly due to the complexity of C7, which increases with M. In the following, we will solve **P3** for the case of $M = 2$, i.e., when there are two co-channel backscatter links in the network.

3.3 Solution of Convex P3

When $B_iC_i - A_iD_i > 0$ for $i \in \{1,2\}$, **P3** is a convex problem with respect to P_a and Y. By employing Lagrange dual decomposition, we obtain

$$\begin{aligned} L(x,Y,\alpha,\beta_i,\theta_i,\phi_i) = {} & \alpha\left(P_{max}-x\right) + \sum_{i=1}^{2}\beta_i\left(x - \frac{PC_t}{g_{i,1}}\right) \\ & + \sum_{i=1}^{2}\theta_i\left[\log_2\left(1+\frac{A_ix-B_i}{C_ix-D_i}\right) - R_{\min}\right] + Y \\ & + \sum_{i=1}^{2}\phi_i\left[\log_2\left(1+\frac{A_ix-B_i}{C_ix-D_i}\right) - Q^*(x+PC_r) - Y\right], \end{aligned} \tag{12}$$

where $\alpha,\beta_i,\theta_i,\phi_i$ are the Lagrange multipliers associated with the constraints of **P3**.

To solve $\frac{\partial L(x,Y,\alpha,\beta_i,\theta_i,\phi_i)}{\partial x} = 0$, we rewrite it as

$$k_1x^4 + k_2x^3 + k_3x^2 + k_4x + k_5 = 0, \tag{13}$$

where $k_1 = Ja_1a_2, k_2 = -J(b_1a_2 + a_1b_2), k_3 = JC_1a_2 + Jb_1b_2 + Ja_1C_2 - Ea_2 - Fa_1, k_4 = Eb_2 + Fb_1 - JC_1b_2 - Jb_1C_2, k_5 = Jc_1c_2 - Ec_2 - Fc_1, a_1 = C_1^2 + A_1C_1, b_1 = 2C_1D_1 + B_1C_1 + A_1D_1, c_1 = B_1D_1 + D_1^2, a_2 = C_2^2 + A_2C_2, b_2 = 2C_2D_2 + B_2C_2 + A_2D_2, c_2 = B_2D_2 + D_2^2, E = (\theta_1+\phi_1)(B_1C_1 - A_1D_1), F = (\theta_2+\phi_2)(B_2C_2 - A_2D_2), J = (\alpha - (\beta_1+\beta_2) + 2Q^*)\ln 2$.

Then we obtain the four roots of (13) as [14]

$$x_{1,2} = \left[-\frac{k_2}{4k_1} - S \pm \frac{\sqrt{-4S^2 - 2p + \frac{q}{s}}}{2}\right]^+, \tag{14}$$

$$x_{3,4} = \left[-\frac{k_2}{4k_1} + S \pm \frac{\sqrt{-4S^2 - 2p - \frac{q}{s}}}{2}\right]^+, \tag{15}$$

where $[X]^+ = \max(0,X), p = \frac{8k_1k_3 - 3k_2^2}{8k_1^2}, q = \frac{k_2^3 - 4k_1k_2k_3 + 8k_1^2k_4}{8k_1^3}, S = \frac{1}{2}\sqrt{-\frac{2}{3}p + \frac{T + \frac{\Delta_0}{T}}{3k_1}}$, $T = \sqrt[3]{\frac{\Delta_1 + \sqrt{\Delta_1^2 - 4\Delta_0^3}}{2}}$, $\Delta_1 = 2k_3^3 - 9k_2k_3k_4 + 27k_2^2k5 + 27k_1k_4^2 - 72k_1k_3k_5$, and $\Delta_0 = k_3^2 - 3k_2k_4 + 12k_1k_5$.

For any given Y, the optimal value of P_a is given by

$$P_a^* = \max(x_1, x_2, x_3, x_4). \tag{16}$$

Substituting (16) into (8), we can calculate Y^* as

$$Y^* = \min_{\{i \in \hat{D}\}} \left(\log_2 \left(1 + \frac{A_i P_a^* - B_i}{C_i P_a^* - D_i} \right) - Q^* \left(P_a^* + PC_r \right) \right). \tag{17}$$

The Lagrange multipliers are updated by using the subgradient method [15].

3.4 Solution of Non-convex P3

If $B_i C_i - A_i D_i \leq 0$ for either $i \in \hat{D}$, then C7 is non-convex and **P3** cannot be solved using convex optimization methods. In the following, we analyze the monotonicity of C7 to solve **P3**. Based on (8), $B_i C_i - A_i D_i$, $i \in \{1,2\}$ can be written as

$$B_1 C_1 - A_1 D_1 = \frac{PC_t g_{1,2}}{\eta} In_{2,1}(g_{2,1} - g_{1,1}) + g_{1,1} g_{1,2} N_0, \tag{18}$$

$$B_2 C_2 - A_2 D_2 = \frac{PC_t g_{2,2}}{\eta} In_{1,2}(g_{1,1} - g_{2,1}) + g_{2,1} g_{2,2} N_0. \tag{19}$$

From (18) and (19), we can see that if $g_{2,1} - g_{1,1} > 0$, then $B_1 C_1 - A_1 D_1 > 0$ and $B_2 C_2 - A_2 D_2 \leq 0$, leading to $f_1''(x) < 0$ and $f_2''(x) \geq 0$; Otherwise, $B_1 C_1 - A_1 D_1 \leq 0$ and $B_2 C_2 - A_2 D_2 > 0$, leading to $f_1''(x) \geq 0$ and $f_2''(x) < 0$.

Without loss of generality, in the following, we assume $B_1 C_1 - A_1 D_1 \leq 0$, thus $f_1''(x) \geq 0$ and $f_2''(x) < 0$. Based on (9)−(11), we can see that $f_1(x)$ is a monotonically decreasing function of x and $f_2(x)$ is a concave function of x while meeting all the constraints of **P3**. The relationship between $f_1(x)$ and $f_2(x)$ can be analyzed by defining

$$h(x) = f_1(x) - f_2(x) = \log_2 \left(1 + \frac{A_1 x - B_1}{C_1 x - D_1} \right) - \log_2 \left(1 + \frac{A_2 x - B_2}{C_2 x - D_2} \right), \tag{20}$$

and calculating

$$h'(x) = \frac{(B_1C_1 - A_1D_1)\log_2 e}{(C_1x - D_1 + A_1x - B_1)(C_1x - D_1)} - \frac{(B_2C_2 - A_2D_2)\log_2 e}{(C_2x - D_2 + A_2x - B_2)(C_2x - D_2)}. \tag{21}$$

Since $B_1C_1 - A_1D_1 \leq 0$, we have $h'(x) \leq 0$, indicating that there is at most one intersection between $f_1(x)$ and $f_2(x)$.

Then we need to find the range of x. Denoting the feasible value range for x by $[x_{min}, x_{max}]$, based on C1, C5 and C6, we obtain that

$$x_{min} = \max\left(\frac{B_i - D_i(2^{R_{\min}} - 1)}{A_i - C_i(2^{R_{\min}} - 1)}, \frac{PC_t}{g_{i,1}\eta}\right), i \in \{1,2\}, \tag{22}$$

$$x_{max} = P_{\max}. \tag{23}$$

Based on the above analysis, we can solve non-convex **P3** under the following 2 conditions.

Condition 1. $h(x_{min})h(x_{max}) > 0$: $f_1(x)$ and $f_2(x)$ do not intersect, and the maximum value of Y is given by

$$Y^* = \min(\max_{\{x\}} f_1(x), \max_{\{x\}} f_2(x)). \tag{24}$$

Since $f_1(x)$ is a monotonically decreasing function of x, $\max\limits_{\{x\}} f_1(x) = f_1(x_{min})$, and $x_1^* = x_{min}$. Since $f_2(x)$ is a concave function, to obtain $x_2^* = \arg\max\limits_{\{x\}} f_2(x)$, we solve $f_2'(x) = 0$ for x and get

$$G = \frac{-u_2 \pm \sqrt{u_2^2 - 4u_1u_3}}{2u_1}, G \in [x_{min}, x_{max}], \tag{25}$$

where $u_1 = (C_2^2 + A_2C_2)$, $u_2 = -(2C_2D_2 + B_2C_2 + A_2D_2)$ and $u_3 = D_2^2 + B_2D_2 - \frac{\log_2 e(B_2C_2 - A_2D_2)}{Q^*}$. Then we have

$$x_2^* = \begin{cases} x_{max}, & G \geq x_{max}, \\ G, & x_{min} < G < x_{max}, \\ x_{min}, & G \leq x_{min}. \end{cases} \tag{26}$$

Therefore, the optimal value of x is given by

$$x^* = \arg\min_{x_1^*, x_2^*}(f_1(x_1^*), f_2(x_2^*)). \tag{27}$$

Condition 2. $h(x_{min})h(x_{max}) \leq 0$: $f_1(x)$ and $f_2(x)$ have one intersection, which can be further divided into the following three cases.

Case (i). If $f_2'(x_{min}) \leq 0$, then $f_2'(x) < 0, x \in [x_{min}, x_{max}]$. In this case, $f_1(x)$ and $f_2(x)$ are both monotonically decreasing functions of x, and we obtain

$$x^* = x_{min}. \tag{28}$$

Case (ii). If $f_2'(x_{max}) \geq 0$, then $f_2'(x) > 0, x \in [x_{min}, x_{max}]$. In this case, $f_2(x)$ is a monotonically increasing function of x, and the optimal x occurs at the intersection. Solving $f_1(x) = f_2(x)$ for x, we obtain

$$x^* = H = \frac{-n_2 \pm \sqrt{n_2^2 - 4n_1n_3}}{2n_1}, x \in [x_{min}, x_{max}], \tag{29}$$

where $n_1 = A_1C_2 - C_1A_2$, $n_2 = D_1A_2 + C_1B_2 - B_1C_2 - A_1D_2$, $n_3 = B_1D_2 - B_2D_1$, and H denotes the intersection value of x.

Case (iii). If $f_2'(x_{min}) > 0$ and $f_2'(x_{max}) < 0$, then $f_2(x)$ first increases and then decreases with x in $[x_{min}, x_{max}]$, and we obtain

$$P_a{}^* = \begin{cases} G, & f_1(x_{min}) > f_2(x_{min}) \ \& \ f_1(G) \geq f_2(G), \\ H, & f_1(x_{min}) > f_2(x_{min}) \ \& \ f_1(G) \leq f_2(G), \\ x_{min}, & f_1(x_{min}) \leq f_2(x_{min}). \end{cases} \tag{30}$$

Based on the obtained solutions to convex **P3** and non-convex **P3**, we propose an iterative algorithm in Algorithm 1 to solve **P3** and obtain the global optimal values of P_a^* and Z_i^*. In Algorithm 1, t is the index of iteration of the main loop; I is the predefined maximum allowed number of iteration of the main loop, and ψ is a very small value set to check whether the objective function in **P3** converges.

Algorithm 1: Iterative algorithm

Input: $\hat{D} = \{1,2\}$.

Output: P_a^*, Z_i^*.

Initialize: $Q^*(t) = Q^*(0), Y(t) = Y(0), I, \psi, t = 0$.

while $t < I$ **do**

  if $B_i C_i - A_i D_i > 0, i \in \hat{D}$ **then**

    for $n = 1$ to I_1 **do**

      for $u = 1$ to I_2 **do**

        We use $Q_u^*(t)$ and $Y_u(t)$ to obtain $P_{a,u}(t+1)$ by calculating (15).

        We use obtained $P_{a,u}(t+1)$ to calculate $Y_u(t+1)$ by calculating (16).

      end for

      $Q_u^*(t+1) = R_i[P_{a,u}(t+1)]/(P_{a,u}(t+1) + PC_r)$.

      We update Lagrange multipliers by using a sub-gradient method.

    end for

  else We obtain $Y(t+1)$ and $P_a(t+1)$ under Condition 1 or Condition 2.

    $Q^*(t+1) = R_i[P_a(t+1)]/(P_a(t+1) + PC_r)$.

  end if

  if $\left| \min_{\{i \in \hat{D}\}} R_i[P_a(t+1)] - Q^*(t+1)(P_a(t+1) + PC_r) \right| \leq \psi$ **then**

    $P_a^* = P_a(t+1)$, obtain Z_i^* using (6), obtain EE_1 and EE_2 using (4).

    Break

20: **end if**

21: $t = t + 1$.

22: **end while**

---

4 Simulation Results

In this section, we present the simulation results to evaluate the performance of our proposed max-min EE resource allocation scheme in comparison with the criterion of maximizing system EE (max-SEE) under the case of two co-channel backscatter links. We consider distance dependent pathloss as large scale fading, where the pathloss exponent is set as 2.5, and rayleigh fading as small scale fading which follows a unit mean exponential distribution. The transmission radius of PB is set as 30 m; the distance between a backscatter transmitter and its receiver is denoted as r, which is less than 15 m for all backscatter links. P_{max}=23 dBm, N_0=$-$114 dBm, $\eta = 0.6$, PC_t=0.1 mw, PC_r=110 mw, R_{min}=3 bits/Hz.

Fig. 2 shows the convergence of the iterative algorithm for three cases with different distance (r) between a backscatter transmitter and its receiver. We can see that the max-min EE converges in the $4th \sim 6th$ iteration, and a higher EE is obtained for a smaller r. It is because the throughput increases for a shorter communication distance, leading to a higher EE. Fig. 2 proves that our proposed iterative algorithm is efficient to converge fast.

In Fig. 3, we compare the EE under max-min fairness and max-SEE versus the channel power gain differences between $g_{i,1}$ and $g_{j,1}$. On the one hand, we can see that the max-SEE algorithm achieves a higher system EE than our proposed Algorithm 1. However, the EE gap between the best user and the worst user is too large, which is significantly reduced by ensuring max-min fairness. On the other hand, in the first case, the EE of the worst user under the max-SEE criterion improves 31.53% by employing max-min fairness; while in the second case, the EE of the worst user improves 25.55%. This indicates that the max-min fairness is less effective when the channel power gain difference between $g_{i,1}$ and $g_{j,1}$ becomes larger. This is

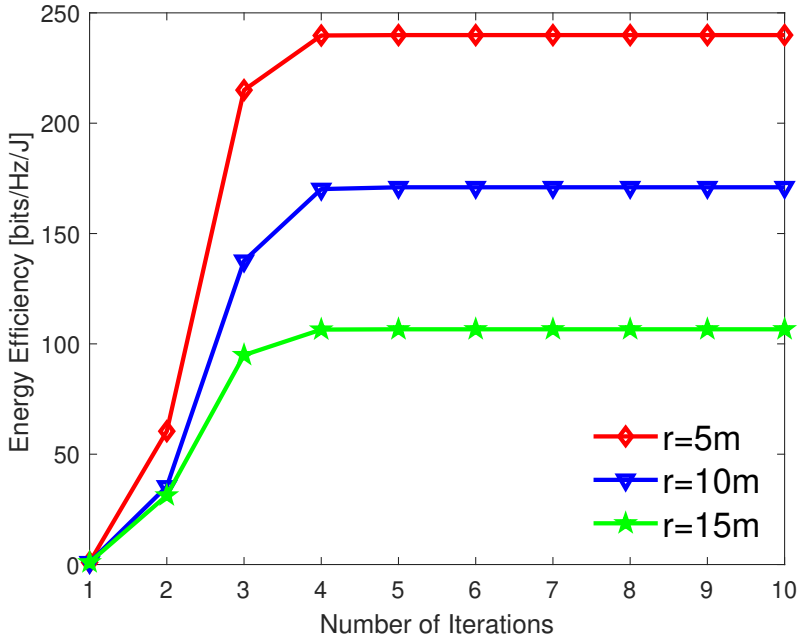

Fig. 2 Iterative algorithm for different value of r.

because when the channel power gain difference becomes larger, the EE difference between the best user and the worst user becomes larger so that it will be harder to achieve fairness. This also proves that the max-SEE algorithm tends to favour the best user.

Fig. 4 shows the EE versus the throughput requirement for backscatter links under the criterions of max-min fairness and max-SEE. A higher throughput requirement reduces the range of P_a, which may change the obtained optimal solution of P_a. Before the throughput requirement increases to 8 bits/Hz, based on the max-SEE, which tends to favour the best user, when the range of P_a reduces, the best user cannot obtain its optimal value of P_a which makes its EE lower. But the worst user forwards to its optimal value so that its EE improves. When we consider max-min fairness, EE of the best user and the worst user keeps unchanged and begins to drop after the throughput requirement greater than 7 bits/Hz, this is because that the obtained optimal solution of P_a first keeps unchanged and then changes for both the best user and the worst user. After the throughput requirement exceeds 8 bits/Hz, the EE of the best user and the worst user under both criterions reduces since both the users cannot obtain their optimal

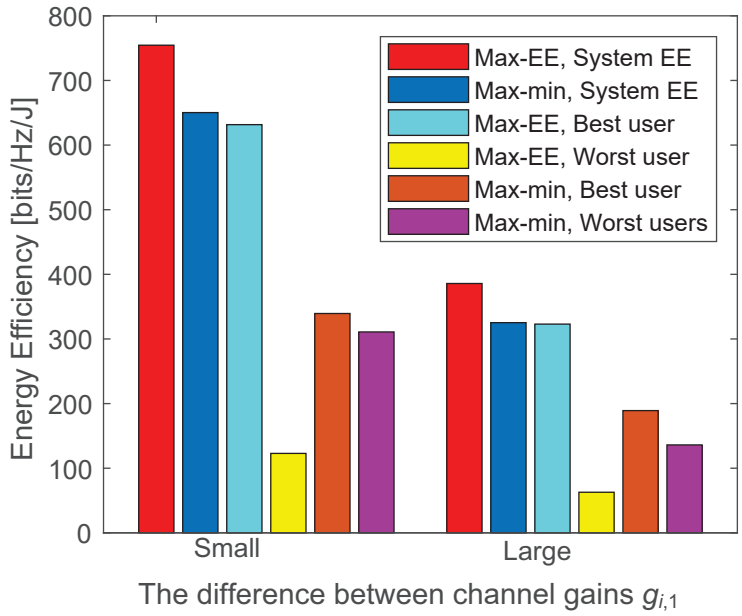

Fig. 3 EE versus channel power gain differences between $g_{i,1}$ and $g_{j,1}$.

value of P_a. Also, the EE gap between the best user and the worst user becomes smaller, and the optimal solutions under the criterions of both max-min fairness and max-SEE are the same.

5 Conclusions

In this letter, we solve the max-min EE resource allocation problem in a wireless powered backscatter network. An iterative algorithms is proposed to solve this problem by jointly optimizing the transmission power of the PB and the reflection coefficients when the optimization problem is convex or non-convex. Simulation results show that the iterative algorithm converges very fast, and the max-min EE resource allocation is more effective when the throughput requirement of the BDs is low and the channel power gain difference from the PB to each backscatter transmitter is small.

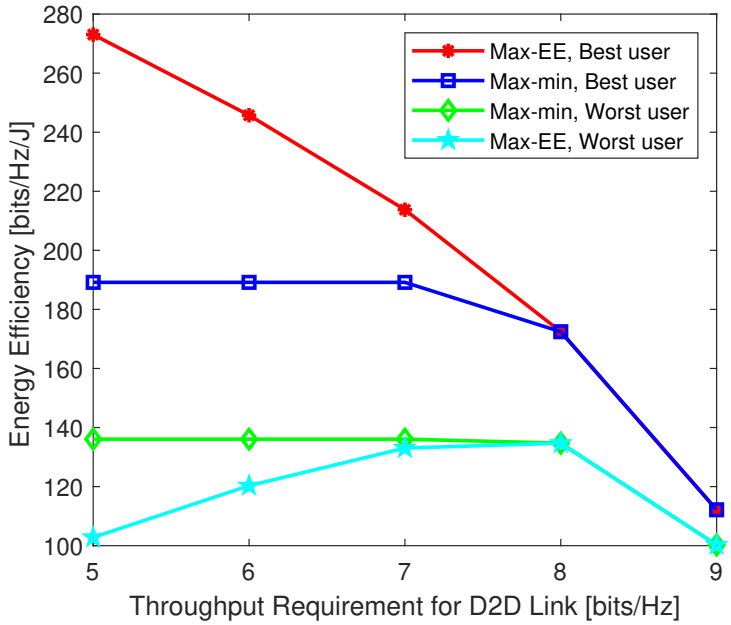

Fig. 4 EE versus throughput requirement for backscatter links.

References

[1] N. Van Huynh, D. T. Hoang, X. Lu, D. Niyato, P. Wang and D. I. Kim, “Ambient Backscatter Communications: A Contemporary Survey," *IEEE Commun. Surv. Tutor.*, vol. 20, no. 4, pp. 2889-2922, Fourthquarter 2018.

[2] B. Lyu, C. You, Z. Yang and G. Gui, “The Optimal Control Policy for RF-Powered Backscatter Communication Networks," *IEEE Trans. Veh. Technol.*, vol. 67, no. 3, pp. 2804-2808, March 2018.

[3] Q. Zhang, H. Guo, Y. Liang and X. Yuan, “Constellation Learning-Based Signal Detection for Ambient Backscatter Communication Systems," *IEEE J. Sel. Areas Commun.,* vol. 37, no. 2, pp. 452-463, Feb. 2019.

[4] B. Kellogg et al., “Wi-Fi Backscatter: Internet Connectivity for Powered Devices," in *Proc. ACM SIGCOMM*, 2014, pp. 607-618.

[5] Y. Ye, L. Shi, R. Q. Hu and G. Lu, “Energy-Efficient Resource Allocation for Wirelessly Powered Backscatter Communications," *IEEE Commun Lett.*, vol. 23, no. 8, pp. 1418-1422, Aug. 2019.

[6] R. Kishore, S. Gurugopinath, P. C. Sofotasios, S. Muhaidat and N. Al-Dhahir, “Opportunistic Ambient Backscatter Communication in RF-Powered Cognitive Radio Networks," *IEEE Trans. Cogn. Commun. Netw.*, vol. 5, no. 2, pp. 413-426, June 2019.

[7] L. Xie, J. Xu and R. Zhang, “Throughput Maximization for UAV-Enabled Wireless Powered Communication Networks,”*IEEE Internet Things J.,* vol. 6, no. 2, pp. 1690-1703, April 2019.

[8] N. Zhao, R. Chai, Q. Hu and J. Zhang, “Energy Efficiency Optimization Based Joint Relay Selection and Resource Allocation for SWIPT Relay Networks”, in *Proc. IEEE ChinaCom*, Shanghai, 2015, pp. 503-508.

[9] C. Boyer and S. Roy, “Backscatter Communication and RFID: Coding, Energy, and MIMO Analysis,”*IEEE Trans. Commun.*, vol. 62, no. 3, pp. 770–785, Mar. 2014.

[10] R. Correia, A. Boaventura, and N. Borges Carvalho, “Quadrature Amplitude Backscatter Modulator for Passive Wireless Sensors in IoT Applications,”*IEEE Trans. Microw. Theory Tech.*, vol. 65, no. 4, pp. 1103–1110, Apr. 2017.

[11] W. Liu, K. Huang, X. Zhou and S. Durrani, “Full-Duplex Backscatter Interference Networks Based on Time-Hopping Spread Spectrum, ”*IEEE Trans. Wireless Commun.*, vol. 16, no. 7, pp. 4361-4377, July 2017.

[12] W. Liu and others, “Backscatter Multiplicative Multiple-Access Systems: Fundamental Limits and Practical Design,”*IEEE Trans. Wireless Commun.*, vol. 17, no. 9, pp. 5713-5728, Sept. 2018.

[13] W. Dinkelbach, “On Nonlinear Fractional Programming," *Manage. Sci.*, vol. 13, no. 7, pp. 492-498, Mar. 1967.

[14] Y. Ye et al., “Dynamic Asymmetric Power Splitting Scheme for SWIPT-Based Two-Way Multiplicative AF Relaying," *IEEE Signal Process. Lett.*, vol. 25, no. 7, pp. 1014-1018, July 2018.

[15] Wei Yu and R. Lui, “Dual methods for nonconvex spectrum optimization of multicarrier systems,”*IEEE Trans. Commun.,* vol. 54, no. 7, pp. 1310-1322, July 2006.

Chapter 6

Paper III

Energy Efficiency Maximization for Symbiotic Radio Networks with Multiple Backscatter Devices

Haohang Yang, Yinghui Ye, Kai Liang and Xiaoli Chu

Published in *IEEE Open Journal of the Communications Society, Volume: 2, Page(s): 1431 - 1444, Date of Publication: 21 June 2021.*

Energy Efficiency Maximization for Symbiotic Radio Networks with Multiple Backscatter Devices

Haohang Yang[1], Yinghui Ye[2], Kai Liang[3] and Xiaoli Chu[1]

[1] Department of Electronic and Electrical Engineering, the University of Sheffield, Sheffield, S1 4ET, United Kingdom

[2] Shaanxi Key Laboratory of Information Communication Network and Security, Xi'an University of Posts & Telecommunications, China

[3] State Key Laboratory of Integrated Service Networks, Xidian University, Xi'an 710071, China

Abstract

Driven by the limited radio spectrum resources and the high energy consumption of wireless devices, symbiotic radio (SR) has recently been proposed to support passive Internet-of-things (IoT) networks, where a primary transmitter (PT) transmits information to a primary reader (PR), while passive backscatter devices (BDs) modulate their own information on the received primary signal and backscatter the modulated signal to the same PR by adjusting their reflection coefficients[1]. Existing works on SR have mainly studied the case of a single BD while without considering the BD's energy harvesting (EH) ability. In this paper, we aim to maximize the energy efficiency (EE) of an SR system that includes multiple BDs each being able to harvest energy while backstattering, by jointly optimizing the PT transmission power and the BDs' reflection coefficients and time division multiple access (TDMA) time slot durations for both the parasitic SR (PSR) and commensal SR (CSR) cases. To solve the formulated non-convex optimization problems, we propose a Dinkelbach-based iterative algorithm that builds on

[1]Compared with relay communication, backscatter communication does not generate RF signal actively. Also, the backscatter device modulates its own information on the incident RF signal and reflects the modulated signal to the receiver for decoding, which means that the receiver decodes the signals from both the backscatter device and the primary transmitter. Therefore, the motivation of using backscatter communication is its low energy consumption and the decoding of both the primary signal and backscattered signal. Some potential applications of backscatter communication are expected, e.g., low-power consumption wearable device, built in biosensor chip, operation and maintenance of railway system, industrial sensor network and underwater Internet of things.

the block coordinated decent (BCD) method and the successive convex programming (SCP) technique. Simulation results show that the proposed algorithm converges fast, and the system EE is maximized when all BDs only achieve the minimum throughput requirements in the PSR case, while in the CSR case, the system EE is maximized when the BD that can provide the highest EE is allocated the maximum allowed time for backscattering while guaranteeing the throughput requirements for the other backscatter links.

1 Introduction

It is predicted that the Internet of Things (IoT) devices will be over 80 billion worldwide by 2030 [1], putting huge pressure on wireless networks concerning the limited radio spectrum resources and soaring energy consumption. In order to support massive IoT connections, cognitive radio (CR) technology has been employed to let IoT devices (as secondary transmitters (STs)) share the same spectrum with incumbent primary transmitters (PTs) [2], [3], [4], [5]. However, the energy efficiency (EE) of a CR system is limited by the energy-consuming active radio frequency (RF) components used in the STs [2], [6].

Different from active RF transmissions, backscatter communications (BackCom) [7], [8], [9], [10], [11], [12] allow a backscatter device (BD) to modulate its own information on the incident RF signal transmitted by a PT and backscatter the modulated signal to the desired receiver by adjusting its reflection coefficient [13], [14], [15], while harvesting energy from the incident RF signal to cover its circuit power consumption [11]. Thus, the energy consumption of passive BackCom is significantly reduced as compared with active transmissions in CR. However, since the BDs have no knowledge of the information transmitted by the PT, the EE of BackCom will be limited by the strong interference caused by the PT [6].

To exploit the synergy between CR and BackCom, symbiotic radio (SR) has been proposed recently [6], where the PT and the primary receiver (PR) are designed to support both the primary and BackCom transmissions, and has attracted a lot of research interest. Depending on whether the BD symbol period is equal to or much longer than the PT symbol period, SR is classified into parasitic SR (PSR) and commensal SR (CSR), respectively [2]. The authors in [2] jointly optimized the transmission power and beamforming vectors of a multi-antenna PT

to maximize the weighted sum-rate and minimize the transmission power separately in an SR system. In [16], the weighted sum-rate of an SR network was maximized through optimizing the PT transmission power and the BD reflection coefficient under either a long-term or short-term PT transmission power constraint. The authors in [17] derived the expressions of the outage probability and the ergodic rate for an SR system, where the base station transmits information to two cellular users and a BD backscatters its information to one of the two cellular users, and analyzed the corresponding diversity orders. In [18], the PT transmission power was minimized by jointly designing the beamforming vector at the PT and the power splitting factor at the full-duplex BD, while guaranteeing the minimum BD rate requirement. The authors in [19] maximized the system EE subject to the throughput requirements of the direct and backscatter links as well as the PT transmit power constraint, by optimizing the PT beamforming vectors in an SR system with a finite block length backscatter link. Nevertheless, the above works considered only a single BD while ignoring the energy harvesting (EH) ability of the BD.

In this paper, we investigate the EE maximization problem of an SR system with multiple BDs, each being able to harvest energy from the incident primary signal to support their circuit power consumption. Our main contributions are summarized as follows:

- We propose an SR system, where following the time division multiple access (TDMA) protocol but allocating a BD-specific time slot duration to each BD, multiple BDs take turn to modulate their own information on the incident primary signal and backscatter the modulated signal to the PR, while harvesting energy from the incident primary signal to support their circuit operation.

- We formulate an optimization problem to maximize the EE of the SR system by jointly optimizing the PT transmission power and the BDs' reflection coefficients and TDMA time slot durations for both the PSR and CSR cases.

- Due to multiple coupled variables in the objective function and the constraints, the formulated problem is non-convex and is hard to solve directly. To solve the problem, in the PSR case, we first introduce auxiliary variables and utilize the Dinkelbach-based method to transform the original problem from a fraction form into a subtraction form,

then employ a block coordinate decent (BCD) method in conjunction with a successive convex programming (SCP) technique to transform the objective function into a convex function, and obtain the sub-optimal solutions of the PT transmission power, the BDs' reflection coefficients, or the BDs' time slot durations, given the other variables by using the interior point method. The closed-form expression of the sub-optimal reflection coefficients is derived by employing the Lagrange dual method. In the case of CSR, as the system EE is a monotonically increasing function of the BDs' reflection coefficients, we first obtain the globally optimal reflection coefficients. Then, employing techniques similar to the PSR case but without using the BCD method, we obtain the sub-optimal solutions of the PT transmission power and the BDs' time slot durations, and derive the closed-form expressions of the optimal reflection coefficients and the sub-optimal PT transmission power. Based on the above obtained solutions, we propose a Dinkelbach based iterative algorithm to solve the formulated problems in the PSR and CSR cases.

- The convergence and computational complexity of the proposed algorithm are analyzed and verified by simulation. The simulation results show that the proposed algorithm converges very fast and the system EE is maximized when all BDs only achieve the minimum throughput requirements in the PSR case, while in the CSR case, the system EE is maximized when a best BD that can contribute the most toward the system EE is allocated the maximum allowed time to backscatter its information to the PR while the other BDs' throughputs being kept at the minimum required level. Furthermore, this best BD is determined by the optimized PT transmission power in the corresponding time slot.

The rest of the paper is organized as follows. The system model is presented in Section 2. In Section 3 and Section 4, the system EE maximization problem is formulated and solved, respectively. Section 5 presents the Dinkelbach based iterative algorithm for maximizing the system EE. Section 6 analyzes the convergence and the computational complexity of the proposed algorithm. In Section 7, the simulation results are presented. Section 8 concludes the paper.

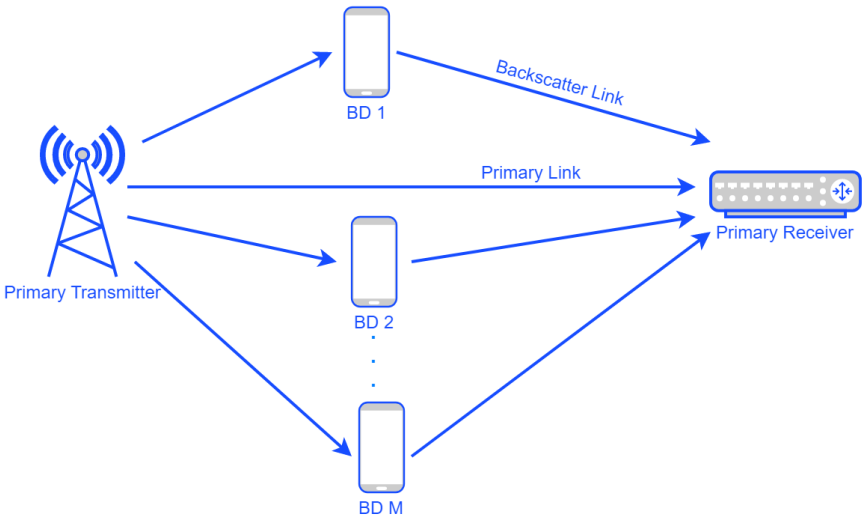

Fig. 1 An SR Network

2 System Model

In this section, we introduce the SR network with multiple BDs, present the throughout analysis for both the PSR and CSR cases, and define the system EE of the network.

2.1 Network Model

As shown in Fig. 1, the SR network consists of a PT, a PR and M BDs, where each BD $i \in \mathscr{M} = \{1, \cdots, M\}$ is equipped with a single antenna, an EH circuit and a passive backscatter circuit[2]. The PT transmits its information to the PR through a direct link, meanwhile BD i modulates its own information on the incident primary signal from the PT and backscatters the modulated signal to the PR by adjusting its reflection coefficient. The BDs share the same RF channel with the primary link. The mutual interference among the BDs during BackCom can be avoided by employing TDMA, where a time block T is divided into M time slots for the M BDs, i.e., $\sum_{i=1}^{M} t_i \leq T$, and t_i is the duration of the ith time slot allocated to BD i for BackCom and EH at the same time, while all the other BDs staying idle. Assuming that there is

[2]BackCom systems can be mainly classified into passive systems and semi-passive systems, where the key benefits of a passive BD without any internal energy storage are its low cost and small size [14], [20]. In this paper, we consider passive BDs where the energy is only harvested for covering circuit power consumption and is not stored in the BDs.

no internal power source or energy storage in the BDs, the harvested energy during BackCom is used up for BD circuit operation and cannot be stored [14].

We use a block flat-fading channel model, where the channel parameters stay constant during each time block T [2]. The channel power gain of the direct link from the PT to the PR is denoted by $h^{t,r} = (d^{t,r})^{-\alpha}\mu^{t,r}$, where $d^{t,r}$, α and $\mu^{t,r}$ are the distance, the path-loss exponent and the Rayleigh fading power gain of the link from the PT to the PR, respectively. We denote the channel power gain from the PT to BD i and that from BD i to the PR by $h_i^{t,b} = (d_i^{t,b})^{-\alpha}\mu_i^{t,b}$ and $h_i^{b,r} = (d_i^{b,r})^{-\alpha}\mu_i^{b,r}$, respectively, where $d_i^{t,b}$ and $d_i^{b,r}$ are the distance from the PT to BD i and that from BD i to the PR, respectively, $\mu_i^{t,b}$ and $\mu_i^{b,r}$ are the Rayleigh fading power gain from the PT to BD i and that from BD i to the PR, respectively.

The amount of energy harvested by BD i during the ith time slot is given by

$$EH_i = t_i P_i h_i^{t,b}(1 - z_i)\eta, \tag{1}$$

where P_i and z_i are the PT transmission power and the reflection coefficient of BD i in the ith time slot, respectively, and η represents the energy conversion efficiency of the EH circuit. We ignore the energy harvested from the thermal noise as it is much lower than the RF energy [15], [21]. Accordingly, the total amount of energy harvested by all the BDs in a time block T is given by $EH_{sum} = \sum_{i=1}^{M} EH_i$.

2.2 Throughput Analysis

Denote the primary signal transmitted from the PT by $s(n)$ with symbol period of T_s and the ith BD's signal by $c_i(l)$ with symbol period of T_c, where n and l are the indices of symbols of the primary signal and the BackCom signal, respectively. The symbol periods T_s and T_c are much shorter than t_i, $i \in \mathscr{M}$. It is assumed that $s(n)$ and $c_i(l)$ follow independent standard circularly symmetric complex Gaussian distribution $\mathscr{CN}(0,1)$. Thus, the backscattered signal from BD i is given by $\sqrt{z_i}c_i(l)$, where $z_i \in [0,1]$ is the reflection coefficient of BD i. Following [2], we consider two cases of SR, one is the PSR with $T_s = T_c$, and the other is the CSR with $T_c = NT_s$, where $N >> 1$ is a positive integer, i.e., the symbol period of the BackCom is much longer

than that of the primary transmission. In the following, we will analyze the throughputs of the primary link and BackCom links for the two cases separately.

2.2.1 PSR

Since $T_s = T_c$, we assume that $l = n$ and the received signal at the PR for the nth primary symbol in the ith time slot is given by

$$y(n)^{(1)} = \sqrt{P_i h^{t,r}} s(n) + \sqrt{P_i z_i h_i^{t,b} h_i^{b,r}} s(n) c_i(n) + k(n), \tag{2}$$

where $k(n)$ is the additive white Gaussian noise (AWGN) with zero mean and power σ^2.

According to (2), the received signal from BD i is weaker than that from the PT. Therefore, the PR can utilize the successive-interference-cancellation (SIC) technique to decode the primary signal $s(n)$ first, then remove $s(n)$ from the received signal $y(n)^{(1)}$, and detect the BackCom signal $c_i(n)$. Since the symbol rates of $s(n)$ and $c_i(n)$ are the same in the PSR case, $c_i(n)$ is regarded as interference when decoding $s(n)$. As we can see from the second term on the right-hand side of (2), the interference is the product of two complex Gaussian signals $s(n)$ and $c_i(n)$, and thus follow a non-Gaussian distribution. The lower bound of the PT-PR link throughput (bits) in a time block is given by [2]

$$R^{s(1)} = \sum_{i=1}^{M} W t_i \log_2 \left(1 + \frac{P_i h^{t,r}}{P_i z_i h_i^{t,b} h_i^{b,r} + \sigma^2} \right), \tag{3}$$

where W is the channel bandwidth.

Assuming that the primary signal is perfectly removed from $y(n)^{(1)}$ by SIC [2], [16], [17], [18], [19], we have

$$y'(n)^{(1)} = \sqrt{P_i z_i h_i^{t,b} h_i^{b,r}} s(n) c_i(n) + k(n). \tag{4}$$

Regarding $s(n)$ as a random channel component imposed on $c_i(n)$, the throughput of backscatter link i in the ith time slot is given by [22]

$$R_i^{c(1)} = W t_i \mathbb{E}_s \left[\log_2 \left(1 + \frac{P_i z_i h_i^{t,b} h_i^{b,r} |s(n)|^2}{\sigma^2} \right) \right], \tag{5}$$

where $|s(n)|^2$ follows the exponential distribution with a unit mean.

2.2.2 CSR

Since $T_c = NT_s, N >> 1$, the BackCom symbol $c_i(l)$ spans N primary symbol periods for $n = 1, \cdots, N$. Accordingly, the received signal at the PR for the nth primary symbol is written as

$$y(n)^{(2)} = \sqrt{P_i h^{t,r}} s(n) + \sqrt{P_i z_i h_i^{t,b} h_i^{b,r}} s(n) c_i(l) + k(n). \tag{6}$$

The second signal term in (6) can be viewed as the output of the primary signal $s(n)$ passing through a slowly varying channel $\sqrt{h_i^{t,b} h_i^{b,r}} c_i(l)$. Thus, the PR first decodes the primary signal $s(n)$ by treating the BD signal as a multipath component. If $c_i(l)$ is negative, the PR can compensate for the negative signal via maximum ratio combing (MRC) and $c_i(l)$ is not be regarded as interference signal. For given $c_i(l)$, the average throughput of the PT-PR link in a time block is given by

$$R^{s(2)''} = \sum_{i=1}^{M} W t_i \mathbb{E}_{c_i} [\log_2 (1 + \gamma_i^s)], \tag{7}$$

where $\gamma_i^s = \frac{P_i h^{t,r} + P_i z_i h_i^{t,b} h_i^{b,r} [c_i(l)]^2}{\sigma^2}$ is the signal-to-noise ratio (SNR).

Lemma 1: γ_i^s follows a noncentral chi-square distribution χ^2 with the freedom of 2, and its probability density function (PDF) is given by

$$f_i(x) = \frac{1}{2\theta_i} e^{\left(-\frac{x+\lambda_i}{2\theta_i}\right)} I_0 \left(\frac{\sqrt{x\lambda_i}}{\theta_i} \right) \tag{8}$$

where the noncentrality parameter $\lambda_i = \frac{P_i h^{t,r}}{\sigma^2}$, the Gaussian variance parameter $\theta_i = \frac{P_i z_i h_i^{t,b} h_i^{b,r}}{2\sigma^2}$, and $I_0(\cdot)$ is a modified Bessel function of the first kind and is given by

$$I_0(v) = \sum_{m=0}^{\infty} \frac{1}{m! \Gamma(m+1)} \left(\frac{v}{2} \right)^{2m}. \tag{9}$$

Based on (7), the expected throughput of the PT-PR link in a time block over all possible values of $c_i(l)$ is given by

$$R^{s(2)\prime} = \sum_{i=1}^{M} Wt_i \int_0^{+\infty} \log_2(1+x) f_i(x)\, dx. \tag{10}$$

Following [2], [16], [17], [18], [19], when $\gamma_i^s \to +\infty$, the expected throughput of the PT-PR link in a time block is given by

$$R^{s(2)} = \sum_{i=1}^{M} Wt_i \left[\log_2\left(\frac{P_i h^{t,r}}{\sigma^2}\right) - \mathrm{Ei}\left(-\frac{h^{t,r}}{z_i h_i^{t,b} h_i^{b,r}}\right) \log_2 e \right], \tag{11}$$

where $\mathrm{Ei}(x) \triangleq \int_{-\infty}^{x} \frac{1}{u} e^u du$.

Assuming that the primary signal is perfectly removed from $y(n)^{(2)}$ via maximum-likelihood (ML) detection [23], for $n = 1, \cdots, N$, we have

$$y'(n)^{(2)} = \sqrt{P_i z_i h_i^{t,b} h_i^{r,b}}\, s(n)\, c_i(l) + k(n). \tag{12}$$

Since $E|s(n)|^2 = 1$, the symbol $c_i(l)$ can be decoded by performing maximal ratio combing (MRC) of $y'(n)^{(2)}$, $n = 1, \cdots, N$, received in N consecutive primary symbol periods, and the throughput of backscatter link i in the ith time slot can be approximately calculated as [2], [16], [17], [18], [19]

$$R_i^{c(2)} = Wt_i \frac{1}{N} \log_2\left(1 + \frac{N P_i z_i h_i^{t,b} h_i^{b,r}}{\sigma^2}\right). \tag{13}$$

2.3 System Energy Efficiency

The system EE of the SR network is defined as the ratio of the total throughput of all links to the total energy consumption of the network in a time block [24], [25], [26], [27]. Letting R_{sum}^{PSR} and R_{sum}^{CSR} denote the total throughput of the network for the PSR and the CSR, respectively, we have

$$R_{sum}^{PSR} = R^{s(1)} + \sum_{i=1}^{M} R_i^{c(1)}, \tag{14}$$

$$R_{sum}^{CSR} = R^{s(2)} + \sum_{i=1}^{M} R_i^{c(2)}. \tag{15}$$

The total energy consumption of the SR network in a time block is given by

$$EC_{sum} = \sum_{i=1}^{M} t_i \left(P_i + P_{cir}^{BD} + P_{cir}^{TR}\right), \tag{16}$$

where P_{cir}^{BD} and P_{cir}^{TR} represent the circuit power consumption of a BD and that of the PT and PR in total, respectively.

Thus, the system EE in the cases of PSR and CSR is given respectively by

$$EE^{PSR} = \frac{R_{sum}^{PSR}}{EC_{sum} - \min(EH_{sum}, \sum_{i=1}^{M} t_i P_{cir}^{BD})}, \tag{17}$$

$$EE^{CSR} = \frac{R_{sum}^{CSR}}{EC_{sum} - \min(EH_{sum}, \sum_{i=1}^{M} t_i P_{cir}^{BD})}, \tag{18}$$

where $\min(EH_{sum}, TP_{cir}^{BD})$ in the denominator on the right-hand side indicates that any excessive energy harvested by BDs will not contribute to a higher system EE, because the BDs do not have any built-in energy storage.

3 PSR System Energy Efficiency Maximization

In this section, we first formulate the system EE maximization problem for the PSR case, then transform the problem into a more tractable form and propose a Dinkelbach-based iterative algorithm to solve it.

3.1 Problem Formulation

We aim to maximize the system EE of the SR network by jointly optimizing the PT transmission power P_i, and BDs' TDMA time slot duration t_i and reflection coefficients z_i, $i \in \mathscr{M}$.

Accordingly, the optimization problem is formulated as

$$
\begin{aligned}
& \mathrm{P}_1: \max_{\{P_i, t_i, z_i\}} \quad EE^{PSR} \\
& \text{s.t.} \\
& \quad \mathrm{C1}: 0 \leq P_i \leq P_{\max}, \forall i; \\
& \quad \mathrm{C2}: 0 \leq z_i \leq 1, \forall i; \\
& \quad \mathrm{C3}: t_i \geq 0, \sum_{i=1}^{M} t_i \leq T, \forall i; \\
& \quad \mathrm{C4}: R^{s(1)} \geq R^{s}_{\min}, R_i^{c(1)} \geq R^{c}_{\min}, \forall i; \\
& \quad \mathrm{C5}: EH_i \geq t_i P_{cir}^{BD}, \forall i,
\end{aligned}
\tag{19}
$$

where $P_{\max}$ is the maximum transmission power of PT, and R^s_{min} and R^c_{min} are the minimum required throughput of the primary link and a backscatter link, respectively; C1 and C2 specify the value ranges of the PT transmission power and BDs' reflection coefficients, respectively; C3 constrains the sum duration of all BDs' time slots in a time block; C4 guarantees the minimum throughput requirements for the primary link and the backscatter links and C5 requires that the harvested energy of each BD should exceed its circuit energy consumption.

We can see that $\mathbf{P_1}$ contains a fractional objective function with multiple variables coupled in it and in the constraints. As it is extremely difficult to solve $\mathbf{P_1}$ directly, we will first transform it into a more tractable form.

3.2 Problem Transformation

Assuming that the harvested energy of each BD is sufficient to cover its circuit power consumption while any excessive harvested energy cannot be stored, letting $A_i = h_i^{t,b} h_i^{r,b}$ and introducing

an auxiliary variable $L_i = P_i z_i t_i$, we transform $\mathbf{P_1}$ as

$$\begin{aligned}
&\mathrm{P}_2: \\
&\max_{\{P_i,t_i,L_i\}} W\frac{\sum\limits_{i=1}^{M} t_i \log_2\left(1+\frac{P_i h^{t,r}}{A_i\frac{L_i}{t_i}+\sigma^2}\right)+\sum\limits_{i=1}^{M} t_i \mathbb{E}_s\left[\log_2\left(1+\frac{A_i L_i |s(n)|^2}{t_i\sigma^2}\right)\right]}{\sum\limits_{i=1}^{M} t_i\left(P_i+P_{cir}^{TR}\right)} \\
&\text{s.t.} \\
&\quad \mathrm{C1}, \mathrm{C3}; \\
&\quad \mathrm{C2}-1: 0 \le L_i \le t_i P_i, \forall i; \\
&\quad \mathrm{C4}-1: R^{s(1)'} \ge R^s_{\min}, R_i^{c(1)'} \ge R^c_{\min}, \forall i; \\
&\quad \mathrm{C5}-1: t_i h_i^{t,b}(P_i - \tfrac{L_i}{t_i})\eta \ge t_i P_{cir}^{BD}, \forall i,
\end{aligned} \tag{20}$$

where $R^{s(1)'} = \sum\limits_{i=1}^{M} W t_i \log_2\left(1+\frac{P_i h^{t,r}}{A_i\frac{L_i}{t_i}+\sigma^2}\right)$, $R_i^{c(1)'} = W t_i \mathbb{E}_s\left[\log_2\left(1+\frac{A_i L_i |s(n)|^2}{t_i\sigma^2}\right)\right]$.

In order to make $\mathbf{P_2}$ more tractable, we use the Dinkelbach-based method [28], [29], [30] to firstly transform the objective function in $\mathbf{P_2}$ from a fraction form into a subtraction form. Then, the maximum system EE, denoted by Q^*, can be achieved if and only if the following equation is satisfied,

$$\begin{aligned}
&\max_{\{P_i,t_i,L_i\}} R^{s(1)'} + \sum_{i=1}^{M} R_i^{c(1)'} - Q^* \sum_{i=1}^{M} t_i\left(P_i + P_{cir}^{TR}\right) \\
&\quad = R^{s(1)'^*} + \sum_{i=1}^{M} R_i^{c(1)'^*} - Q^* \sum_{i=1}^{M} t_i^*\left(P_i^* + P_{cir}^{TR}\right) = 0,
\end{aligned} \tag{21}$$

where $R^{s(1)'^*}, R_i^{c(1)'^*}, t_i^*$ and P_i^* are the optimal value of the throughput of the PT-PR link, the throughput for BD i in the ith time slot, the TDMA time slot duration and the PT transmit power, respectively.

According to (21), $\mathbf{P_2}$ is further transformed into

$$\begin{aligned}
&\mathrm{P}_3: \max_{\{P_i,t_i,L_i\}} R^{s(1)'} + \sum_{i=1}^{M} R_i^{c(1)'} - Q^* \sum_{i=1}^{M} t_i\left(P_i + P_{cir}^{TR}\right) \\
&\text{s.t.} \\
&\quad \mathrm{C1}, \mathrm{C2}-1, \mathrm{C3}, \mathrm{C4}-1, \mathrm{C5}-1.
\end{aligned} \tag{22}$$

3.3 Problem Solution

We note that $\mathbf{P_3}$ is still non-convex due to multiple coupled variables. To this end, we propose a BCD method to solve $\mathbf{P_3}$ alternatively, i.e., to optimize L_i, t_i under a fixed P_i and then optimize P_i under the updated L_i, t_i.

For a fixed P_i, we apply the successive convex programming (SCP) technique on $R^{s(1)'}$ to transform it into a convex form and successively maximize a lower bound of the objective function of $\mathbf{P_3}$ in an iterative manner based on the following lemma.

Lemma 2: For any given $X_i^{(j)} = \frac{L_i^{(j)}}{t_i^{(j)}}, j > 0$, where $L_i^{(j)}$ and $t_i^{(j)}$ denote the obtained values after the jth iteration, we have

$$R^{s(1)'}(X_i) \geq R^{s(1)'}\left(X_i^{(j)}\right), \forall i, \tag{23}$$

where

$$R^{s(1)'}\left(X_i^{(j)}\right) = W t_i \left[\log_2\left(1+\frac{P_i h^{t,r}}{A_i X_i^{(j)}+\sigma^2}\right) - \frac{P_i h^{t,r} A_i \log_2 e}{\left(A_i X_i^{(j)}+\sigma^2+P_i h^{t,r}\right)\left(A_i X_i^{(j)}+\sigma^2\right)}\left(X_i - X_i^{(j)}\right)\right], \tag{24}$$

and the equalities only hold when $X_i = X_i^{(j)}$.

Proof. Please see Appendix A. ■

By substituting (24) into (22) and after some manipulations, $\mathbf{P_3}$ is equivalently formulated as

$$\begin{aligned}
\mathrm{P}_{3.1}: \ \{t_i^*, L_i^*\} = F_1 = \arg\max_{\{t_i, L_i\}} & \sum_{i=1}^{M} W \left[t_i \log_2\left(1+\frac{P_i h^{t,r}}{A_i X_i^{(j)}+\sigma^2}\right) \right. \\
& \left. - \frac{P_i h^{t,r} A_i \log_2 e}{\left(A_i X_i^{(j)}+\sigma^2+P_i h^{t,r}\right)\left(A_i X_i^{(j)}+\sigma^2\right)}\left(L_i - t_i X_i^{(j)}\right)\right] \\
& + \sum_{i=1}^{M} W t_i \mathbb{E}_s\left[\log_2\left(1+\frac{A_i L_i |s(n)|^2}{t_i \sigma^2}\right)\right] - Q^* \sum_{i=1}^{M} t_i \left(P_i + P_{cir}^{TR}\right) \\
\text{s.t.} & \\
& \mathrm{C2}-1, \mathrm{C3}, \mathrm{C5}-1; \\
& \mathrm{C4}-2: R^{s(1)'}\left(X_i^{(j)}\right) \geq R_{\min}^{s}, R_i^{c(1)'} \geq R_{\min}^{c}, \forall i.
\end{aligned} \tag{25}$$

It is easy to verify that the first and third terms of the objective function in $\mathbf{P_{3.1}}$ are linear with respect to L_i and t_i, and the second term of the objective function is a standard log-form convex function. Thus, $\mathbf{P_{3.1}}$ is jointly convex with respect to L_i and t_i, and it can be efficiently solved by standard convex optimization methods, e.g., the interior point method [31] and CVX tool in Matlab.

For the obtained L_i and t_i, $\mathbf{P_3}$ is equivalently formulated as

$$\begin{aligned} &\mathrm{P}_{3.2}: F_2 = \max_{\{P_i\}} R^{s(1)'} + \sum_{i=1}^{M} R_i^{c(1)'} - Q^* \sum_{i=1}^{M} t_i \left(P_i + P_{cir}^{TR}\right) \\ &\text{s.t.} \\ &\quad \mathrm{C1}, \mathrm{C2}-1, \mathrm{C4}-1, \mathrm{C5}-1. \end{aligned} \tag{26}$$

It is easy to verify that $\mathbf{P_{3.2}}$ is convex with respect to P_i since the first and third terms of the objective function are convex and linear with respect to P_i, respectively, while the second term of the objective function is constant for the obtained L_i and t_i. Thus, we can easily solve $\mathbf{P_{3.2}}$ by applying the interior point method or using CVX tool in Matlab.

Lemma 3: To gain more insights, we derive the closed form expressions of the optimal reflection coefficient z_i and the optimal PT transmission power P_i by employing the Lagrange dual method as follows.

$$z_i^* = \frac{1}{P_i} \times \left[\frac{(1+\delta_i)\log_2 e}{\mu_i + \varepsilon_i + (1+\beta)\frac{P_i h^{t,r} A_i \log_2 e}{\left(A_i X_i^{(j)} + \sigma^2 + P_i h^{t,r}\right)\left(A_i X_i^{(j)} + \sigma^2\right)}} - \frac{\sigma^2}{A_i} \right], \tag{27}$$

$$P_i^* = \frac{(1+\beta)\log_2 e}{Q^* + \frac{\mu_i - \varepsilon_i}{t_i}} - \frac{A_i X_i + \sigma^2}{h^{t,r}}, \tag{28}$$

where $\beta, \delta_i, \mu_i, \varepsilon_i$ are the Lagrange multipliers associated with C4-1, C2-1 and C5-1, respectively.

Proof. Please see Appendix B. ■

Remark 1: As we can see in (27), the optimal reflection coefficient is lower with higher PT transmission power, indicating that the EE of the primary link dominates the system EE. This can be explained as follows. Increasing the PT transmission power will lead to higher

interference power from the backscatter links to the primary link. Since the EE of the primary link dominates the system EE, the system EE can be increased by the BDs reducing their reflection coefficients so as to reduce their interference to the primary link and to increase the primary link EE. According to (28), the optimal PT transmission power in a time slot increases with a better channel condition of the primary link, i.e., $h^{t,r}$, as well as a longer duration of the time slot, i.e., t_i. The above insights will be verified by simulations.

4 CSR System Energy Efficiency Maximization

In this section, we first formulate the system EE maximization problem for the CSR network, then transform the problem into a more tractable form and propose a Dinkelbach-based iterative algorithm to solve it.

4.1 Problem Formulation

Similar to the PSR case, the system EE maximization for the CSR case is formulated as

$$\begin{aligned} \mathrm{P}_4: \quad & \max_{\{P_i,t_i,z_i\}} EE^{CSR} \\ \text{s.t.} \quad & \\ & \mathrm{C1},\mathrm{C2},\mathrm{C3},\mathrm{C5}; \\ & \mathrm{C4}-3: R^{s(2)} \geq R^{s}_{\min}, R_i^{c(2)} \geq R^{c}_{\min}, \forall i; \end{aligned} \tag{29}$$

Similar to $\mathbf{P_1}$, $\mathbf{P_4}$ is extremely difficult to solve due to the fractional objective function and multiple coupled variables. Next, we transform $\mathbf{P_4}$ into a more tractable form.

4.2 Problem Transformation

Since the numerator of the objective function of $\mathbf{P_4}$, i.e., R_{sum}^{CSR} in (15), is a monotonically increasing function of z_i, the system EE is maximized when the harvested energy of each BD

equals their circuit power consumption, that is

$$t_i P_i h_i^{t,b} (1 - z_i) \eta = t_i P_{cir}^{BD}, \tag{30}$$

and the optimal reflection coefficient z_i^* is obtained as

$$z_i^* = 1 - \frac{P_{cir}^{BD}}{P_i h_i^{t,b} \eta}. \tag{31}$$

Remark 2: According to (31), the optimal reflection coefficient in the CSR case increases with higher PT transmission power, which is opposite to the PSR case. This is because in CSR, the backscatter links not only cause no interference to the primary link, but also enhance the throughout of the primary link.

Based on (31) and letting $B_i = \frac{P_{cir}^{BD} h_i^{r,b}}{\eta}$, $\mathbf{P_4}$ is transformed into

$$\begin{aligned}
&\mathrm{P}_5: \max_{\{P_i, t_i\}} W \frac{\sum\limits_{i=1}^{M} t_i \left[\log_2 \left(\frac{P_i h^{t,r}}{\sigma^2} \right) - \mathrm{Ei}\left(-\frac{h^{t,r}}{A_i - \frac{B_i}{P_i}} \right) \log_2 e \right] + \sum\limits_{i=1}^{M} t_i \frac{1}{N} \log_2 \left(1 + \frac{N(P_i A_i - B_i)}{\sigma^2} \right)}{\sum\limits_{i=1}^{M} t_i \left(P_i + P_{cir}^{TR} \right)} \\
&\text{s.t.} \\
&\mathrm{C1}, \mathrm{C3}, \mathrm{C4} - 3; \\
&\mathrm{C2} - 2: 0 \leq 1 - \frac{P_{cir}^{BD}}{P_i h_i^{t,b} \eta} \leq 1, \forall i.
\end{aligned} \tag{32}$$

Then, by introducing the auxiliary variables $U_i = (P_i A_i - B_i) t_i, i \in \mathscr{M}$, substituting $P_i = B_i / A_i + U_i / (t_i A_i)$ into (32) and employing the Dinkelbach-based method on the objective

function of $\mathbf{P_5}$, we transform $\mathbf{P_5}$ into

$$\begin{aligned}
\mathrm{P}_6: \max_{\{t_i,U_i\}} & W\sum_{i=1}^{M} t_i\left[\log_2\left(\frac{\left(B_i+\frac{U_i}{t_i}\right)h^{t,r}}{A_i\sigma^2}\right)-\mathrm{Ei}\left(-\frac{h^{t,r}}{A_i-\frac{A_iB_i}{(B_i+\frac{U_i}{t_i})}}\right)\log_2 e\right] \\
& +W\sum_{i=1}^{M} t_i\tfrac{1}{N}\log_2\left(1+\tfrac{NU_i}{t_i\sigma^2}\right)-Q^*\sum_{i=1}^{M} t_i\left(\frac{B_i+\frac{U_i}{t_i}}{A_i}+P_{cir}^{TR}\right) \\
& \text{s.t.} \\
& \mathrm{C3}; \\
& \mathrm{C1}-1: 0\le\tfrac{B_i+\frac{U_i}{t_i}}{A_i}\le P_{\max},\forall i; \\
& \mathrm{C2}-3: 0\le 1-\frac{P_{cir}^{BD}A_i}{\left(B_i+\frac{U_i}{t_i}\right)h_i^{t,b}\eta}\le 1,\forall i; \\
& \mathrm{C4}-4: {R^{s(2)}}'\ge R_{\min}^{s},{R_i^{c(2)}}'\ge R_{\min}^{c},\forall i,
\end{aligned} \tag{33}$$

where ${R^{s(2)}}' = W\sum_{i=1}^{M} t_i\left[\log_2\left(\frac{\left(B_i+\frac{U_i}{t_i}\right)h^{t,r}}{A_i\sigma^2}\right)-\mathrm{Ei}\left(-\frac{h^{t,r}}{A_i-\frac{A_iB_i}{(B_i+\frac{U_i}{t_i})}}\right)\log_2 e\right]$ and ${R_i^{c(2)}}'=$ $W\sum_{i=1}^{M} t_i\frac{1}{N}\log_2\left(1+\frac{NU_i}{t_i\sigma^2}\right)$.

4.3 Problem Solution

To solve $\mathbf{P_6}$, we apply the SCP technique on ${R^{s(2)}}'$ to transform it into a convex form and successively maximize the lower bound of the objective function in an iterative manner based on the following lemma.

Lemma 4: For any given $P_i^{(j)}=B_i^{(j)}/A_i+U_i^{(j)}/(t_i^{(j)}A_i), j>0$, where $P_i^{(j)}$, $B_i^{(j)}$, $U_i^{(j)}$ and $t_i^{(j)}$ denote the obtained parameter values after the jth iteration, we have

$$R^{s(2)}(P_i)\ge R^{s(2)}\left(P_i^{(j)}\right),\forall i, \tag{34}$$

where

$$\begin{aligned} & R^{s(2)}\left(P_i^{(j)}\right) \\ & = W\sum_{i=1}^{M} t_i\left[\log_2\left(\frac{P_i^{(j)}h^{t,r}}{\sigma^2}\right) - \mathrm{Ei}\left(-\frac{h^{t,r}}{A_i-\frac{B_i}{P_i^{(j)}}}\right)\log_2 e\right. \\ & \left. + \left(\frac{\log_2 e}{P_i^{(j)}} + \frac{B_i exp\left(-\frac{h^{tr}}{A_i-\frac{B_i}{P_i^{(j)}}}\right)\log_2 e}{A_i\left(P_i^{(j)}\right)^2 - B_i P_i^{(j)}}\right)\left(P_i - P_i^{(j)}\right)\right], \end{aligned} \tag{35}$$

and the equalities in (34) only hold when $P_i = P_i^{(j)}$.

Proof. Please see Appendix C. ■

By substituting (35) into (33) and after some manipulations, $\mathbf{P_6}$ is equivalently formulated as

$$\begin{aligned} & \mathrm{P}_{6.1}: \{U_i^*, t_i^*\} = F_3 = \arg\max_{\{U_i,t_i\}} W\sum_{i=1}^{M} t_i\left[\log_2\left(\frac{P_i^{(j)}h^{t,r}}{\sigma^2}\right)\right. \\ & -\mathrm{Ei}\left(-\frac{h^{t,r}}{A_i-\frac{B_i}{P_i^{(j)}}}\right)\log_2 e + \left(\frac{\log_2 e}{P_i^{(j)}} + \frac{B_i exp\left(-\frac{h^{tr}}{A_i-\frac{B_i}{P_i^{(j)}}}\right)\log_2 e}{A_i P_i^{(j)} - B_i P_i^{(j)}}\right) \\ & \left.\left(\frac{B_i+\frac{U_i}{t_i}}{A_i} - P_i^{(j)}\right)\right] + W\sum_{i=1}^{M}\frac{U_i}{A_i}\left(\frac{\log_2 e}{P_i^{(j)}} + \frac{B_i exp\left(-\frac{h^{tr}}{A_i-\frac{B_i}{P_i^{(j)}}}\right)\log_2 e}{A_i P_i^{(j)} - B_i P_i^{(j)}}\right) \\ & + W\sum_{i=1}^{M} t_i \frac{1}{N}\log_2\left(1+\frac{NU_i}{t_i\sigma^2}\right) - Q^*\sum_{i=1}^{M}\left(\frac{B_i t_i + U_i}{A_i} + P_{cir}^{TR}\right) \\ & \text{s.t.} \\ & \mathrm{C3}; \mathrm{C4}-4; \\ & \mathrm{C1}-2: U_i \le t_i\left(P_{\max}A_i - B_i\right), \forall i; \\ & \mathrm{C2}-4: U_i \ge 0, \forall i. \end{aligned} \tag{36}$$

It is observed that the first term and the third term of the objective function in (36) are linear with respect to U_i and t_i, and the second term of the objective function is a standard log-form

convex function. Therefore, $\mathbf{P_{6.1}}$ is jointly convex with respect to U_i and t_i, and can be solved by employing the interior point method or using CVX tool in Matlab.

Lemma 5: To gain more insights, we derive the closed form expression of the optimal PT transmission power P_i by employing the Lagrange dual method as follows.

$$P_i^* = \frac{B_i}{A_i} + \frac{1}{NA_i} \times \left[\frac{A_i(1+\delta_i)\log_2 e}{Y - (1+\beta)\left(\frac{\log_2 e}{P_i^{(j)}} + \frac{B_i exp\left(-\frac{h^{t,r}}{A_i - \frac{B_i}{P_i^{(j)}}} \right) \log_2 e}{A_i P_i^{(j)} - B_i P_i^{(j)}} \right)} - \sigma^2 \right], \tag{37}$$

where $Y = Q^* + A_i\varepsilon_i$, and $\beta, \delta_i, \varepsilon_i$ are the Lagrange multipliers associated with C4-4 and C1-2, respectively.

Proof. Please see Appendix D. ■

5 Dinkelbach Based Iterative Algorithm

Based on the solutions obtained in Sections 3 and 4, we propose a Dinkelbach-based iterative algorithm in **Algorithm 1** to solve $\mathbf{P_3}$ and $\mathbf{P_6}$ for the PSR and CSR cases, respectively, where v is the iteration index for updating the maximum system EE Q^*, and ε is the convergence threshold imposed on the objective function in $\mathbf{P_3}$ and $\mathbf{P_6}$, by meeting which the algorithm terminates.

Algorithm 1: Dinkelbach based iterative algorithm

1: **Input:** $\mathscr{M}$.

2: **Output:** $Q^*, t_i^*, L_i^*, P_i^*, U_i^*$.

3: **Initialize:** $j=1, v=1, Q^*(v), \varepsilon$.
In the case of PSR

4: **repeat**

5: **repeat**

6: Initialize $L_i^{(j)}, t_i^{(j)}$;

7: **repeat**

8: Obtain t_i, L_i by solving $\mathbf{P_{3.1}}$;

9: $j = j+1$;

10: **until** the objective function value in $\mathbf{P_{3.1}}$ converges;

11: Obtain P_i by solving $\mathbf{P_{3.2}}$;

12: **until** the objective function value in $\mathbf{P_3}$ converges;

13: Compute $R^{s(1)'}$ and $R_i^{c(1)'}$ in (20);

14: $v = v+1$;

15: Update $Q^*(v) = \frac{R^{s(1)'} + \sum_{i=1}^{M} R_i^{c(1)'}}{\sum_{i=1}^{M} t_i\left(P_i + P_{cir}^{BD}\right)}$;

16: **until** $|\min_{i\in\mathscr{M}} R^{s(1)'} + \sum_{i=1}^{M} R_i^{c(1)'} - Q^*(v) \sum_{i=1}^{M} t_i\left(P_i + P_{cir}^{BD}\right)| \leq \varepsilon$.
In the case of CSR

17: **repeat**

18: Initialize $U_i^{(j)}, t_i^{(j)}$;

19: **repeat**

20: Obtain U_i, t_i by solving $\mathbf{P_{6.1}}$;

21: $j = j+1$;

22: **until** the objective function value in $\mathbf{P_{6.1}}$ converges;

23: Compute $R^{s(2)'}$ and $R_i^{c(2)'}$ in (33);

24: $v = v+1$;

25: Update $Q^*(v) = \frac{R^{s(2)'} + \sum_{i=1}^{M} R_i^{c(2)'}}{\sum_{i=1}^{M} t_i\left(P_i + P_{cir}^{BD}\right)}$;

26: **until** $|\min_{i\in M} R^{s(2)'} + \sum_{i=1}^{M} R_i^{c(2)'} - Q^*(v) \sum_{i=1}^{M} t_i\left(P_i + P_{cir}^{BD}\right)| \leq \varepsilon$.

6 Convergence and Running Time Analysis

We first analyze the convergence of **Algorithm 1**. The SCP based iterative method applied for solving $\mathbf{P_{3.1}}$ and $\mathbf{P_{6.1}}$ ensures that the objective function value of them monotonically increases with the iteration, because the objective functions in $\mathbf{P_{3.1}}$ and $\mathbf{P_{6.1}}$ are the lower bound functions of those in $\mathbf{P_3}$ and $\mathbf{P_6}$, respectively. Meanwhile, $\mathbf{P_{3.1}}$ and $\mathbf{P_{6.1}}$ are upper bounded by their constraints. Thus, the SCP based iterative method is guaranteed to converge to a locally optimal solution. The BCD method used to solve $\mathbf{P_3}$ also ensures that the solution converges to a locally optimal value, because the objective function value of $\mathbf{P_3}$ is nondecreasing with updated variables after each iteration, and it is also upper bounded by its associated constraints.

Then, we evaluate the running time of **Algorithm 1**, the simulations are performed using CVX in MATLAB 2018 and a laptop with the following configurations: Intel(R) Core(TM) i7-9750H CPU @ 2.6GHZ, RAM 16 GB. For the PSR case, the number of iterations of the BCD process and SCA process is denoted as Δ_1 (3-4 steps) and Δ_2 (2-3 steps), respectively. Also, the running time for solving $\mathbf{P_{3.1}}$ is around 1.25s and each step of Δ_2 cost around 1.28s. Thus, the running time of the PSR case is around Δ_1(1.25+$\Delta_2$1.28)s. For the CSR case, the number of iterations of the SCA process is denoted as Δ_3 (2-3 steps) and each step costs around 1.29s. Thus, the running time of the CSR case is 1.29Δ_3s.

7 Simulation Results

In this section, we present the simulation results to evaluate the system EE performance versus the system parameters, e.g., the PT-PR distance, and the throughput requirements for the backscatter link and the primary link. The convergence of **Algorithm 1** and the throughput performance are also evaluated. The simulation parameters are set as follows unless otherwise specified. The number of the BDs $M = 5$, $N = 100$ for the CSR case, the PT-PR distance $r = 20$m, the pathloss exponent $\alpha = 3$, the channel bandwidth $W = 10k$Hz, the AWGN power spectral density is -130dBm/Hz [3], the maximum PT transmission power $P_{max} = 23$dBm, the energy conversion efficiency $\eta = 0.6$, the backscatter circuit power consumption $P_{cir}^{BD} = 200\mu$W, the PT and PR's total circuit power consumption $P_{cir}^{TR} = 2$mW, and the convergence threshold $\varepsilon = 10^{-10}$. We assume that the minimum throughput requirement for each backscatter link is the same.

7.1 Convergence of Algorithm 1

Fig. 2 shows the convergence of **Algorithm 1**. We can see that the system EE in both the PSR and CSR cases converges quickly after the 3rd iteration. The system EE in the PSR case is higher than that in the CSR case. This is because due to the long BD symbol period, the throughout of the backscatter link in the CSR case is lower than that in the PSR case, thus the system EE is reduced. Moreover, the throughout of the primary link in the CSR case is higher than that in the PSR case, but the system EE improvement brought by the higher throughput cannot compensate for the EE loss due to the higher PT transmission power for meeting R_{min}^{c}. Therefore, the system EE decreases with higher power consumption. In addition, the system EE increases with higher maximum PT transmission power in both the PSR and CSR cases. This is because the optimal PT transmission power for maximizing the system EE is capped at P_{max} and a higher P_{max} leads to a higher system EE.

[3] A higher noise power density will not lose the generality and will not affect the optimization process of the proposed EE maximization problem. Also, the AWGN generated by the receiver mainly consists of the thermal noise (also known as the antenna noise) and the baseband noise. -174 dBm/Hz is only the power spectral density of the thermal noise at the room temperature, and the practical power spectral density of the AWGN is usually much higher than -174 dBm/Hz due to the baseband noise [46].

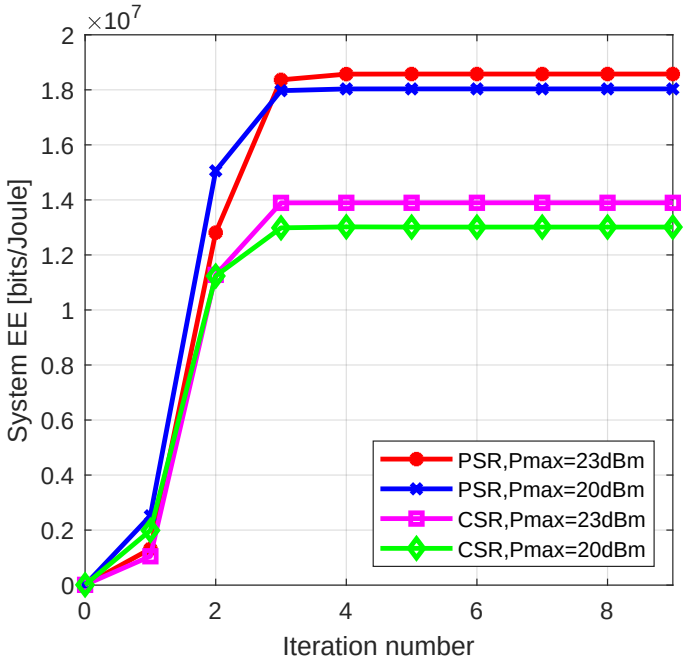

Fig. 2 Convergence of Algorithm 1

7.2 System EE and Throughput Performance

Fig. 3 plots the system EE versus the PT-PR distance r for different values of N. It can be seen that the system EE in both the PSR and CSR cases reduce with a longer r. The reason is that the longer r decreases the received power at the PR, which reduces the throughput of the primary link and the system EE. In addition, the system EE in the CSR case is higher with a lower N. This is because the backscatter link can achieve a higher throughput with a shorter BD symbol period. When the value of N reaches 200, the system EE of the CSR case reduces to 0 when r is longer than 15m. This is because the throughout requirements of the BDs in the CSR case cannot be satisfied due to the very long symbol period of the BackCom for $N = 200$.

Fig. 4(a) illustrates the system EE versus R^c_{min} in the PSR case under different R^s_{min}. We can see that the system EE decreases with a higher R^c_{min}. This is because a higher backscatter link throughput requirement needs the PT to increase its transmission power, while the EE improvement due to a higher backscatter link throughput cannot compensate for the EE loss due to more energy consumption. However, the system EE keeps the same when R^s_{min} increases from 3M bits/s to 4M bits/s. This indicates that the primary link throughput obtained under the

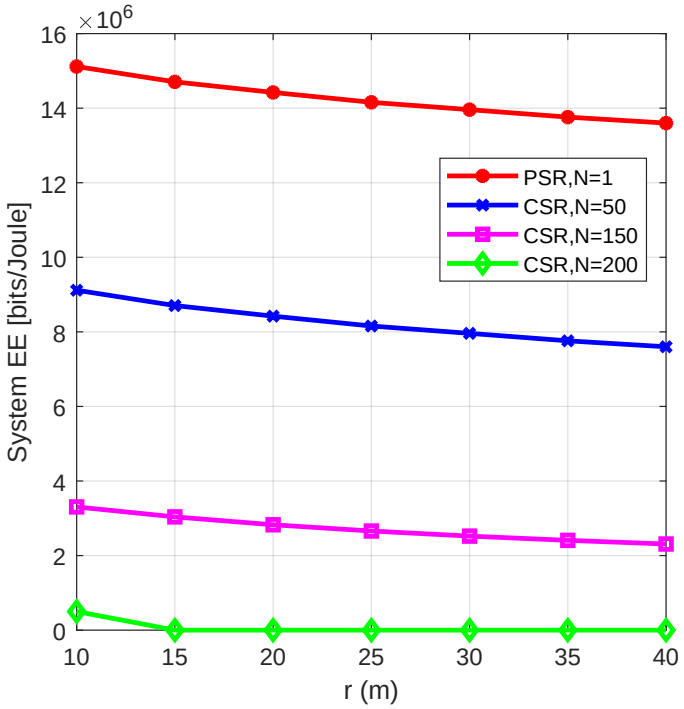

Fig. 3 System EE versus PT-PR distance r

optimal solution for maximizing the system EE is higher than 4M bits/s. When R^s_{min} increases beyond 4.7M bits/s, the PT needs to increase its transmission power, which results in system EE reduction.

Fig. 4(b) demonstrates the system EE versus R^c_{min} in the CSR case under different R^s_{min}. We can see that the system EE decreases with R^c_{min} in the CSR case much faster than that in the PSR case. This is because due to long BD symbol period in CSR, higher PT transmission power is required to meet R^c_{min}, which greatly reduces the system EE. When R^c_{min} exceeds 17k bits/s, even the maximum PT transmission power cannot let the BDs meet the throughput requirement, thus the system EE drops to 0.

By comparing Fig. 4(a) with Fig. 4(b), we find that the system EE in the CSR case exceeds that in the PSR case when R^c_{min} is between 3k bits/s and 13k bits/s and R^s_{min} is larger than 47k bits/s. Since the BD signal is regarded as an interference signal in the PSR case while being treated as a multipath component in the CSR case, the PT needs to transmit at a higher power

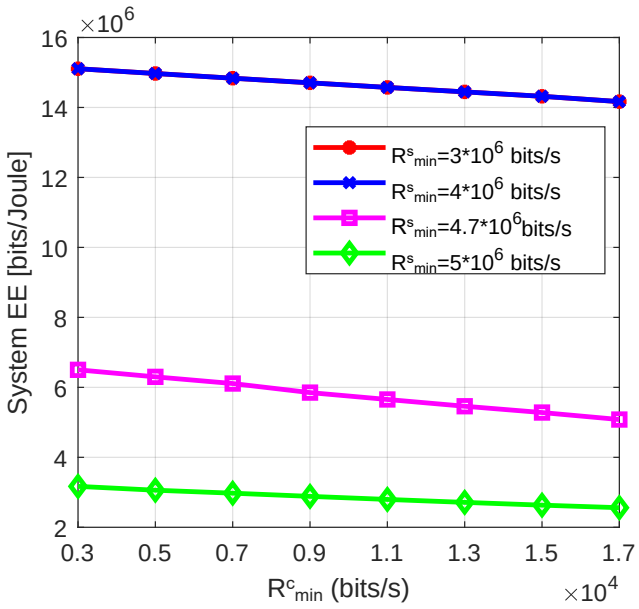

Fig. 4(a) System EE versus R^c_{min} (PSR)

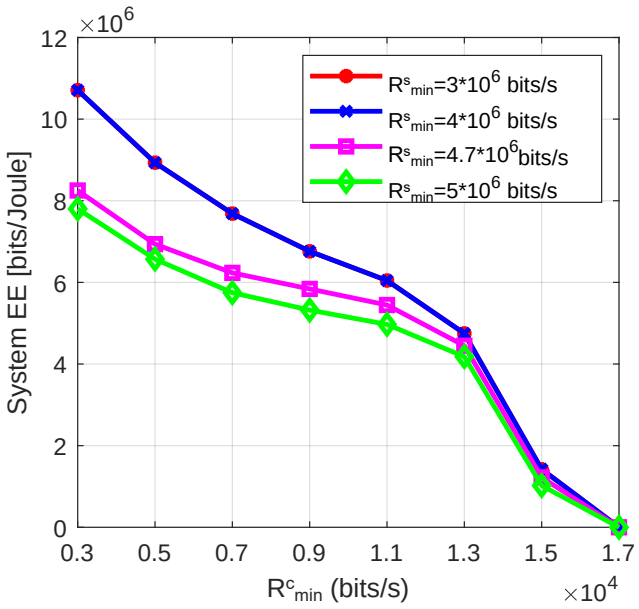

Fig. 4(b) System EE versus R^c_{min} (CSR)

level to meet the primary link throughput requirement in PSR than in CSR, which reduces the system EE in the PSR case.

Fig. 5(a) shows the throughout of each Backscatter link under different R^s_{min} and R^c_{min} in the PSR. It is clear to see that each backscatter link maintains the minimum required throughput R^c_{min} even when R^s_{min} is changed. This proves that the primary link dominates the system EE and the maximum system EE is achieved when each BD adjusts its reflection coefficient to minimize its interference to the primary link while meeting its own throughput requirement R^c_{min}.

Fig 5(b) plots the primary link throughput versus R^c_{min} under different R^s_{min} in the PSR case. For R^s_{min} being 3M bits/s and 4M bits/s, the primary link throughput is the same and it reduces with a higher R^c_{min}. This is because a higher R^c_{min} needs a higher reflection coefficient, but then the interference power from each BD also becomes larger and the primary link throughput reduces. In addition, when R^s_{min} is higher than 4.7M bits/s, the maximum system EE is achieved when the PT transmission power is just sufficient to meet R^s_{min} which would be sufficient to meet all the considered values of R^c_{min} as well. Thus, increasing R^c_{min} does not affect the primary

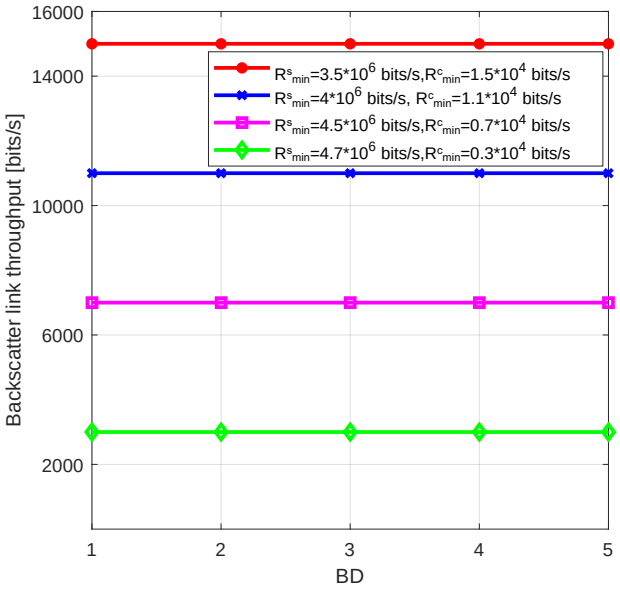

Fig. 5(a) Backscatter link throughput for different BD (PSR)

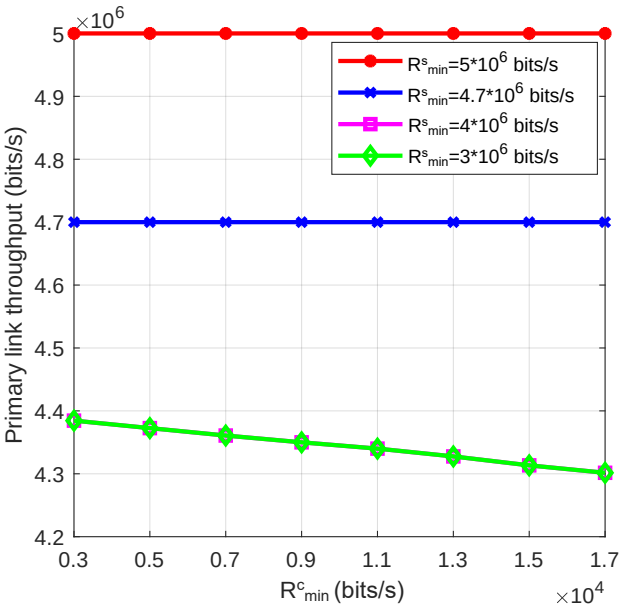

Fig. 5(b) Primary link throughput versus R^c_{min} (PSR)

link throughput, while any increase of the PT transmission power beyond the sufficient level will decrease the system EE.

Fig. 6(a) illustrates the throughout of each Backscatter link under different R^s_{min} for R^c_{min} =3k bits/s in the CSR case. We find that for each considered value of R^s_{min}, only one BD achieves a throughput higher than R^c_{min}. This is because that this BD has the potential to contribute more to the system EE than the other BDs, thus is allocated the maximum allowed time for backscattering, while the remained time is allocated to the other BDs for meeting R^c_{min}. Moreover, the BD that is allocated the maximum allowed time for backscattering may change with different R^s_{min}. This is because different values of R^s_{min} may require different PT transmission power, which affects the backscatter link throughput achievable by each BD.

Fig. 6(b) demonstrates the primary link throughput versus R^c_{min} under different R^s_{min} in the CSR case. When R^s_{min} is lower than 4M bits/s and R^c_{min} is no larger than 15k bit/s, the primary link throughput increases with R^c_{min}. This is because the PT transmission power for meeting low values of R^s_{min} is not sufficient to meet R^c_{min} and the PT transmission power has to increase for a higher R^c_{min}, thus resulting in a higher primary link throughput. When R^s_{min} exceeds 4.7M

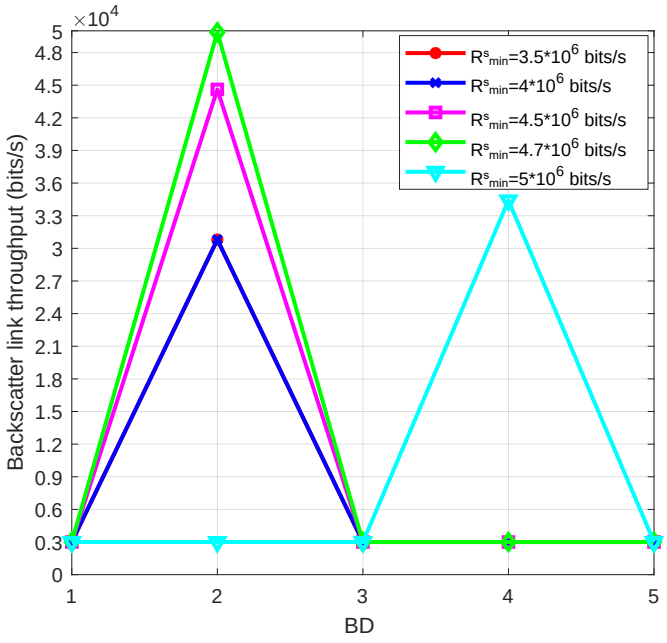

Fig. 6(a) Backscatter link throughput for different BDs (CSR)

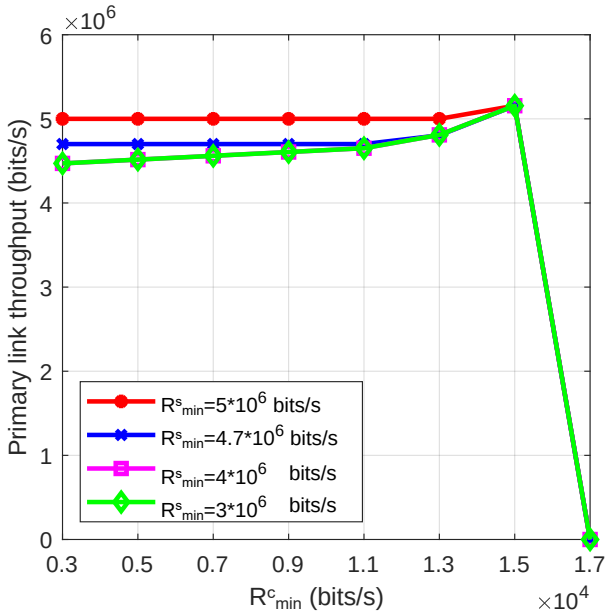

Fig. 6(b) Primary link throughput versus R^c_{min} (CSR)

bits/s, the primary link throughput first keeps constant and then increases with R^c_{min}. This is because the PT transmission power for meeting large values of R^s_{min} can satisfy relatively small values of R^c_{min} but will have to increase for meeting larger values of R^c_{min}. When R^c_{min} reaches 17k bit/s, R^c_{min} cannot be satisfied, while the PT transmission power being capped at P_{max}, hence the primary link throughput drops to 0.

Fig. 7 demonstrates that the sum throughput of the primary link and the backscatter links increases linearly with the number of BDs in both the PSR and CSR cases. This is because in the PSR case, the increase of the sum throughput is mainly brought by the more backscatter links, each maintaining the minimum throughput requirement, i.e., $R^c_{\min}$; while similarly in the CSR case, apart from one BD achieving a throughput higher than $R^c_{\min}$, all the other BDs also maintain the minimum throughput requirement, hence the sum throughput increases linearly with more BDs. For each considered number of BDs, the sum throughput of the CSR case is higher than that of the PSR case. This is because in the CSR case, one BD can achieve a throughput much higher than $R^c_{\min}$, while the backscatter links helping improve the throughput of the primary link.

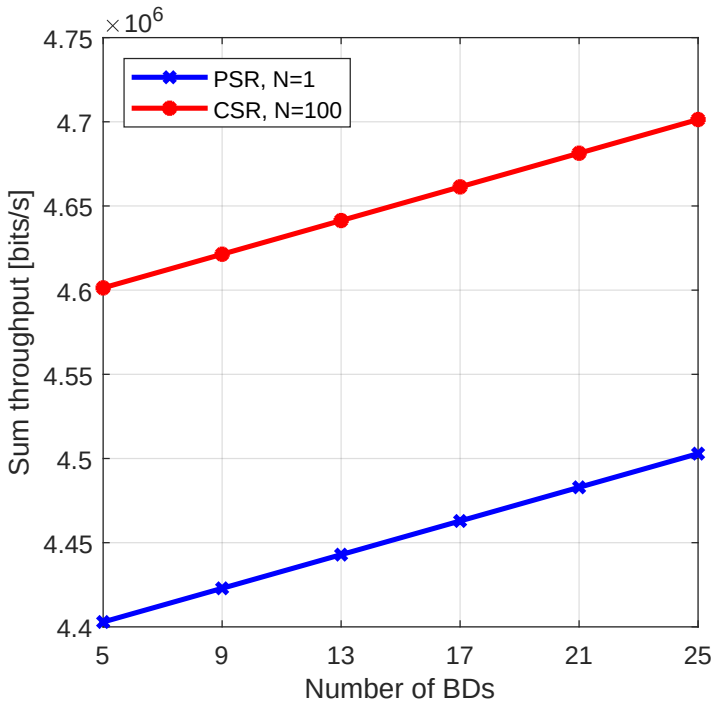

Fig. 7 Sum throughput versus the number of BDs ($R^c_{\min} = 5kbits/s$)

8 Conclusions

In this paper, we have investigated the system EE maximization problem in an SR system, where multiple BDs share the same RF channel with a primary link, for both the PSR and CSR cases. Since the formulated system EE maximization problem is extremely difficult to solve directly, we propose a Dinkelbach-based iterative algorithm to first transform the optimization problem into a more tractable form by introducing auxiliary variables and using the generalized fractional programming, then employ the BCD method and the SCP technique to solve the transformed problem in an iterative manner. The simulation results demonstrate that the proposed algorithm converges very fast and the maximized system EE reduces with a longer PT-PR distance and a higher throughput requirement per link. Moreover, we find that the primary link dominates the system EE and the maximum system EE in the PSR case is maximized when all the BDs only achieve the minimum throughput requirement. However, the system EE in the CSR case is maximized when the BD that has the potential to obtained the highest throughput among all BDs (which depends on the PT transmission power in the

corresponding time slot) is allocated the maximum allowed time for backscattering, while guaranteeing the throughput requirement of the other BDs.

Appendix A

Proof of Lemma 2

Let us define a function given by $f_1 = \log_2\left(1+\frac{P_i h^{t,r}}{A_i X_i+\sigma^2}\right)$, where f_1 is convex with respect to X_i. Since the first-order Taylor expansion of a convex function is a global under-estimator of its function values. For any given $X_i^{(j)}$, we have

$$f_1 \geq \log_2\left(1+\frac{P_i h^{t,r}}{A_i X_i^{(j)}+\sigma^2}\right) - \frac{P_i h^{t,r} A_i \log_2 e}{\left(A_i X_i^{(j)}+\sigma^2+P_i h^{t,r}\right)\left(A_i X_i^{(j)}+\sigma^2\right)}\left(\frac{L_i}{t_i}-X_i^{(j)}\right), \tag{A.1}$$

where the equalities hold when $\frac{L_i}{t_i} = X_i^{(j)}$. The proof is completed.

Appendix B

Proof of Lemma 3

Based on the Lagrange dual method, $\mathbf{P_{3.1}}$ is equivalently transformed into

$$\begin{aligned}
&\mathbb{L}_1 \\
&= \min_{\beta,\delta_i,\lambda,\mu_i,\varepsilon_i} \max_{L_i,t_i} \; F_1 + \beta W \Bigg[t_i \log_2 \left(1 + \frac{P_i h^{t,r}}{A_i X_i^{(j)} + \sigma^2}\right) \\
&- \frac{P_i h^{t,r} A_i \log_2 e}{\left(A_i X_i^{(j)} + \sigma^2 + P_i h^{t,r}\right)\left(A_i X_i^{(j)} + \sigma^2\right)} \left(L_i - t_i X_i^{(j)}\right) - R^s_{\min} \Bigg] \\
&+ \sum_{i=1}^{M} \delta_i W \left[\mathbb{E}_s \left[t_i \log_2 \left(1 + \frac{A_i L_i |s(n)|^2}{t_i \sigma^2}\right)\right] - R^c_{\min} \right] \\
&+ \lambda \left(T - \sum_{i=1}^{M} t_i\right) + \sum_{i=1}^{M} \mu_i \left(P_i t_i - L_i\right) + \sum_{i=1}^{M} \varepsilon_i \left[t_i \left(P_i - \frac{P^{BD}_{cir}}{h_i^{t,b}\eta}\right) - L_i \right].
\end{aligned} \tag{B.1}$$

Since $\mathbf{P_{3.1}}$ is convex, (B.1) is convex. Applying the KKT conditions and letting $\frac{\partial \mathbb{L}_1}{\partial L_i} = 0$, we obtain

$$X_i = \frac{L_i}{t_i} = \frac{(1+\delta_i)\log_2 e}{\mu_i + \varepsilon_i + (1+\beta)\frac{P_i h^{t,r} A_i \log_2 e}{\left(A_i X_i^{(j)} + \sigma^2 + P_i h^{t,r}\right)\left(A_i X_i^{(j)} + \sigma^2\right)}} - \frac{\sigma^2}{A_i \mathbb{E}_s |s(n)|^2}. \tag{B.2}$$

By substituting (B.2) into $z_i = \frac{X_i}{P_i}$, z_i^* is obtained.

$\mathbf{P_{3.2}}$ can also be transformed into

$$\begin{aligned}
&\mathbb{L}_2 \\
&= \min_{\beta,\mu_i,\varepsilon_i} \max_{P_i} F_2 + \beta W \left[\sum_{i=1}^{M} t_i \log_2 \left(1 + \frac{P_i h^{t,r}}{A_i X_i + \sigma^2}\right) - R^s_{\min} \right] \\
&+ \sum_{i=1}^{M} \mu_i \left(P_{\max} - P_i\right) + \sum_{i=1}^{M} \varepsilon_i \left(P_i - X_i - \frac{P^{BD}_{cir}}{h_i^{t,b}\eta} \right).
\end{aligned} \tag{B.3}$$

Since $\mathbf{P_{3.2}}$ is convex, (B.3) is convex. Applying the KKT conditions and letting $\frac{\partial \mathbb{L}_2}{\partial P_i} = 0$, we obtain

$$P_i^* = \frac{(1+\beta)\log_2 e}{Q + \frac{\mu_i - \varepsilon_i}{t_i}} - \frac{A_i X_i + \sigma^2}{h^{t,r}}. \tag{B.4}$$

The optimal values of z_i and P_i are obtained and the proof is completed.

Appendix C

Proof of Lemma 4

Let us define a function $f_2 = \log_2\left(\frac{P_i h^{t,r}}{\sigma^2}\right) - \mathrm{Ei}\left(-\frac{h^{t,r}}{A_i - \frac{P_{cir}^{BD} h_i^{r,b}}{P_i \eta}}\right)\log_2 e$, where f_2 is convex with respect to P_i. Since the first-order Taylor expansion of a convex function is a global under-estimator of its function values. For any given $P_i^{(j)}$, we have

$$f_2 \geq \log_2\left(\frac{P_i^{(j)} h^{t,r}}{\sigma^2}\right) - \mathrm{Ei}\left(-\frac{h^{t,r}}{A_i - \frac{P_{cir}^{BD} h_i^{r,b}}{P_i^{(j)} \eta}}\right)\log_2 e + \left(\frac{\log_2^e}{P_i^{(j)}} + \frac{B_i e^{-\frac{h^{tr}}{A_i - \frac{B_i}{P_i^{(j)}}}} \log_2^e}{A_i P_i^{(j)} - B_i P_i^{(j)}}\right)\left(P_i - P_i^{(j)}\right), \tag{C.1}$$

where the equalities hold when $P_i = P_i^{(j)}$. The proof is completed.

Appendix D

Proof of Lemma 5

Based on the Lagrange dual method, $\mathbf{P_{6.1}}$ is equivalently transformed into

$$\begin{aligned}
&\mathbb{L}_3 \\
&= \min_{\beta,\delta_i,\lambda,\varepsilon_i} \max_{U_i,t_i} \quad F_3 + \beta\left(W\sum_{i=1}^{M} t_i\left[\log_2\left(\frac{P_i^{(j)} h^{t,r}}{\sigma^2}\right) - \mathrm{Ei}\left(-\frac{h^{t,r}}{A_i - \frac{P_{cir}^{BD} h_i^{r,b}}{P_i^{(j)}\eta}}\right)\log_2 e\right.\right. \\
&\left.\left. + \left(\frac{\log_2^e}{P_i^{(j)}} + \frac{B_i e^{-\frac{h^{tr}}{A_i - \frac{B_i}{P_i^{(j)}}}} \log_2^e}{A_i P_i^{(j)} - B_i P_i^{(j)}}\right)\left(\frac{B_i + \frac{U_i}{t_i}}{A_i} - P_i^{(j)}\right)\right] + W\sum_{i=1}^{M}\frac{U_i}{A_i}\left(\frac{\log_2^e}{P_i^{(j)}} + \frac{B_i e^{-\frac{h^{tr}}{A_i - \frac{B_i}{P_i^{(j)}}}} \log_2^e}{A_i P_i^{(j)} - B_i P_i^{(j)}}\right) - R_{\min}^s\right) \\
&+ \sum_{i=1}^{M}\delta_i W\left[\sum_{i=1}^{M} t_i \frac{1}{N}\log_2\left(1 + \frac{NU_i}{t_i\sigma^2}\right) - R_{\min}^c\right] + \lambda\left(T - \sum_{i=1}^{M} t_i\right) + \sum_{i=1}^{M}\varepsilon_i\left[t_i\left(P_{\max}A_i - B_i\right) - U_i\right].
\end{aligned} \tag{D.1}$$

Since $\mathbf{P_{6.1}}$ is convex, (D.1) is convex. Applying the KKT conditions and letting $\frac{\partial \mathbb{L}_3}{\partial U_i} = 0$, we obtain

$$\frac{U_i}{t_i} = \frac{1}{N}\left[\frac{(1+\delta_i)\log_2 e}{(1+\beta)\left(\frac{\log_2^e}{P_i^{(j)}} + \frac{B_i e^{-\frac{h^{tr}}{A_i - \frac{B_i}{P_i^{(j)}}}} \log_2^e}{A_i P_i^{(j)} - B_i P_i^{(j)}}\right)} - \sigma^2\right]. \tag{D.2}$$

Substituting (D.2) into $P_i = \frac{B_i + \frac{U_i}{t_i}}{A_i}$, the optimal value of P_i is obtained and the proof is completed.

References

[1] L. Chettri and R. Bera, "A comprehensive survey on internet of things (IoT) toward 5g wireless systems," *IEEE Internet of Things Journal*, vol. 7, no. 1, pp. 16–32, 2020.

[2] R. Long, Y. Liang, H. Guo, G. Yang, and R. Zhang, "Symbiotic radio: A new communication paradigm for passive internet of things," *IEEE Internet of Things Journal*, vol. 7, no. 2, pp. 1350–1363, 2020.

[3] Y. Liang, K. Chen, G. Y. Li, and P. Mahonen, "Cognitive radio networking and communications: an overview," *IEEE Transactions on Vehicular Technology*, vol. 60, no. 7, pp. 3386–3407, 2011.

[4] A. A. Khan, M. H. Rehmani, and A. Rachedi, "Cognitive-radio-based internet of things: Applications, architectures, spectrum related functionalities, and future research directions," *IEEE Wireless Communications*, vol. 24, no. 3, pp. 17–25, 2017.

[5] L. Zhang, Y. Liang, and M. Xiao, "Spectrum sharing for internet of things: A survey," *IEEE Wireless Communications*, vol. 26, no. 3, pp. 132–139, 2019.

[6] Y. C. Liang, Q. Zhang, E. G. Larsson, and G. Y. Li, "Symbiotic radio: Cognitive backscattering communications for future wireless networks," *IEEE Transactions on Cognitive Communications and Networking*, vol. 6, no. 4, pp. 1242–1255, 2020.

[7] X. Kang, Y. Liang, and J. Yang, "Riding on the primary: A new spectrum sharing paradigm for wireless-powered iot devices," *IEEE Transactions on Wireless Communications*, vol. 17, no. 9, pp. 6335–6347, 2018.

[8] G. Yang, D. Yuan, Y. Liang, R. Zhang, and V. C. M. Leung, "Optimal resource allocation in full-duplex ambient backscatter communication networks for wireless-powered iot," *IEEE Internet of Things Journal*, vol. 6, no. 2, pp. 2612–2625, 2019.

[9] Y. Zhang, B. Li, F. Gao, and Z. Han, "A robust design for ultra reliable ambient backscatter communication systems," *IEEE Internet of Things Journal*, vol. 6, no. 5, pp. 8989–8999, 2019.

[10] D. Li, "Two birds with one stone: Exploiting decode-and-forward relaying for opportunistic ambient backscattering," *IEEE Transactions on Communications*, vol. 68, no. 3, pp. 1405–1416, 2020.

[11] C. Boyer and S. Roy, "— invited paper — backscatter communication and RFID: Coding, energy, and mimo analysis," *IEEE Transactions on Communications*, vol. 62, no. 3, pp. 770–785, 2014.

[12] B. Ji, Z. Chen, S. Chen, B. Zhou, C. Li, and H. Wen, "Joint optimization for ambient backscatter communication system with energy harvesting for IoT," *Mechanical Systems and Signal Processing*, vol. 135, p. 106412, 2020.

[13] H. Yang, Y. Ye, and X. Chu, "Max-min energy-efficient resource allocation for wireless powered backscatter networks," *IEEE Wireless Communications Letters*, vol. 9, no. 5, pp. 688–692, 2020.

[14] N. Van Huynh, D. T. Hoang, X. Lu, D. Niyato, P. Wang, and D. I. Kim, "Ambient backscatter communications: A contemporary survey," *IEEE Communications Surveys Tutorials*, vol. 20, no. 4, pp. 2889–2922, 2018.

[15] B. Lyu, C. You, Z. Yang, and G. Gui, "The optimal control policy for RF-powered backscatter communication networks," *IEEE Transactions on Vehicular Technology*, vol. 67, no. 3, pp. 2804–2808, 2018.

[16] H. Guo, Y. Liang, R. Long, S. Xiao, and Q. Zhang, "Resource allocation for symbiotic radio system with fading channels," *IEEE Access*, vol. 7, pp. 34333–34347, 2019.

[17] Q. Zhang, L. Zhang, Y. Liang, and P. Y. Kam, "Backscatter-NOMA: An integrated system of cellular and internet-of-things networks," in *2019-2019 IEEE International Conference on Communications (ICC)*, pp. 1– 6, 2019.

[18] R. Long, H. Guo, and Y. Liang, "Symbiotic radio with full-duplex backscatter devices," in *2019 - 2019 IEEE International Conference on Communications (ICC)*, pp. 1–6, 2019.

[19] Z. Chu, W. Hao, P. Xiao, M. Khalily, and R. Tafazolli, "Resource allocations for symbiotic radio with finite blocklength backscatter link," *IEEE Internet of Things Journal*, vol. 7, no. 9, pp. 8192–8207, 2020.

[20] X. Lu, D. Niyato, H. Jiang, D. I. Kim, Y. Xiao, and Z. Han, "Ambient backscatter assisted wireless powered communications," *IEEE Wireless Communications*, vol. 25, no. 2, pp. 170–177, 2018.

[21] Y. Ye, L. Shi, R. Qingyang Hu, and G. Lu, "Energy-efficient resource allocation for wirelessly powered backscatter communications," *IEEE Communications Letters*, vol. 23, no. 8, pp. 1418–1422, 2019.

[22] D. Tse and P. Viswanath, "Fundamentals of wireless communication," Cambridge, U.K.: Cambridge Univ. Press, 2005.

[23] G. Yang, Q. Zhang, and Y.-C. Liang, "Cooperative ambient backscatter communications for green internet-of-things," *IEEE Internet of Things Journal*, vol. 5, no. 2, pp. 1116–1130, 2018.

[24] Y. Xin, D. Wang, J. Li, H. Zhu, J. Wang, and X. You, "Area spectral efficiency and area energy efficiency of massive mimo cellular systems," *IEEE Transactions on Vehicular Technology*, vol. 65, no. 5, pp. 3243– 3254, 2016.

[25] S. Guo, Y. Shi, Y. Yang, and B. Xiao, "Energy efficiency maximization in mobile wireless energy harvesting sensor networks," *IEEE Transactions on Mobile Computing*, vol. 17, no. 7, pp. 1524–1537, 2018.

[26] T. Liu, X. Qu, F. Yin, and Y. Chen, "Energy efficiency maximization for wirelessly powered sensor networks with energy beamforming," *IEEE Communications Letters*, vol. 23, no. 12, pp. 2311–2315, 2019.

[27] H. Zhang, M. Feng, K. Long, G. K. Karagiannidis, V. C. M. Leung, and H. V. Poor, "Energy efficient resource management in SWIPT enabled heterogeneous networks with NOMA," *IEEE Transactions on Wireless Communications*, vol. 19, no. 2, pp. 835–845, 2020.

[28] W. Dinkelbach, "On nonlinear fractional programming," Management Science, vol. 13, pp. 492–498, March 1967, Available: http://www.jstor. org/stable/2627691.

[29] D. W. K. Ng, E. S. Lo, and R. Schober, "Energy-efficient resource allocation in OFDMA systems with large numbers of base station antennas," *IEEE Transactions on Wireless Communications*, vol. 11, no. 9, pp. 3292–3304, 2012.

[30] D. W. K. Ng, E. S. Lo, and R. Schober, "Wireless information and power transfer: Energy efficiency optimization in OFDMA systems," *IEEE Transactions on Wireless Communications*, vol. 12, no. 12, pp. 6352– 6370, 2013.

[31] J. Gondzio and T. Terlaky, "A computational view of interior point methods," JE Beasley. *Advances in Linear and Integer Programming. Oxford Lecture Series in Mathematics and its Applications*, vol. 4, pp. 103–144, 1996.

[32] H. Zhang, C. Jiang, N. C. Beaulieu, X. Chu, X. Wen, and M. Tao, "Resource allocation in spectrum-sharing OFDMA femtocells with heterogeneous services," *IEEE Transactions on Communications*, vol. 62, no. 7, pp. 2366–2377, 2014.

Chapter 7

Paper IV

Energy Efficiency Maximization for UAV-Enabled Hybrid Backscatter-Harvest-then-Transmit Communications

Haohang Yang, Yinghui Ye, Xiaoli Chu and Sumei Sun

Published in *IEEE Transactions on Wireless Communication*, DOI: 10.1109/TWC.2021.3116509, Date of Publication: 06 October 2021.

Energy Efficiency Maximization for UAV-Enabled Hybrid Backscatter-Harvest-then-Transmit Communications

Haohang Yang[1], Yinghui Ye[2], Xiaoli Chu[1] and Sumei Sun[3]

[1] Department of Electronic and Electrical Engineering, the University of Sheffield, Sheffield, S1 4ET, United Kingdom

[2] Shaanxi Key Laboratory of Information Communication Network and Security, Xi'an University of Posts & Telecommunications, China

[3] Institute for Infocom Research, A*STAR, 138632, Singapore

Abstract

Wireless powered communication via backscatter and/or harvest-then-transmit (HTT) has been considered a promising solution to connecting nodes in the Internet of things (IoT) networks. However, the harvested energy at an IoT node is heavily limited by the distance between the node and the power beacon (PB) due to the high propagation loss. In this paper, we propose to employ an unmanned aerial vehicle (UAV) as a mobile PB to provide energy signals on demand to the IoT nodes, which convey their information to a reader via backscattering or active transmission using the harvested energy. We maximize the total energy efficiency (EE) of all the IoT nodes powered by the UAV by jointly optimizing the UAV's transmit power and trajectory, the IoT nodes' backscatter reflection coefficients and their transmit power for active transmission, and the time allocation between backscattering and active transmission. To solve the formulated non-linear fractional programming problem, we use the generalized fractional programming theory and a block coordinated decent method to decompose it into two sub-problems: one optimizes the communication resource allocation under a fixed UAV trajectory, and the other optimizes the UAV trajectory with given communication resource allocation. We then devise a Dinkelbach-based iterative algorithm to solve the two sub-problems by employing a Lagrangian dual method and a successive convex programming technique, respectively and iteratively. Simulation results show that our proposed iterative algorithm

converges very fast, and the optimized UAV-enabled hybrid backscatter-HTT communication achieves a much higher EE of all the IoT nodes than the benchmark schemes including the UAV-enabled backscatter, UAV-enabled HTT, and hybrid BackCom-HTT with a fixed PB.

1 Introduction

Due to the limited battery capacity of low-powered Internet of Things (IoT) nodes, wireless powered communication networks (WPCNs) have been proposed to support IoT, where the IoT nodes can either harvest RF energy from an energy source and then use the harvested energy to convey information via active transmission, i.e., harvest-then-transmit (HTT) [1]-[4], or modulate and backscatter the incident radio frequency (RF) signal to carry its information to the associated receiver without requiring an active transceiver [5]-[8]. The circuit power consumption of backscatter communications (BackCom) is very low and can be supported by the harvested RF energy. However, BackCom cannot realize when the incident signals are not available. Meanwhile, HTT can solve this problem but its energy consumption is normally high [5]-[8]. To exploit the complementarity of BackCom and HTT, hybrid BackCom-HTT communications have been proposed. The authors in [8] solved a max-min throughput problem among multiple sensor nodes for a wireless powered IoT network. In [9], the wireless powered nodes were allowed to operate in backscatter mode when the harvested energy from the dedicated RF signals is not sufficient to support HTT, where the time allocated for backscattering was optimized to maximize the throughput. The authors in [10] proposed hybrid BackCom-HTT for a cognitive WPCN, where the throughput of the secondary communication system was maximized by optimizing the time allocation between backscattering and energy harvesting and that between the bistatic backscatter mode and the HTT mode. In [11], the time allocation between data backscattering and energy harvesting, as well as the time sharing among multiple transmitters were optimized to maximize the throughput of a RF-powered backscatter cognitive radio network. The authors in [12] maximized the energy efficiency (EE) of all the devices in a hybrid BackCom-HTT network by optimizing the transmit power of the power beacon (PB) and hybrid devices, and the time allocation among energy harvesting, the backscatter mode and the HTT mode.

Although the above works [9]-[12] demonstrated the superior performance of hybrid BackCom-HTT over BackCom or HTT in terms of throughput and EE, they considered a fixed RF energy source, e.g., a PB, where the received power at IoT nodes is limited by their distance to the PB due to severe RF propagation loss [13]. Recently, unmanned aerial vehicles (UAVs) have been employed as mobile PB to provide RF energy to IoT nodes via line-of-sight (LoS) links. In [14], the UAV's trajectory was optimized to maximize the total energy harvested by all the IoT nodes wirelessly powered by it. In [15], a max-min throughput problem was solved in a UAV-enabled WPCN, where a UAV was dispatched as a mobile access point (AP). In [16], the system throughput of a UAV-aided BackCom network was maximized by optimizing the time allocation, backscatter reflection coefficient, and UAV trajectory for two protocols, namely transmit-backscatter and transmit-backscatter-relay, where the direct link from the backscatter device to the receiver of the latter protocol is not available. In [17], two UAVs were used to wirelessly power two IoT devices and collect information from them, and the minimum uplink throughput of the two IoT devices was maximized through jointly optimizing the trajectories of the two UAVs and the downlink/uplink wireless resource allocation. The above works indicate that the UAV-enabled networks can achieve better performance in terms of throughput and energy transmission compared with fixed PB based networks. However, we note that UAV-carried mobile PB has not been exploited for emerging hybrid BackCom-HTT networks. This motivates us to configure a new network which fully makes the use of the advantages of UAV and BackCom-HTT.

In this paper, we propose a novel UAV-enabled hybrid BackCom-HTT communication system to connect multiple IoT nodes to a reader, where a UAV is dispatched as a mobile PB to provide RF energy for all the IoT nodes. Based on a time-division multiple access (TDMA) protocol, an IoT node first backscatters the incident RF signal from the UAV to carry its own information to the reader, while harvesting the RF power for supporting its circuit operation together with the other IoT nodes, and then utilizes the remaining energy to transmit information to the reader via active transmission. We then maximize the total EE of all the IoT nodes wirelessly powered by the UAV.

Our main contributions are summarized as follows:

- We propose a novel system model, namely the UAV-enabled hybrid BackCom-HTT communication network, where a UAV works as a mobile energy source to provide RF energy for all the ground IoT nodes. The IoT nodes utilize the incident RF signal to communicate with a reader via a hybrid BackCom-HTT scheme.

- To exploit the synergy between hybrid BackCom-HTT communications and UAV, we formulate a problem to maximize the EE of all the IoT nodes in the UAV-enabled hybrid BackCom-HTT system by jointly optimizing the UAV's transmit power and trajectory and the allocation of communication resources, including the backscatter reflection coefficients, the transmit power of IoT nodes during active transmission, and the time allocation between BackCom and active transmission.

- Since the EE of multiple IoT nodes are jointly maximized, the formulated optimization problem involves many variables that are coupled in the objective function and/or the constraints. Through theoretical analysis, we reveal that letting the UAV transmit with the maximum power maximizes the EE of all the IoT nodes. Leveraging this finding and the generalized fractional programming theory, we transform the original optimization problem into a more tractable but still non-convex problem. Then, we use a block coordinated decent (BCD) method to decompose the transformed problem into two sub-problems: one optimizes the communication resource allocation with a fixed UAV trajectory and the other optimizes the UAV trajectory with given communication resource allocation. We employ a Lagrangian dual method to solve the former sub-problem optimally and apply a successive convex programming (SCP) technique to obtain a locally optimal solution to the latter sub-problem. The closed-form expressions for the optimal reflection coefficient and active transmit power of each IoT node are derived. Based on the obtained solutions, we propose a Dinkelbach based iterative algorithm to maximize the EE of all the IoT nodes in the UAV-enabled hybrid BackCom-HTT system.

- We perform extensive simulations to evaluate the optimized UAV trajectory, time allocation for BackCom and active transmission, the convergence of our proposed iterative algorithm, and the EE of all the IoT nodes achieved by our proposed algorithm in com-

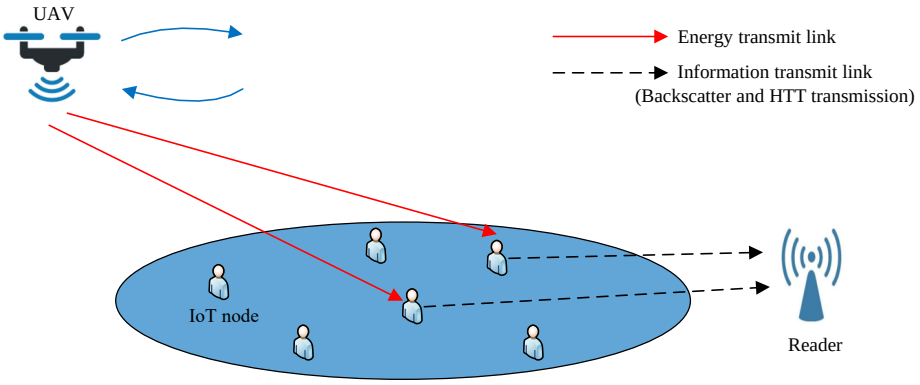

Fig. 1 UAV-enabled hybrid BackCom-HTT network.

parison with that of several benchmark schemes including the UAV-enabled backscatter, UAV-enabled HTT, energy consumption minimization, and hybrid BackCom-HTT with a fixed PB. The simulation results show that the proposed algorithm has a fast convergence speed, and can achieve a much higher total EE than the benchmark schemes. In addition, we observe that a higher EE is achieved for all the IoT nodes when more time is allocated to those IoT nodes with better channel conditions to the UAV and the reader for BackCom and active transmissions, repectively. Also, the UAV tends to fly towards to those IoT nodes with better channel condition.

The rest of the paper is organized as follows. The system model of a UAV-enabled hybrid BackCom-HTT network is built in Section 2. In Section 3, the total EE maximization problem is formulated and solved. Section 4 analyzes the convergence and computational complexity of our proposed algorithms. In Section 5, the numerical results are presented. Section 6 concludes the paper.

2 System Model

In this section, we present the system model, and the associated throughput analysis and definition of the total EE.

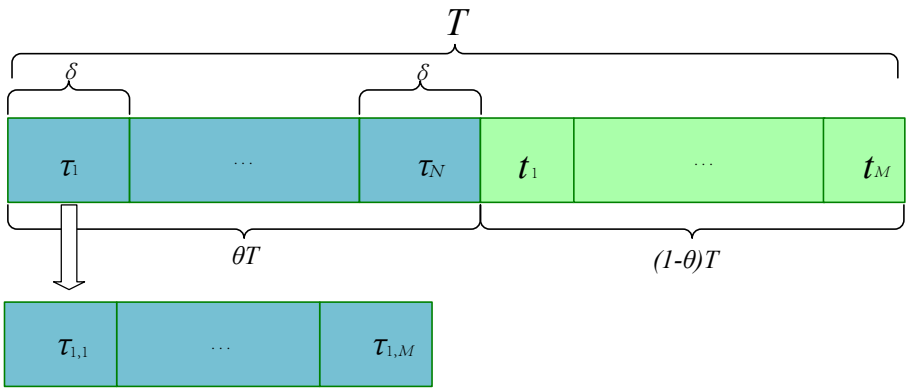

Fig. 2 Time allocation scheme.

2.1 Network Model

As illustrated in Fig. 1, the proposed UAV-enabled hybrid BackCom-HTT network consists of one UAV, M IoT nodes and one reader, where the IoT nodes harvest energy from the UAV's RF transmission and transmit information to the reader through hybrid BackCom and HTT within the time block T. We assume that each IoT node is equipped with a backscatter circuit, an EH module, and an active RF transmitter such that they can operate in the BackCom and HTT modes. Each IoT node $i \in \mathscr{M} = \{1, \cdots, M\}$ is deployed at a fixed location $q_i^g = (x_i, y_i)$ on the ground in a 2-D Cartesian coordinate system. The reader is fixed at the location $q^r = (x^r, y^r)$. The UAV is assumed to fly at a fixed altitude $H > 0$ above the ground, and the location of the UAV in the 2D horizontal plane at altitude H at any time instant $t \in T$ is denoted by $q_t^u = (x_t^u, y_t^u)$. We assume that all the IoT nodes are inside a region on the ground, while the UAV is dispatched from an initial location $q_{ini}^u = (x_{ini}^u, y_{ini}^u)$ outside this region to provide energy for the IoT nodes and then flies back to q_{ini}^u at the end of the BackCom time period.

The entire time block T is divided into two time periods, i.e., θT $(0 < \theta \leq 1)$ for BackCom and $(1-\theta)T$ for HTT active transmission by utilizing the energy harvested within θT, as shown in Fig. 2. During the first time period, a UAV is dispatched to provide energy for the IoT nodes to backscatter their own information to the reader via BackCom, and the IoT node-to-reader BackComs follow a TDMA protocol. For simplicity, the first time period of θT is equally divided into N time slots, where the n-th time slot $\tau_n, n \in \mathscr{N} = \{1, 2, \cdots, N\}$, has a duration of $\delta = \frac{\theta T}{N}$. We assume that the value of N is sufficiently large so that the UAV can be

considered as static at each time slot [14]-[16], and $N >> M$. Let q_n^u denote the location of the UAV at time slot n. Thus, the distance between the UAV and IoT node i at time slot n is given by

$$d_{i,n}^u = \sqrt{||q_n^u - q_i^g||^2 + H^2}, \tag{1}$$

where $||\cdot||$ denotes the Euclidean norm of a vector.

Following [16], [18], [19], we adopt the following Rician fading channel model for UAV communications:

$$h_{i,n}^u = \beta_0 (d_{i,n}^u)^{-2} ||\mu_{i,n}^{(1)}||^2 = \frac{\beta_0 ||\mu_{i,n}^{(1)}||^2}{||q_n^u - q_i^g||^2 + H^2}, \tag{2}$$

where β_0 denotes the channel power gain at a reference distance of $d_0 = 1$m, and $\mu_{i,n}^{(1)}$ denotes the small-scale fading and is modeled as

$$\mu_{i,n}^{(1)} = \sqrt{\frac{K}{K+1}} \hat{\mu}_{i,n}^{(1)} + \sqrt{\frac{1}{K+1}} \hat{\hat{\mu}}_{i,n}^{(1)}, \tag{3}$$

where $\hat{\mu}_{i,n}^{(1)}$ denotes the LoS channel coefficient with $||\hat{\mu}_{i,n}^{(1)}|| = 1$, $\hat{\hat{\mu}}_{i,n}^{(1)}$ represents the non-LoS channel coefficient, which is a circularly symmetric complex Gasussian random variable with mean zero and variance 1, and K is the Rician factor. In this paper, it is reasonable to assume that the channel from the UAV to an IoT node is dominated by the LoS path [20]-[23]. Thus, the Rician factor K is very large, and the channel model in (2) approximately reduces to $h_{i,n}^u = \beta_0 (d_{i,n}^u)^{-2} ||\hat{\mu}_{i,n}^{(1)}||^2$, which is equivalent to a free-space path-loss model [16]. Hence, the channel from the UAV to an IoT node can be estimated based on the locations of the UAV and IoT nodes.

To ensure that every IoT node has a chance to backscatter its information to the reader in each time slot, a time slot is further divided into M sub-slots [15], where the ith sub-slot is allocated to IoT node i. Let $\tau_{i,n}$ denote the backscattering time for IoT node i at time slot n and $\sum_{i=1}^{M} \tau_{i,n} = \frac{\theta T}{N}$ holds for $\forall n \in \mathcal{N}$.

When IoT node i is in the backscatter mode, its received RF signal from the UAV is divided into two parts [7]: a $Z_{i,n}$ portion of the received power is used for BackCom to the reader, and the rest is harvested for supporting its circuit consumption, where $Z_{i,n} \in [0,1]$ is the reflection

coefficient[1]. Accordingly, the total amount of energy harvested by IoT node i during the first time period θT is given by

$$EH_i = \sum_{n=1}^{N} \left(P^u \eta h_{i,n}^u (1 - Z_{i,n}) \tau_{i,n} + P^u \eta h_{i,n}^u \left(\frac{\theta T}{N} - \tau_{i,n} \right) \right) = \sum_{n=1}^{N} P^u \eta h_{i,n}^u \left(\frac{\theta T}{N} - \tau_{i,n} Z_{i,n} \right). \tag{4}$$

where P^u represents the UAV transmit power, η is the energy conversion efficiency of the EH circuit, which is assumed to include the EH circuit power consumption. We ignore the energy harvested from the signals backscattered by the other IoT nodes and the thermal noise, since their power is much smaller than P^u [9], [10], [12]. During the second time period of $(1-\theta)T$, the IoT nodes utilize the remaining harvested energy (after deducting the circuit energy consumption) to transmit information to the reader via active transmission. Same as in BackCom period, TDMA is used. We divide $(1-\theta)T$ into M time slots, where the ith time slot of duration t_i is allocated to the ith IoT node for active transmission, and we have $\sum_{i=1}^{M} t_i = (1-\theta)T$.

2.2 Throughput of BackCom and HTT

The sum received power at the reader from IoT node i via BackCom and from the UAV at time slot n is given by [22]

$$P_{i,n}^{r,B} = P^u Z_{i,n} h_{i,n}^u h_i^r + P^u h_n^{u,r}, \tag{5}$$

where $h_i^r = \beta_0 (d_i^r)^{-\alpha} ||\mu_i^{(2)}||^2$ denotes the channel power gain from IoT node i to the reader and $d_i^r = ||q_i^g - q^r||$, where α is the free space path loss exponent and $||\mu_i^{(2)}||^2$ represents the Rayleigh fading power gain. The channel power gain from the UAV to the reader is denoted as $h_n^{u,r}$. Since the UAV serves as the dedicated energy source, its transmitted signal is a priori known to the reader, and the interference $P^u h^{u,r}$ can be removed by the reader. After the UAV

[1]The backscattered signal is composed of two components: the structural mode scattering component and the antenna mode scattering component. In this paper, we only consider the antenna mode scattering component, which is characterized by the reflection coefficient, because the structural mode scattering is determined by the geometrical layout of the reflective device antenna and the electromagnetic properties of the material, and can be regarded as a constant value [24].

interference has been removed, the received power at the reader at time slot n is rewritten as $P_{i,n}^{r,B'} = P^u Z_{i,n} h_{i,n}^u h_i^r$ [26].

Thus, the BackCom throughput of IoT node i-to-reader link at time slot n can be calculated as

$$R_{i,n}^B = W\tau_{i,n}\log_2\left(1+\frac{\varphi P_{i,n}^{r,B'}}{W\sigma^2}\right), \tag{6}$$

where W is the system bandwidth. Since BackCom usually transmits modulated signals from a finite constellation, which is very different from Gaussian signaling widely adopted in conventional active communications, thus the conventional achievable rate formula cannot perfectly match with that in BackCom. We introduce φ to represent the performance gap between the active transmission and the BackCom [8]-[12], and σ^2 denotes the noise power spectral density.

The received power at the reader from the active transmission of IoT node i is given by

$$P_i^{r,H} = P_i h_i^r, \tag{7}$$

where P_i denotes the transmit power of IoT node i.

Then, the active transmission throughput of IoT node i-to-reader link is calculated as

$$R_i^H = Wt_i\log_2\left(1+\frac{P_i^{r,H}}{W\sigma^2}\right). \tag{8}$$

2.3 Total Energy Efficiency

The total EE of all the IoT nodes is defined as the ratio of the total throughput achieved by the IoT nodes to the total energy consumption of the IoT nodes [27][2]. Letting R_{sum} denote the total

[2]In this paper, we aim to maximize the total EE of all the IoT nodes by jointly optimizing how they harvest and use the RF energy transmitted by the UAV, which can be regarded as maximizing the efficiency of the IoT nodes in utilizing the RF energy provided by the UAV [12], [27]. The system EE that includes the UAV's energy consumption will be studied in our future work.

throughput achieved by all the IoT nodes in T, we have

$$R_{sum} = \sum_{i=1}^{M} \sum_{n=1}^{N} R_{i,n}^{B} + \sum_{i=1}^{M} R_{i}^{H}. \tag{9}$$

The energy consumption of IoT node i is given by $EC_i = \sum_{n=1}^{N} P_{cir}^{B} \tau_{i,n} + (P_{cir}^{H} + P_i) t_i$, where P_{cir}^{B} and P_{cir}^{H} represent the constant circuit power consumption for BackCom and active transmission, respectively, and they are assumed to be the same for all M IoT nodes.

The total energy consumption of all the IoT nodes is given by

$$EC_{sum} = \sum_{i=1}^{M} \sum_{n=1}^{N} P_{cir}^{B} \tau_{i,n} + \sum_{i=1}^{M} \left(P_{cir}^{H} + P_i\right) t_i, \tag{10}$$

Then, the total EE of all the IoT nodes is given by

$$EE_{sum} = \frac{R_{sum}}{EC_{sum}}. \tag{11}$$

3 Energy Efficiency Maximization

In this section, we first formulate the EE maximization problem for the considered UAV-aided hybrid BackCom-HTT IoT system, then we propose a Dinkelbach-based iterative algorithm to solve the optimization problem.

3.1 Problem Formulation

We propose to maximize the EE of all the IoT nodes by jointly optimizing the UAV's transmit power P^u, transmit time factor θ, and trajectory vector $\mathbf{q} = [q_1^u, q_2^u, ..., q_N^u]$, as well as the IoT nodes' BackCom reflection coefficient vectors $\mathbf{Z}_n = [Z_{1,n}, Z_{2,n}, \cdots, Z_{M,n}], n \in \mathcal{N}$, BackCom time allocation vectors $\boldsymbol{\tau}_n = [\tau_{1,n}, \tau_{2,n}, \cdots, \tau_{M,n}], n \in \mathcal{N}$, active transmission time allocation vector $\mathbf{t} = [t_1, t_2, \cdots, t_M]$, and active transmission power vector $\mathbf{P} = [P_1, P_2, \cdots, P_M]$. Accord-

ingly, the optimization problem is formulated as

$$
\begin{aligned}
\mathbf{P_1}: \quad & \max_{\{P^u,\theta,\mathbf{Z}_n,\boldsymbol{\tau}_n,\mathbf{t},\mathbf{P},\mathbf{q}\}} EE_{sum} \\
\text{s.t.} \quad & \\
& \text{C1}: \ 0 \le \theta \le 1, 0 \le Z_{i,n} \le 1, \tau_{i,n} \ge 0, t_i \ge 0, \forall i, \forall n; \\
& \text{C2}: \ 0 \le P^u \le P_{\max}^{\text{UAV}}, 0 \le P_i \le P_{\max}^{\text{node}}, \forall i; \\
& \text{C3}: \ \sum_{i=1}^{M} \tau_{i,n} = \frac{\theta T}{N}; \ \sum_{i=1}^{M} t_i = (1-\theta)T, \forall n; \\
& \text{C4}: \ \sum_{n=1}^{N} R_{i,n}^{B} + R_i^{H} \ge R_{\min}, \forall i; \\
& \text{C5}: \ 0 \le P_i t_i \le EH_i - \sum_{n=1}^{N} P_{cir}^{B} \tau_{i,n} - P_{cir}^{H} t_i, \forall i; \\
& \text{C6}: \ EH_i - EC_i \ge 0, \forall i; \\
& \text{C7}: \ ||q_n^u - q_{n-1}^u|| \le V_{\max}\delta, \forall n; \\
& \text{C8}: \ q_1^u = q_{ini}^u, q_N^u = q_{ini}^u;
\end{aligned}
\tag{12}
$$

In (12), C1 specifies the value ranges of the transmit time factor, the reflection coefficient factors, and the transmit time allocation factors for both BackCom and active transmission. $P_{\max}^{\text{UAV}}$ and $P_{\max}^{\text{node}}$ in C2 denote the maximum transmit power of the UAV and the IoT nodes, respectively. C3 constrains the total transmit time for both BackCom and active transmission. C4 guarantees the long-term minimum throughput requirement for each IoT node. In C5, the transmit power consumption of each IoT node cannot exceed the remaining harvested energy after BackCom. C6 ensures that the power consumption of each IoT node during BackCom and active transmission should not exceed the energy harvested by the IoT node within θT. C7 constrains the maximum speed of the UAV, $V_{\max}$, by limiting its flight distance during each time slot. In C8, the UAV is dispatched from an initial location and flies back to the initial location at the end of the first time period.

The formulated problem $\mathbf{P_1}$ is a non-convex fractional optimization problem with multiple variables coupling in both the objective function and the constraints, i.e., P^u, $\mathbf{Z}_n$, $\boldsymbol{\tau}_n$, $\mathbf{t}$, $\mathbf{P}$ and $\mathbf{q}$. Thus, it would be extremely difficult to solve $\mathbf{P_1}$ directly. In order to make this optimization problem more tractable, we first determine the optimal transmit power of the UAV, as summarized in Lemma 1.

Lemma 1: In our proposed system model, the optimal transmit power of the UAV for maximizing the total EE of all the IoT nodes is the maximum UAV transmit power, i.e., $P^{u*} = P_{\max}^{\text{uav}}$, where * denotes the optimal solution.

Proof. Please see Appendix A. ■

Remark 1: Lemma 1 indicates that letting the UAV transmit with the maximum allowed power can maximize the EE of all the ground IoT nodes. For BackCom, since the IoT nodes reflect the incident RF signal from the UAV, the throughput of BackCom improves with higher UAV transmit power without increasing the IoT node's power consumption, thus the EE of IoT nodes increases. For active transmission, the higher UAV transmit power reduces the time for harvesting energy, and the IoT nodes will have more time to transmit information to the reader, thus increasing the throughput and the EE. This insight can be supported by Remark 3, where the whole time block needs to be used up for achieving the maximum EE.

3.2 Problem Transformation

Based on Lemma 1, $\mathbf{P_1}$ is transformed into

$$\mathbf{P_2}: \max_{\{\theta,\mathbf{Z}_n,\boldsymbol{\tau}_n,\mathbf{t},\mathbf{P},\mathbf{q}\}} \frac{\sum_{i=1}^{M}\sum_{n=1}^{N} W\tau_{i,n}\log_2\left(1+\frac{\varphi P_{\max}^{\text{uav}} h_{i,n}^{tt} Z_{i,n} h_i^r}{W\sigma^2}\right)+\sum_{i=1}^{M} W t_i \log_2\left(1+\frac{P_i h_i^r}{W\sigma^2}\right)}{\sum_{i=1}^{M}\sum_{n=1}^{N} P_{cir}^{B}\tau_{i,n}+\sum_{i=1}^{M}(P_{cir}^{H}+P_i)t_i}$$

$$\text{s.t.} \quad \text{C1}, \text{C3}, \text{C4}, \text{C6}, \text{C7}, \text{C8}; \quad \text{C2}-1: \ 0 \le P_i \le P_{\max}^{\text{node}}, \forall i; \tag{13}$$

Next, we employ Dinkelbach's method to transform the fractional objective function into a subtractive form. Letting Q^* denote the maximum EE, based on [28], Q^* can be achieved if and only if the following equation holds:

$$\max_{\{\theta,\mathbf{Z_n},\boldsymbol{\tau_n},\mathbf{t},\mathbf{P},\mathbf{q}\}} \sum_{i=1}^{M}\sum_{n=1}^{N} R_{i,n}^{B} + \sum_{i=1}^{M} R_i^H - Q^* EC_{sum} = \sum_{i=1}^{M}\sum_{n=1}^{N} R_{i,n}^{B\,*} + \sum_{i=1}^{M} R_i^{H*} - Q^* EC_{sum}^* = 0. \tag{14}$$

Based on (13), $\mathbf{P_2}$ is transformed into

$$\begin{aligned} \mathbf{P_3}: \quad & \max_{\{\theta,\mathbf{Z}_n,\boldsymbol{\tau}_n,\mathbf{t},\mathbf{P},\mathbf{q}\}} \sum_{i=1}^{M}\sum_{n=1}^{N} R_{i,n}^{B} + \sum_{i=1}^{M} R_i^{H} - Q^* EC_{sum} \\ & \text{s.t. } \mathrm{C1}, \mathrm{C2}-1, \mathrm{C3}, \mathrm{C4}, \mathrm{C6}, \mathrm{C7}, \mathrm{C8}. \end{aligned} \tag{15}$$

where Q denotes a small positive value that is used as the initial value of Q*. Although $\mathbf{P_3}$ is more tractable than P_2, it is still non-convex due to the coupling between $\mathbf{Z}_n$ and $\boldsymbol{\tau}_n$, $\mathbf{P}$ and $\mathbf{t}$. We solve this coupling issue by introducing the following auxiliary vectors: $\mathbf{X}_n = [X_{1,n}, X_{2,n}, \cdots, X_{M,n}], n \in \mathscr{N}$ and $\mathbf{Y} = [Y_1, Y_2, \cdots, Y_M]$, where $X_{i,n} = Z_{i,n}\tau_{i,n}$ and $Y_i = P_i t_i$. Then, $\mathbf{P_3}$ is transformed into

$$\begin{aligned} \mathbf{P_4}: \quad & \max_{\{\theta,\mathbf{X}_n,\boldsymbol{\tau}_n,\mathbf{t},\mathbf{Y},\mathbf{q}\}} \sum_{i=1}^{M}\sum_{n=1}^{N} R_{i,n}^{B\,'} + \sum_{i=1}^{M} R_i^{H'} - Q^* EC_{sum}{}' \\ & \text{s.t.} \\ & \quad \mathrm{C3}, \mathrm{C7}, \mathrm{C8}; \\ & \quad \mathrm{C1}-1: \ 0 \le \theta \le 1, \tau_{i,n} \ge 0, \mathbf{t} \ge 0, \forall i, \forall n; \\ & \quad \mathrm{C2}-2: \ 0 \le X_{i,n} \le \tau_{i,n}, 0 \le Y_i \le t_i P_{\max}^{node}, \forall i, \forall n; \\ & \quad \mathrm{C4}-1: \ \sum_{n=1}^{N} R_{i,n}^{B\,'} + R_i^{H'} \ge R_{\min}, \forall i, \forall n; \\ & \quad \mathrm{C6}-1: \ EH_i' - EC_i' \ge 0, \forall i, \end{aligned} \tag{16}$$

where $R_{i,n}^{B\,'} = W\tau_{i,n}\log_2\left(1 + \frac{\varphi P_{max}^{uav} X_{i,n} h_{i,n}^u h_i^r}{\tau_{i,n} W\sigma^2}\right), R_i^{H'} = W\, t_i \log_2\left(1 + \frac{Y_i h_i^r}{t_i W\sigma^2}\right), EC_i' = \sum_{n=1}^{N} PC^B \tau_{i,n}$ $+(PC^H\ t_i + Y_i)$, and the total amount of energy harvested by IoT node i during BackCom is rewritten as

$$\begin{aligned} EH_i' &= \sum_{n=1}^{N} \left[P_{max}^{uav} \eta h_{i,n}^u (\tau_{i,n} - X_{i,n}) + P_{max}^{uav} \eta h_{i,n}^u \left(\frac{\theta T}{N} - \tau_{i,n}\right) \right] \\ &= \sum_{n=1}^{N} P_{max}^{uav} \eta h_{i,n}^u \left(\frac{\theta T}{N} - X_{i,n}\right). \end{aligned} \tag{17}$$

3.3 Problem Solution

We note that $\mathbf{P_4}$ is still non-convex and challenging to solve due to the coupling among the UAV trajectory $\mathbf{q}$, $\mathbf{X}_n$ and $\boldsymbol{\tau}_n$ in the objective function, C4-1 and C6-1. To this end, we

propose a BCD method to decompose $\mathbf{P_4}$ into two sub-problems, namely, the optimization of communication resource allocation including θ, $\mathbf{X}_n$, $\mathbf{Y}$, $\boldsymbol{\tau}_n$, and $\mathbf{t}$ with fixed UAV trajectory, and the optimization of the UAV trajectory optimization for a given communication resource allocation. Then, we solve $\mathbf{P_4}$ by solving these two subproblems alternately. This process leads to a Dinkelbach based iterative algorithm given in **Algorithm 1**.

3.3.1 Communication resource allocation optimization

For a given UAV trajectory $\mathbf{q}$, the communication resource allocation sub-problem is formulated as

$$\begin{aligned}\mathbf{P_{4.1}}: \ & \max_{\{\theta,\mathbf{X}_n,\boldsymbol{\tau}_n,\mathbf{Y},\mathbf{t}\}} \sum_{i=1}^{M}\sum_{n=1}^{N} {R_{i,n}^{B}}' + \sum_{i=1}^{M} {R_i^{H}}' - Q^* {EC_{sum}}' \\ & \text{s.t.} \\ & \quad \text{C1}-1, \text{C2}-2, \text{C3}, \text{C4}-1, \text{C6}-1.\end{aligned} \tag{18}$$

It is easy to verify that $\mathbf{P_{4.1}}$ is a standard convex optimization problem. In the following, we will solve this problem by using the Karush-Kuhn-Tucker (KKT) conditions. First, the Lagrangian function for $\mathbf{P_{4.1}}$ is given by

$$\begin{aligned}&\mathbb{L}(\theta,\mathbf{X}_n,\boldsymbol{\tau}_n,\mathbf{Y},\mathbf{t},\boldsymbol{\alpha}_n^{(1)},\boldsymbol{\alpha}^{(2)},\boldsymbol{\beta}^{(1)},\beta^{(2)},\boldsymbol{\gamma},\boldsymbol{\phi}) \\ &= \sum_{i=1}^{M}\sum_{n=1}^{N} W\tau_{i,n}\log_2\left(1+\frac{\varphi P_{\max}^{uav} h_{i,n}^{u} X_{i,n} h_i^{r}}{\tau_{i,n} W\sigma^2}\right) \\ &+ \sum_{i=1}^{M} W t_i \log_2\left(1+\frac{Y_i h_i^{r}}{t_i W\sigma^2}\right) - Q^*\left(\sum_{i=1}^{M}\sum_{n=1}^{N} PC^{B}\tau_{i,n} + \sum_{i=1}^{M}\left(PC^{H} t_i + Y_i\right)\right) \\ &+ \sum_{i=1}^{M}\sum_{n=1}^{N} \alpha_{i,n}^{(1)}(\tau_{i,n}-X_{i,n}) + \sum_{i=1}^{M}\alpha_i^{(2)}(t_i P_{\max}^{node}-Y_i) + \sum_{n=1}^{N}\beta^{(1)}(\frac{\theta T}{N}-\sum_{i=1}^{M}\tau_{i,n}) \\ &+\beta^{(2)}\left((1-\theta)T-\sum_{i=1}^{M} t_i\right) + \sum_{i=1}^{M}\gamma_i\left(\sum_{n=1}^{N}{R_{i,n}^{B}}' + {R_i^{H}}' - R_{\min}\right) + \sum_{i=1}^{M}\phi_i(EH_i' - {EC_{sum}}'),\end{aligned} \tag{19}$$

where $\boldsymbol{\alpha}_n^{(1)} = [\alpha_{1,n}^{(1)}, \alpha_{2,n}^{(1)}, \cdots, \alpha_{M,n}^{(1)}] \succeq \mathbf{0}, n \in \mathcal{N}$, $\boldsymbol{\alpha}^{(2)}$=$[\alpha_1^{(2)}, \alpha_2^{(2)}, \cdots, \alpha_M^{(2)}] \succeq \mathbf{0}$, $\boldsymbol{\beta}^{(1)}$=$[\beta_1^{(1)}, \beta_2^{(1)}, \cdots, \beta_N^{(1)}] \succeq \mathbf{0}$, $\beta^{(2)} \geq 0$, $\boldsymbol{\gamma}$=$[\gamma_1, \gamma_2, \cdots, \gamma_M] \succeq \mathbf{0}$ and $\boldsymbol{\phi}$=$[\phi_1, \phi_2, \cdots, \phi_M] \succeq \mathbf{0}$ are the Lagrange multipliers associated with C2-2, C3, C4-1 and C5-2, respectively. Please note that the non-negativity constraints in C1-1 and C2-2, i.e., $\theta \geq 0, \tau_{i,n} \geq 0, \mathrm{t_i} \geq 0$ and $X_{i,n} \geq 0, Y_i \geq 0$, are considered in the optimal solution in the following. Accordingly, the dual function of $\mathbf{P_{4.1}}$ is

denoted by $\mathbb{G}\left(\boldsymbol{\alpha}_n^{(1)}, \boldsymbol{\alpha}^{(2)}, \boldsymbol{\beta}^{(1)}, \beta^{(2)}, \boldsymbol{\gamma}, \boldsymbol{\phi}\right) = \max_{\theta, \mathbf{X}_n, \boldsymbol{\tau}_n, \mathbf{Y}, \mathbf{t}} \mathbb{L}\left(\theta, \mathbf{X}_n, \boldsymbol{\tau}_n, \mathbf{Y}, \mathbf{t}\right)$, and the Lagrangian dual optimization problem can be formulated as

$$\min_{\boldsymbol{\alpha}_n^{(1)}, \boldsymbol{\alpha}^{(2)}, \boldsymbol{\beta}^{(1)}, \beta^{(2)}, \boldsymbol{\gamma}, \boldsymbol{\phi}} \max_{\theta, \mathbf{X}_n, \boldsymbol{\tau}_n, \mathbf{Y}, \mathbf{t}} \mathbb{L}. \tag{20}$$

Since $\mathbf{P_{4.1}}$ is a standard convex optimization problem, it satisfies Slater's condition so that the duality gap between $\mathbf{P_{4.1}}$ and (20) is zero. Thus, we can solve $\mathbf{P_{4.1}}$ by maximizing $\mathbb{L}\left(\theta, \mathbf{X}_n, \boldsymbol{\tau}_n, \mathbf{Y}, \mathbf{t}\right)$ for given $\boldsymbol{\alpha}_n^{(1)}, \boldsymbol{\alpha}^{(2)}, \boldsymbol{\beta}^{(1)}, \beta^{(2)}, \boldsymbol{\gamma}, \boldsymbol{\phi}$, and minimizing $\mathbb{G}\left(\boldsymbol{\alpha}_n^{(1)}, \boldsymbol{\alpha}^{(2)}, \boldsymbol{\beta}^{(1)}, \beta^{(2)}, \boldsymbol{\gamma}, \boldsymbol{\phi}\right)$ for given $\theta, \mathbf{X}_n, \boldsymbol{\tau}_n, \mathbf{Y}, \mathbf{t}$. The details are provided as follows.

For given Lagrange multipliers, based on the KKT conditions, we take the derivative of $\mathbb{L}$ with respect to $X_{i,n}, Y_i, \tau_{i,n}, t_i$ and θ, respectively, yielding

$$\frac{\partial \mathbb{L}}{\partial X_{i,n}} = \frac{W(1+\gamma_i)\log_2 e}{\frac{X_{i,n}}{\tau_{i,n}} + \frac{W\sigma^2}{\varphi P_{\max}^{uav} h_{i,n}^u h_i^r}} - \alpha_{i,n}^{(1)} - \phi_i P_{\max}^{uav} \eta h_{i,n}^u, \tag{21}$$

$$\frac{\partial \mathbb{L}}{\partial Y_i} = \frac{W(1+\gamma_i)\log_2 e}{\frac{Y_i}{t_i} + \frac{W\sigma^2}{h_i^r}} - \alpha_i^{(2)} - Q^* - \phi_i, \tag{22}$$

$$\begin{aligned}\frac{\partial \mathbb{L}}{\partial \tau_{i,n}} = W(1+\gamma_i)&\left(\log_2\left(1 + \frac{\varphi P_{\max}^{uav} h_{i,n}^u h_i^r \frac{X_{i,n}}{\tau_{i,n}}}{W\sigma^2}\right) - \frac{\log_2 e}{1 + \frac{W\sigma^2}{\varphi P_{\max}^{uav} h_{i,n}^u h_i^r \frac{X_{i,n}}{\tau_{i,n}}}}\right) \\ &- Q^* P C^B + \alpha_{i,n}^{(1)} - \beta_n^{(1)} - \phi_i P C^B,\end{aligned} \tag{23}$$

$$\frac{\partial \mathbb{L}}{\partial t_i} = W(1+\gamma_i)\left(\log_2\left(1 + \frac{h_i^r \frac{Y_i}{t_i}}{W\sigma^2}\right) - \frac{\log_2 e}{1 + \frac{W\sigma^2}{h_i^r \frac{Y_i}{t_i}}}\right) - Q^* P C^H + \alpha_i^{(2)} P_{\max}^{node} - \beta^{(2)} - \phi_i P C^H, \tag{24}$$

$$\frac{\partial \mathbb{L}}{\partial \theta} = \sum_{n=1}^{N} \beta_n^{(1)} \frac{T}{N} - \beta^{(2)} T + \sum_{i=1}^{M} \sum_{n=1}^{N} \phi_i P_{\max}^{uav} \eta h_{i,n}^{u} \frac{T}{N}. \tag{25}$$

By letting (21) and (22) equal to 0, we obtain

$$Z_{i,n}^{*} = \frac{X_{i,n}}{\tau_{i,n}} = \min(1, W\left[\frac{(1+\gamma_i)\log_2 e}{\alpha_{i,n}^{(1)} + \phi_i P_{\max}^{uav} \eta h_{i,n}^{u}} - \frac{\sigma^2}{\varphi P_{\max}^{uav} h_{i,n}^{u} h_i^{r}}\right]^{+}), \tag{26}$$

$$P_i^{*} = \frac{Y_i}{t_i} = \min(P_{max}^{node}, W\left[\frac{(1+\gamma_i)\log_2 e}{\alpha_i^{(2)} + Q^{*} + \phi_i} - \frac{\sigma^2}{h_i^{r}}\right]^{+}), \tag{27}$$

where $Z_{i,n}^{*}$ and P_i^{*} denote the optimal reflection coefficient of IoT node i at time slot n during BackCom and the optimal transmit power of IoT node i during active transmission, respectively, and $[x]^{+} \triangleq \max\{x, 0\}$.

Remark 2: From (26), we find that $Z_{i,n}^{*}$ increases with higher h_i^{r}, indicating that an IoT node closer to the reader uses a higher reflection coefficient to backscatter information. The reason is that the UAV can afford to backscatter a higher portion of the incident RF signal power for achieving a higher EE, given that its circuit power consumption for BackCom is constant. From (27), we can see that P_i^{*} increases with h_i^{r}, which is the channel gain from IoT node i to the reader. That is, an IoT node with a better channel to the reader should transmit with higher power during active transmission. The resulting higher throughput will overweight the increased power consumption and lead to a higher EE.

Based on (25) and substituting (26) and (27) into (23) and (24), respectively, we find that the Lagrangian function $\mathbb{L}$ is linear with respect to $\tau_{i,n}, t_i$ and θ. This indicates that the optimal values of $\tau_{i,n}, t_i$ and θ can be found at the vertices of the feasible region. By substituting (26), (27) into $\mathbf{P_{4.1}}$ and after some manipulations, we obtain an equivalent optimization problem as

follows,

$$\begin{aligned}
&\max_{\theta,\boldsymbol{\tau}_n,\mathbf{t}} \sum_{i=1}^{M}\sum_{n=1}^{N} W\tau_{i,n}\left(\log_2\left(1+\frac{\varphi P_{\max}^{uav} h_{i,n}^{u} h_i^{r} Z_{i,n}^{*}}{W\sigma^2}\right)-Q^{*}PC^{B}\right)+\sum_{i=1}^{M} Wt_i\left(\log_2\left(1+\frac{h_i^{r}P_i^{*}}{W\sigma^2}\right)-Q^{*}(P_i^{*}+PC^{H})\right)\\
&\text{s.t.}\\
&\quad \text{C1}-1,\text{C3};\\
&\quad \text{C4}-2:\ \sum_{n=1}^{N} {R_{i,n}^{B}}'' + {R_i^{H}}'' \geq R_{\min},\forall i;\\
&\quad \text{C6}-2:\ {EH_i}'' - {EC_i}'' \geq 0,\forall i,
\end{aligned} \tag{28}$$

where ${R_{i,n}^{B}}'' = W\tau_{i,n}\log_2\left(1+\frac{\varphi P_{\max}^{uav} h_{i,n}^{u} h_i^{r} Z_{i,n}^{*}}{W\sigma^2}\right)$, ${R_i^{H}}'' = Wt_i\log_2\left(1+\frac{h_i^{r}P_i^{*}}{W\sigma^2}\right)$, ${EH_i}'' = P^{u}\eta h_{i,n}^{u}(\frac{\theta T}{N} - \tau_{i,n}Z_{i,n}^{*})$, and ${EC_i}'' = \sum_{n=1}^{N} PC^{B}\tau_{i,n} + (PC^{H}+P_i{}^{*})t_i$.

It is obvious that problem (28) is a linear programming problem with respect to $\tau_{i,n}, t_i$ and θ. Thus, we can solve problem (28) efficiently by using standard convex optimization tools, e.g., CVX tool. Then, $X_{i,n}$ and Y_i can be obtained by substituting $\tau_{i,n}$ and t_i back into (26) and (27), respectively.

Remark 3: In (28), the objective function is the weighted sum of $\tau_{i,n}$ and t_i. Thus, the maximum EE of all the ground IoT nodes can be achieved by allowing the IoT nodes to use up all the available time, i.e., T, for BackCom and active transmission. Furthermore, in order to maximize the EE, more time for BackCom and active transmission should be allocated to the IoT nodes with better channel conditions from themselves to the UAV and to the reader. For those IoT nodes whose channel conditions are not good enough to allow for EE improvement, the time allocated to them will guarantee that they can achieve their minimum throughput requirement. The above remark will be verified in Section 5.

Since the dual optimization problem in (20) is convex as is $\mathbf{P_{4.1}}$, for given $\tau_{i,n}, t_i$ and θ, we use a gradient based method to update the Lagrange multipliers $\boldsymbol{\alpha}_n^{(1)}, \boldsymbol{\alpha}^{(2)}, \boldsymbol{\beta}^{(1)}, \beta^{(2)}, \boldsymbol{\gamma}, \boldsymbol{\phi}$ as

follows,

$$\alpha_{i,n}^{(1)}(l+1) = \left[\alpha_{i,n}^{(1)}(l) - s_1(\tau_{i,n} - X_{i,n})\right]^+, \forall i, \forall n; \tag{29}$$

$$\alpha_i^{(2)}(l+1) = \left[\alpha_i^{(2)}(l) - s_2(t_i P_{\max}^{node} - Y_i)\right]^+, \forall i; \tag{30}$$

$$\beta_n^{(1)}(l+1) = \left[\beta_n^{(1)}(l) - s_3\left(\frac{\theta T}{N} - \sum_{i=1}^{M}\tau_{i,n}\right)\right]^+, \forall n; \tag{31}$$

$$\beta^{(2)}(l+1) = \left[\beta^{(2)}(l) - s_4\left((1-\theta)T - \sum_{i=1}^{M} t_i\right)\right]^+; \tag{32}$$

$$\gamma_i(l+1) = \left[\gamma_i(l) - s_5\left(\sum_{n=1}^{N} {R_{i,n}^{B}}' + R_i^{H'} - R_{\min}\right)\right]^+, \forall i; \tag{33}$$

$$\phi_i(l+1) = \left[\phi_i(l) - s_6({EH_i}' - {EC_{sum}}')\right]^+, \forall i, \tag{34}$$

where l is the iteration index for updating the Lagrange multipliers, s_1, s_2, s_3, s_4, s_5 and s_6 are the step sizes for the associated Lagrange multipliers. How to choose the values of the step sizes in a gradient method has been discussed in [29] and is thus omitted here for brevity. Then, we use the updated Lagrange multipliers to update $\tau_{i,n}, t_i$ and θ in problem (28).

3.3.2 UAV trajectory optimization

For given communication resource allocation in terms of $X_{i,n}, Y_i, \tau_{i,n}, t_i$ and θ, the UAV trajectory optimization sub-problem is formulated as

$$\begin{aligned} \mathbf{P_{4.2}}: \ & \max_{\{\mathbf{q}\}} \sum_{i=1}^{M}\sum_{n=1}^{N} {R_{i,n}^{B}}' + \sum_{i=1}^{M} {R_i^{H}}' - Q^* {EC_{sum}}' \\ & \text{s.t.} \\ & \quad \text{C4}-1, \text{C6}-1, \text{C7}, \text{C8}. \end{aligned} \tag{35}$$

$\mathbf{P_{4.2}}$ is still non-convex due to the non-convex vectors $\mathbf{q}$ in the objective function and the constraints. An SCP based technique is employed to obtain a locally optimal solution by successively maximizing a lower bound of the objective function in an iterative manner. Specifically, let $\mathbf{q^0} = [q_1^0, q_2^0, ..., q_N^0]$ denote the initial UAV trajectory and $\mathbf{q}^{l'} = [q_1^{l'}, q_2^{l'}, ..., q_N^{l'}]$ denote the obtained UAV trajectory after the l'th iteration. Accordingly, we propose the following lemma to transform ${R_{i,n}^{B}}'$ and ${EH_i}'$ into convex formulations [15], [16], [30].

Lemma 2: For any given $\mathbf{q}^{l'}, l' \geq 0$, we have

$${R_{i,n}^{B}}'(\mathbf{q}) \geq {R_{i,n}^{B}}'(\mathbf{q}^{l'}), \forall i, \forall n; \tag{36}$$

$${EH_i}'(\mathbf{q}) \geq {EH_i}'(\mathbf{q}^{l'}), \forall i, \tag{37}$$

where

$$\begin{aligned} {R_{i,n}^{B}}'(\mathbf{q}^{l'}) = & W\tau_{i,n}\log_2\left(1+\frac{\varphi P_{\max}^{uav} h_i^r X_{i,n}\beta_0\mu}{W\sigma^2\tau_{i,n}(H^2+F_0)}\right) \\ & - \frac{W\tau_{i,n}\log_2 e}{\left(1+\frac{W\sigma^2\tau_{i,n}(H^2+F_0)}{\varphi P_{\max}^{uav} h_i^r X_{i,n}\beta_0\mu}\right)(H^2+F_0)}(F-F_0), \forall i, \forall n, \end{aligned} \tag{38}$$

$${EH_i}'(\mathbf{q}^{l'}) = \frac{P_{\max}^{uav}\eta\beta_0\mu\left(\frac{\theta T}{N}-X_{i,n}\right)}{H^2+F_0} - \frac{P_{\max}^{uav}\eta\beta_0\mu\left(\frac{\theta T}{N}-X_{i,n}\right)}{(H^2+F_0)^2}(F-F_0), \forall i, \forall n, \tag{39}$$

$$F = ||q_n^{l'} - q_i^g||^2, F_0 = ||q_n^0 - q_i^g||^2, \forall i, \forall n, \tag{40}$$

the equations in (36) and (37) only hold when $\mathbf{q}^0 = \mathbf{q}^{l'}$.

Proof. Please see Appendix B. ■

Based on Lemma 2, we optimize the UAV trajectory $\mathbf{q}$ by replacing $R_{i,n}^{B\,'}$ and $EH_i^{'}$ in $\mathbf{P_{4.2}}$ with their respective lower bounds $R_{i,n}^{B\,'}(\mathbf{q}^{l'})$ and $EH_i^{'}(\mathbf{q}^{l'})$ in (38) and (39) at each iteration l'. By substituting (38) and (39) into problem (35), $\mathbf{P_{4.2}}$ can be equivalently formulated as

$$\begin{aligned}
&\mathbf{q}^* = \arg\max_{\{\mathbf{q}^{l'}\}} \sum_{i=1}^{M}\sum_{n=1}^{N} R_{i,n}^{B\,'}(\mathbf{q}^{l'}) + \sum_{i=1}^{M} R_i^{H'} - Q^* EC_{sum}{}^{'} \\
&\text{s.t.} \\
&\quad \text{C7, C8,} \\
&\quad \text{C4}-3: \sum_{n=1}^{N} R_{i,n}^{B\,'}(\mathbf{q}^{l'}) + R_i^{H'} \geq R_{\min}, \forall i, \forall n, \\
&\quad \text{C6}-3: EH_i^{'}(\mathbf{q}^{l'}) - EC_i^{'} \geq 0, \forall i.
\end{aligned} \tag{41}$$

Since (38) and (39) are convex with respect to $\mathbf{q}^{l'}$, problem (41) is a convex optimization problem and can be efficiently solved by using standard convex optimization methods, e.g., the CVX tool or the Lagrange dual method.

Remark 4: The factor '$F - F_0$' in (39) indicates that a higher amount of energy can be harvested when the UAV is closer to the IoT nodes, as the received power will be higher. In order to maximize the objective function of (41), which is equivalent to maximizing the total EE of all the ground IoT nodes, the UAV needs to be closer to the IoT nodes that can achieve a higher throughput than the other IoT nodes during BackCom. Meanwhile, the time allocation for BackCom and active transmission will guarantee the minimum throughput requirements for all IoT nodes. That is to say, the IoT nodes allocated less time during BackCom will have enough time to transmit information actively to meet the minimum throughput requirement during active transmission. The above remark will be verified in Section 5.

3.4 Dinkelbach-Based Iterative Algorithm

We propose a Dinkelbach-based iterative algorithm in Algorithm 1 to summarize the optimization process in Section 3.3.

Algorithm 1: Dinkelbach based iterative algorithm

Input: $\mathscr{M}, \mathscr{N}$.

Output: $Q^*, \mathbf{Z}_n^*, \boldsymbol{\tau}_n^*, \mathbf{t}^*, \mathbf{P}^*, \mathbf{q}^*$.

Initialize: $k = 1, Q^*(k) = Q^*(0), \varepsilon$.

repeat

  Initialize $\mathbf{q}$;

  repeat

    repeat

      Initialize $\boldsymbol{\alpha}_n^{(1)}, \boldsymbol{\alpha}^{(2)}, \boldsymbol{\beta}^{(1)}, \beta^{(2)}, \boldsymbol{\gamma}, \boldsymbol{\phi}$;

      Obtain $\theta, \mathbf{X}_n, \boldsymbol{\tau}_n, \mathbf{Y}, \mathbf{t}$ by solving $\mathbf{P_{4.1}}$;

      Update the Lagrange multipliers $\boldsymbol{\alpha}_n^{(1)}, \boldsymbol{\alpha}^{(2)}, \boldsymbol{\beta}^{(1)}, \beta^{(2)}, \boldsymbol{\gamma}, \boldsymbol{\phi}$ in (28)-(33), respectively;

    until $\boldsymbol{\alpha}_n^{(1)}, \boldsymbol{\alpha}^{(2)}, \boldsymbol{\beta}^{(1)}, \beta^{(2)}, \boldsymbol{\gamma}, \boldsymbol{\phi}$ converge;

    repeat

      Initialize $\mathbf{q^0}$;

      Obtain $\mathbf{q}^*$ by solving $\mathbf{P_{4.2}}$;

      Update the obtained UAV trajectory $\mathbf{q}^{\mathbf{l}'}$;

    until $\mathbf{q}^*$ converges;

17: **until** $\boldsymbol{\alpha}_n^{(1)}, \boldsymbol{\alpha}^{(2)}, \boldsymbol{\beta}^{(1)}, \beta^{(2)}, \boldsymbol{\gamma}, \boldsymbol{\phi}$ and $\mathbf{q}$ converge after $k = 2$;

18: Compute $R_{i,n}^B, R_i^H$ and EC_{sum} in (6), (7) and (9), respectively;

19: $k = k + 1$;

20: Update $Q^*(k) = \frac{R_{sum}}{EC_{sum}}$;

21: **until** $|\min_{i\in M, n\in N} \sum_{i=1}^{M}\sum_{n=1}^{N} R_{i,n}^B + \sum_{i=1}^{M} R_i^H - Q^*(k)EC_{sum}| \leq \varepsilon$.

In Algorithm 1, k is the iteration index for updating Q^*, i.e., the maximum EE, and ε is set to control the convergence of the objective function in $\mathbf{P_4}$.

4 Convergence and Computational Complexity Analysis

We first analyze the convergence of Algorithm 1, which includes two layers of iteration, where the two inner layer iterative loops aim to achieve the convergence of Lagrange multipliers for solving $\mathbf{P_{4.1}}$ and the convergence of the UAV's trajectory, respectively, and the outter layer iteration seeks the convergence of the BCD algorithm that decomposes $\mathbf{P_4}$ into $\mathbf{P_{4.1}}$ and $\mathbf{P_{4.2}}$. Since $\mathbf{P_{4.1}}$ is a standard convex optimization problem, the iterative updates of $\theta, \boldsymbol{\tau}, \mathbf{t}$ and the Lagrange multipliers $\boldsymbol{\alpha}_n^{(1)}, \boldsymbol{\alpha}^{(2)}, \boldsymbol{\beta}^{(1)}, \beta^{(2)}, \boldsymbol{\gamma}, \boldsymbol{\phi}$ are guaranteed to converge to the optimal solution of $\mathbf{P_{4.1}}$. To solve $\mathbf{P_{4.2}}$, successive convex programming (SCP) method is used. We denote the maximum EE obtained by solving $\mathbf{P_{4.2}}$ in the $(l+1)$th iteration by $EE(l+1)$, and denote the maximum EE obtained through solving (41) in the lth and the $(l+1)$th iteration by $EE_{lb}(l)$ and $EE_{lb}(l+1)$, respectively. Based on [30], we have

$$EE_{lb}(l) \leq EE_{lb}(l+1), \tag{42}$$

$$EE_{lb}(l+1) \leq EE(l+1), \tag{43}$$

where l is the iteration number, (42) holds since $EE_{lb}(l+1)$ is the optimal solution of (41), and (43) holds since a convex function is globally lower bounded by its first-order Taylor expansion.

The inequalities in (42) and (43) imply that the achieved maximal EE is non-decreasing after each iteration and is upper bounded, and the approximate problem (41) of $\mathbf{P_{4.2}}$ is solved optimally locally in each iteration. Therefore, the SCP based method for solving $\mathbf{P_{4.2}}$ is guaranteed to converge to a locally optimal solution. After each iteration of the BCD algorithm that alternately solves $\mathbf{P_{4.1}}$ and $\mathbf{P_{4.2}}$, the objective function value of $\mathbf{P_4}$ is nondecreasing with updated variables. Meanwhile, $\mathbf{P_4}$ is also upper bounded by its associated constraints, thus the BCD algorithm is guaranteed to converge to a solution of $\mathbf{P_4}$.

Next, we evaluate the computational complexity of Algorithm 1. The computational complexity of the Lagrange dual method in (19) for solving $\mathbf{P_{4.1}}$ is $\mathscr{O}(\Delta_1 MN)$ [31], where Δ_1 is the number of iterations for updating the Lagrange multipliers. The number of iterations for using SCP method to solve problem (41) is denoted as Δ_2. The iterations needed for the convergence of the BCD algorithm and Q^* are denoted by Δ_3 and Δ_4, respectively. Thus, the total computational complexity of Algorithm 1 is $\mathscr{O}[(\Delta_1 MN + \Delta_2)\Delta_3\Delta_4]$. According to our simulations, the values of Δ_1 , Δ_2, Δ_2 and Δ_4 are in the ranges of 2-5, 2-3, 2-4 and 3-5, respectively.

5 Simulation Results

In this section, we present simulation results to evaluate the time allocation, the UAV trajectory, the convergence of Algorithm 1, and the EE performance versus different parameters based on our proposed Algorithm 1, in comparison with the benchmark schemes, i.e., the UAV-enabled BackCom scheme, the UAV-enabled HTT scheme, the energy consumption minimization scheme, and the fixed PB based hybrid BackCom-HTT scheme. The details of the benchmark schemes are provided in Appendix C. We consider a network, where all the IoT nodes are located within a 2-D region of $10 \times 10\, m^2$ [33], the UAV's original position and the location of the reader are respectively 10 m and 30 m away from the center of this region, which is set as the origin of the 2D ground plane. The values of the other fixed system parameters are listed in Table 1 [14], [15], [25], [34].

Table 1 Simulation Parameters

Simulation parameter	Value
Number of IoT nodes M	5
Number of time slots N	50
Altitude of UAV H	10m
Maximum speed of UAV V_{max}	10m/s
Coordinate of UAV's original location	$(-10,0)$
Coordinate of reader location	(30,0)
Channel bandwidth W	10 kHz
Noise power spectral density σ^2	-130 dBm/Hz
Channel power gain at reference distance β_0	-30 dB
Rician factor	7 dB
Pathloss exponent of UAV-node channel	2
Pathloss exponent of node-reader channel	3
Maximum UAV transmit power P_{max}^{uav}	40 dBm
Maximum IoT node transmit power P_{max}^{node}	23 dBm
Energy conversion efficiency η	0.5
Backscatter circuit power consumption P_{cir}^{B}	200 μw
HTT circuit power consumption P_{cir}^{H}	1 mw

5.1 Time Allocation Versus Backscatter Performance Gap

Fig. 3 illustrates the impact of backscatter performance gap φ on the time allocation for BackCom, i.e., θ. It is easy to verify that θ is always 1 for the UAV-enabled backscatter scheme since it only includes BackCom. For the UAV-enabled HTT scheme, θ keeps the same value as 0.28 with different φ, this is also easy to verify that during BackCom in the UAV-enabled HTT scheme, the IoT nodes only harvest energy and then transmit information to the reader during active transmission. For our proposed Algorithm 1, when φ is smaller than -50 dB, θ is the same as that in the UAV-enabled HTT scheme, since the EE provided by BackCom is too low and the minimum throughput requirement R_{min} cannot be met in this case. Same as in the UAV-enabled HTT, the IoT nodes only harvest energy during BackCom and transmit information to the reader during active transmission. θ slightly increases with the improvement of φ from -50dB to -40dB, then it dramatically increases when φ is greater than -40dB. This is because that BackCom of some IoT nodes at some time slots can gain more EE with higher φ so that more time is allocated to BackCom. It also indicates that θ is sensitive to φ, where θ improves dramatically after exceeding -40 dB. When φ is bigger than -25 dB, θ is

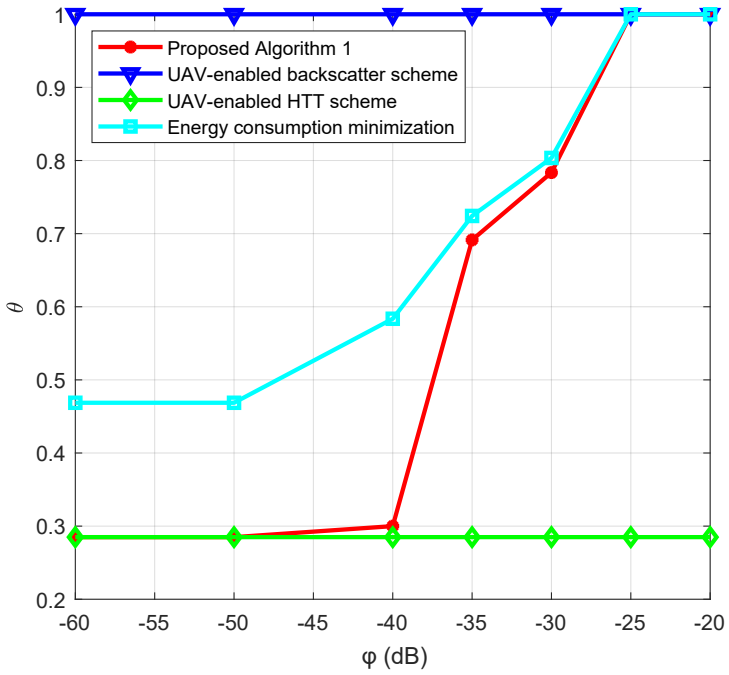

Fig. 3 Portion of time allocated for BackCom versus BackCom performance gap ($R_{min} = 5 \times 10^4$ bit/s).

always one, which indicates that BackCom dominates the over all time period, and the active transmission of any IoT node at any time slot cannot provide higher EE than that in BackCom.

Comparing the energy consumption minimization scheme with our proposed Algorithm 1, θ in energy consumption minimization scheme is no smaller than that in our proposed Algorithm 1. This is because BackCom consumes much less energy than active transmission due to the low backscatter circuit consumption without transmit power consumption. Specifically, when φ is smaller than -50 dB, the throughput requirement cannot be met by BackCom. Thus, the IoT nodes only harvest energy during BackCom, and transmit information during active transmission. However, in order to minimize the energy consumption, more time is allocated to BackCom for energy harvesting but without energy consumption, since the throughput of all the IoT nodes only need to equal to R_{min}. θ significantly increases from 0.48 to 0.8 with φ increasing from -50 dB -30 dB, which indicates that more time is allocated to BackCom for saving energy while satisfying R_{min} with active transmission/BackCom. Also, the gap between our proposed Algorithm 1 and the energy consumption minimization scheme becomes

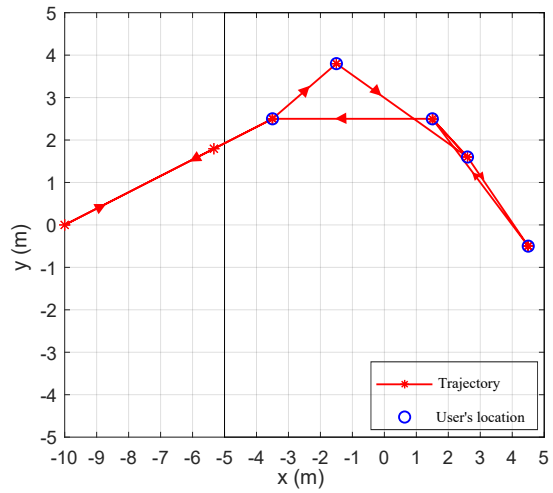

Fig. 4(a) UAV trajectory for a UAV-enabled backscatter network ($R_{min} = 5 \times 10^4$ bit/s).

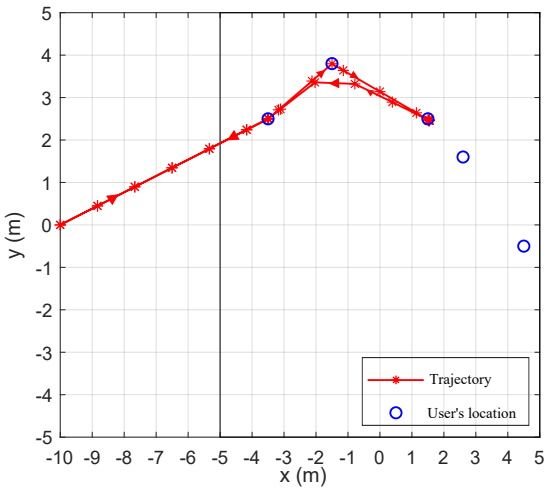

Fig. 4(b) UAV trajectory for a UAV-enabled HTT network ($R_{min} = 5 \times 10^4$ bit/s).

smaller since higher φ can both improve the EE and minimize the energy consumption. After φ exceeds -25 dB, the BackCom dominate the over all time period as in our proposed Algorithm 1. We can also see that the EE of each scheme stays constant when φ is less than -50dB or more than -25dB.

5.2 UAV Trajectory

In Fig. 4 (a), the UAV trajectory is illustrated where $\theta = 1$, which means that BackCom dominates the whole time period. The UAV is dispatched to provide energy for the IoT nodes from the left side outside the region where all the IoT nodes are located in, and then flies back to the initial location at the end of the BackCom time period. As we can see, the UAV flies to and hovers above each IoT node to make sure all the IoT nodes meet R_{min}. Also, the UAV takes the longest time to hover above the node on the right side of the network, since this IoT node is closest to the reader which can provide more EE for the EE of all the IoT nodes. In addition, the UAV returns to the initial location immediately after passing through the IoT node on the left side of the network, this is because that the UAV focuses on providing energy for the IoT nodes, and it needs to take the shortest time to return to the initial location. That is to say, the UAV returns straightly to the initial location after leaving the IoT node which is located on the

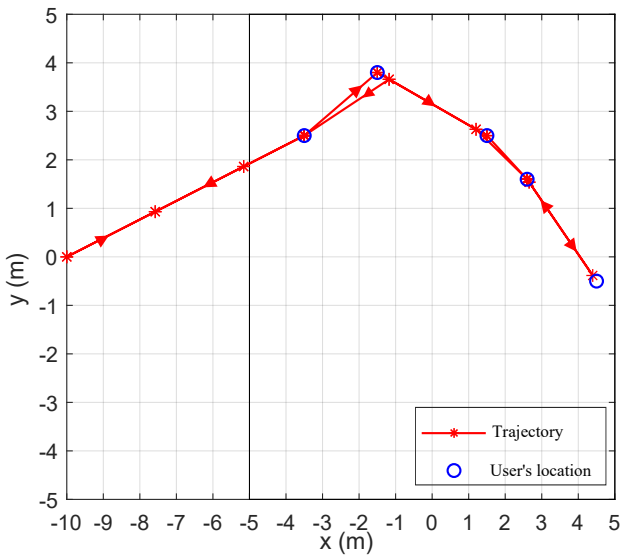

Fig. 4(c) UAV trajectory for a UAV-enabled hybrid network ($R_{min} = 5 \times 10^4$ bit/s).

left side of the network. Same reasons can be used to explain the straight trajectory after UAV being dispatched. Thus, the trajectory of the UAV after being dispatched and before returned is overlapped.

In Fig. 4 (b), the UAV trajectory is illustrated where $\theta = 0.27$, which means that HTT dominates the whole time period. The UAV in this figure only flies to and hover above three IoT nodes and spends the most time hovering above the IoT node at the middle of the network. This is because that the throughput of each IoT node is only provided during active transmission in this case, sufficient energy for active transmission needs to be harvested during BackCom. Thus, the UAV needs to fly to a middle position to ensure that each IoT node can harvest enough energy for meeting the throughput requirements. However, more time of active transmission is allocated to the two IoT nodes that are closer to the reader for achieving higher throughput and EE, while other IoT nodes only achieve the minimum throughput requirements.

Fig. 4 (c) shows the UAV trajectory for $\theta = 0.52$, which refers to a hybrid BackCom-HTT network. We can see that the UAV trajectory is similar to that in Fig. 4 (a), where the UAV flies to and hover above each IoT node and returns to the initial location via a straight line. The difference is that the UAV spends less time hovering above the IoT node that is closest to the reader and other IoT nodes achieve higher throughput with longer BackCom transmission time.

This is because the maximum EE of all the IoT nodes is achieved when the IoT node that is closest to the reader is allocated the most time during active transmission while other IoT node only achieve the minimum throughput requirement during the whole time block. Thus, more time of BackCom is allocated to other IoT nodes for meeting the throughput requirements.

Based on the above results and **Remark 4**, we summarize the insights into the UAV trajectory as follows. First, the UAV tends to fly to the IoT nodes that are closer to the reader for the above three cases, and such IoT nodes can achieve higher throughput and provide higher EE of all the IoT nodes. Second, if BackCom dominates the network, the UAV will fly above each IoT node to ensure that all the IoT nodes satisfy the throughput requirement, and the IoT node that is closest to the reader is allocated the most time for maximizing the EE of all the IoT nodes. Third, if HTT dominates the network, the UAV spends the most time hovering above the IoT node that is around the middle position of all the IoT nodes, but the IoT nodes that are closer to the reader achieve higher throughput and provide higher EE. Fourth, in the case of hybrid backscatter-HTT, the UAV trajectory is similar to that in pure BackCom network, but the UAV spends less time to hover above the IoT node that is closest to the reader for meeting the throughput requirements of other IoT nodes. Fifth, if the reader's location is changed, the UAV will fly to the IoT nodes that are closer to the updated location of the reader. Last but not least, if the time block is long enough, the UAV trajectory will be a straight line from the initial location to the IoT node closest to the reader for maximizing the total EE, since the throughput requirement of other IoT nodes can be satisfied through BackCom or HTT for a sufficiently long time.

5.3 Convergence of Algorithm 1

Fig. 5 illustrates the convergence of our proposed Algorithm 1 versus different maximum UAV transmit power. It can be observed that our proposed algorithm always converges to the optimal EE after 4_{th} step under any given UAV transmit power. This proves that our proposed Algorithm 1 is computationally efficient. Also, based on Lemma 1, where maximum UAV transmit power is proved to be the optimal value for maximum EE. We can see that higher

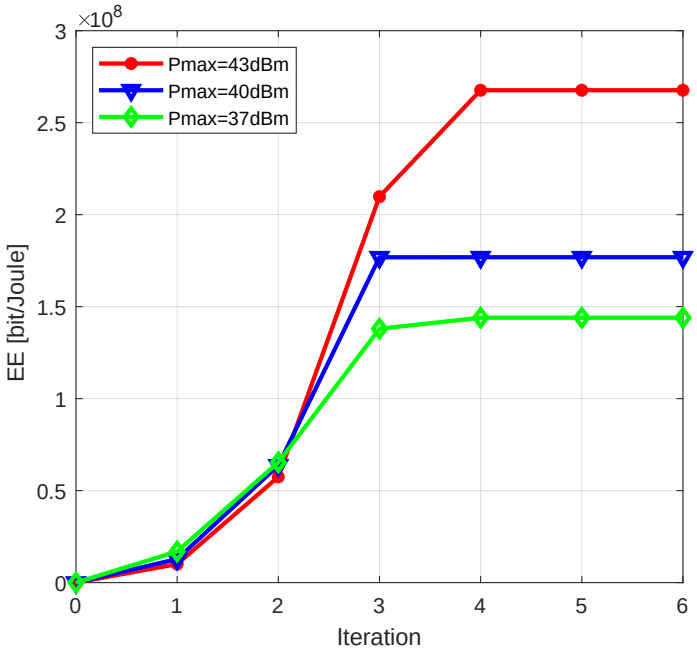

Fig. 5 Convergence of Algorithm 1 ($R_{min} = 5 \times 10^4$ bit/s, $\varphi = -30$ dB).

maximum UAV transmit power achieve higher EE than other cases with lower UAV transmit power in Fig. 5.

5.4 Total EE Performance

5.4.1 Total EE versus φ

Fig. 6 illustrates the total EE of all the IoT nodes versus φ. We can see that the total EE of our proposed Algorithm 1 outperforms all other schemes. Next, we describe and explain each curve of each scheme as follows. Firstly, the total EE of UAV-enabled HTT scheme is constant, i.e., 7.2×10^7 bits/s, since the IoT nodes during the first time period in the UAV-enabled HTT scheme only harvest energy, and then transmit information to the reader during active transmission. Thus, the backscatter performance gap of BackCom has no impact on the UAV-enabled HTT scheme. Secondly, the EE of our proposed algorithm is constant when φ is smaller than -40 dB since the IoT nodes under this condition are the same as the IoT nodes in the UAV-enabled HTT scheme in order to meet R_{min}. Then the total EE of our proposed

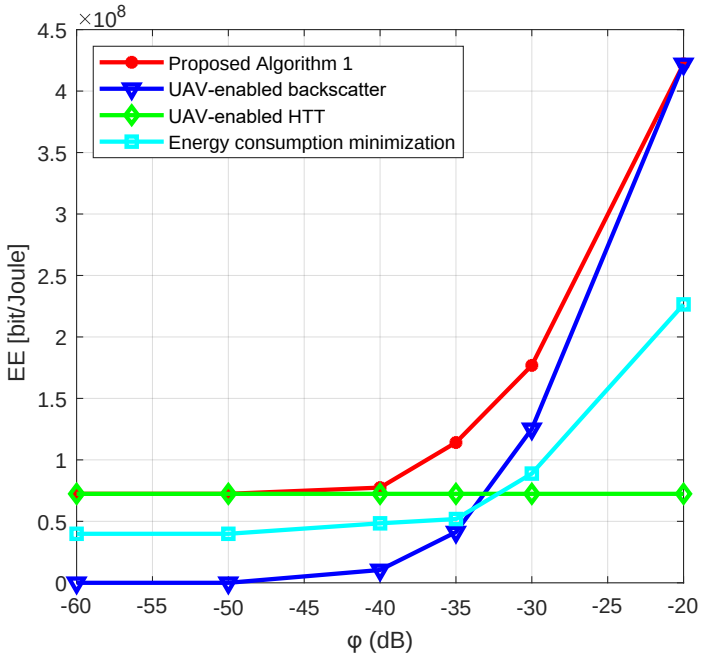

Fig. 6 Flow chart of Total EE versus BackCom performance gap φ ($R_{min} = 5 \times 10^4$ bit/s).

algorithm increases sharply when φ improves from -40 to -20 dB, which indicates that BackCom provide much more EE than active transmission with low φ.

In addition, the total EE of the energy consumption minimization scheme is still constant when φ is smaller than -40 dB due to the same reason explained above, then it gradually increase with the improvement of φ. Also, the total EE of the energy consumption minimization scheme exceeds that of the UAV-enabled HTT scheme after φ is greater than -35 dB due to the longer time allocated to BackCom for saving energy. This also indicates that BackCom can provide more EE with higher φ. The EE of the UAV-enabled backscatter scheme is 0 when φ is smaller than -40 dB, this is because that the IoT nodes cannot meet R_{min}, which fails to contribute EE. When φ increases beyond -20 dB, the total EE of the UAV-enabled backscatter scheme becomes the same as that of our proposed algorithm. This is because BackCom occupies the entire time block in our proposed algorithm when φ is greater than -20 dB.

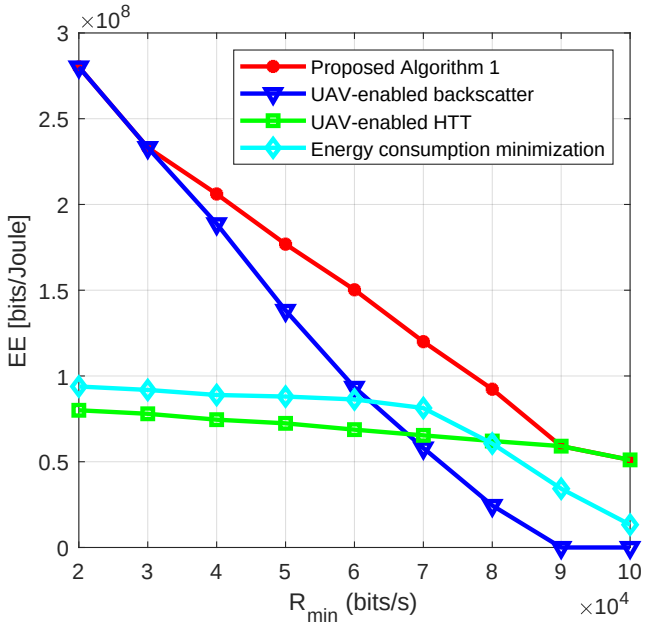

Fig. 7 Total EE versus minimum throughput requirement R_{min} ($\varphi = -30$ dB).

5.4.2 Total EE versus R_{min}

Fig. 7 plots the total EE of all the IoT nodes versus R_{min}. The total EE of our proposed Algorithm 1 still out performs than that of other schemes. Similarly, the total EE of all schemes decreases with higher R_{min}, since a higher R_{min} makes some IoT nodes at some time slots fail to preform BackCom which greatly decreases the EE. Also, the EE improvement due to a higher throughput cannot compensate for the loss of EE caused by the high energy consumption for meeting a higher throughput requirement. As we can see the total EE of our proposed algorithm significantly decreases but the decreasing rate becomes smaller with the improvement of R_{min}, this is because that more IoT nodes or more time slots are allocated for active transmission, and the EE loss during active transmission is only caused by a higher energy consumption which is smaller than the EE loss due to the low time allocation to BackCom. For the UAV-enabled backscatter scheme, the total EE drops sharply with higher R_{min}, since some IoT nodes cannot meet R_{min} and fail to join the network. Thus, the total EE drops to 0 when R_{min} is too high, e.g., 9 $\times 10^4$ bits/s. The total EE of our proposed Algorithm 1 and that of the UAV-enabled backscatter scheme are the same when R_{min} is smaller than 3×10^4 bits/s, because BackCom

occupies the whole time block for such low R_{min}. When R_{min} is larger than 3×10^4 bits/s, the proposed Algorithm 1 achieves the highest EE among the four considered schemes. As R_{min} further increases, the EE achieved by Algorithm 1 gradually reduces to be the same as that of the UAV-enabled HTT scheme. This is because for very high values of R_{min}, active transmission occupies the whole time block.

The total EE of the UAV-enabled HTT scheme reduces steadily with increasing R_{min}, since the EE loss is only caused by the high energy consumption for meeting a higher throughput requirement. However, the total EE did improve due to higher throughput, thus, the total EE of the UAV-enabled HTT scheme decreases steadily. For the energy consumption minimization scheme, the total EE is around 8.7×10^8 bits/Joule from 3×10^4 bits/s to 6×10^4 bits/s, and then suddenly drops to 2.8×10^7 bits/Joule at $R_{min} = 9 \times 10^4$ bits/s. Since the time allocated to BackCom is more than that allocated to active transmission, the EE obtained by this scheme decreases slowly. After R_{min} exceed 6×10^4 bits/s, active transmission takes a longer time, and the sudden decreasing of the total EE is due to a much higher energy consumption during active transmission. Furthermore, the EE of each scheme will increase with the minimum throughput requirement below the value of $3 * 10^4$.

5.4.3 Total EE versus V_{max}

Fig. 8 shows the total EE of all the IoT nodes versus the maximum UAV flying speed V_{max}. It is obvious that the total EE of all the schemes shows the same trend, where our proposed Algorithm 1 achieves the highest EE. Specifically, the total EE of all the schemes gradually increases with higher V_{max} and converges to a certain value after V_{max} exceeds 40 m/s. The reason for that is a higher V_{max} allows the UAV quickly fly to and stay at some positions which can lead to higher EE while satisfying the constraints, e.g., R_{min}, the amount of energy harvested requirement. Thus, the total EE improves with better UAV trajectory. However, the EE improvement is not large as compared to fig. 6 and fig. 7, this is because V_{max} can only change the optimal trajectory, where the network size is small. Since the UAV can easily travel around a small network, it will not contribute too much EE improvement. Also, the optimal UAV trajectory is constant after V_{max} exceed 40 m/s, which indicates that the UAV has enough

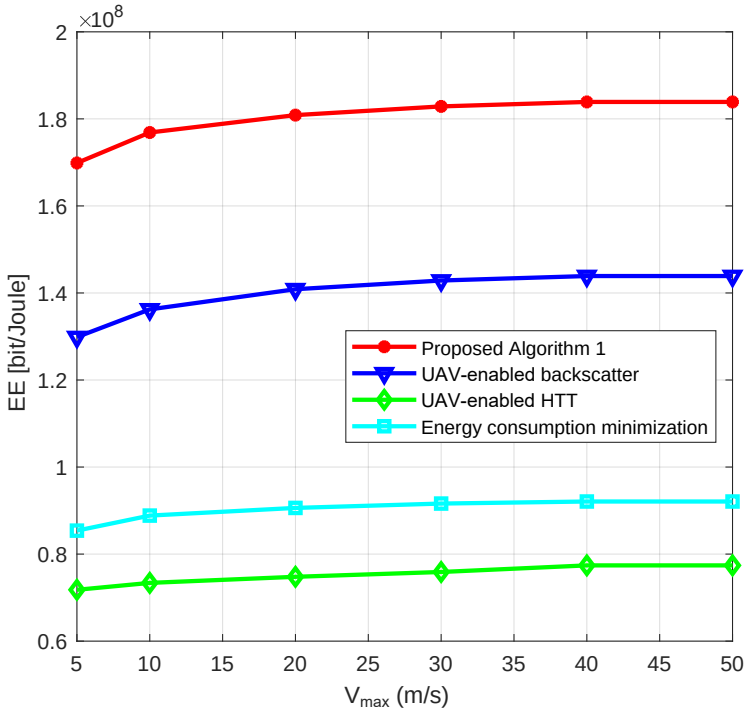

Fig. 8 Total EE versus maximum UAV speed V_{max} ($R_{min} = 5 \times 10^4$ bit/s, $\varphi = -30$ dB).

speed to make an optimal trajectory. Thus, the total EE of all the schemes converges after the optimal UAV trajectory is fixed.

Same reasons can be explained for the total EE of energy consumption minimization scheme despite this scheme aims to minimize the energy consumption. In addition, the total EE of the UAV-enabled backscatter scheme does not drop like in fig. 7 and fig. 8, this is easy to be verified, the serious drop of the EE for the UAV-enabled backscatter scheme is that the IoT nodes cannot meet R_{min}. However, the IoT node can easily meet R_{min} with high UAV speed.

5.4.4 Total EE versus fixed PB or UAV initial location

Fig. 9 shows the total EE versus the fixed PB location or the UAV initial location under two schemes, i.e., our proposed Algorithm 1 and the fixed PB based BackCom-HTT scheme. The total EE of both schemes increases with shorter distance from the UAV initial location or the PB location to the IoT nodes. It is easy to be verified that the harvested energy utilization and the throughput increases with short communication distance, which improves the EE.

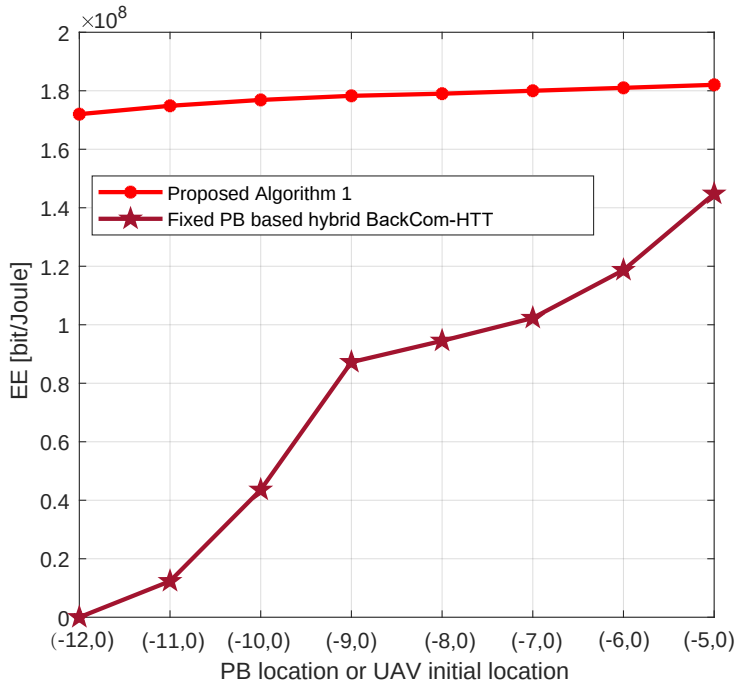

Fig. 9 Total EE versus fixed PB or UAV initial location ($R_{min} = 5 \times 10^4$ bit/s, $\varphi = -30$ dB).

Specifically, the total EE of the fixed PB based BackCom-HTT scheme is very low when the distance from the PB to the IoT nodes is long, i.e., (-12, 0), (-11, 0) and (-10, 0). This is because that the minimum throughput requirement of some users cannot be met, and none of the users could meet this requirement after the PB location is farther than (-12, 0). Then the total EE significantly increases with shorter distance from the PB to the IoT nodes with less increasing rate. Also, the increasing trend of the total EE of our proposed algorithm is very stable, which is due to the high mobility of the UAV. Since the UAV works as a mobile power station, it can quickly fly to the region, where all the IoT nodes are located. Thus, the impact of the small distance difference of initial UAV locations on the EE is not obvious.

However, our proposed algorithm gain much more total EE than the fixed PB based BackCom-HTT scheme does. This is due to the high propagation loss of the long distance from the fixed PB to the IoT nodes, and the energy harvested by the IoT nodes is much decreased due to the same reason. Such high propagation loss seriously degrades the total EE performance as illustrated in Fig. 9. In addition, the EE gap between the two schemes becomes small, since the

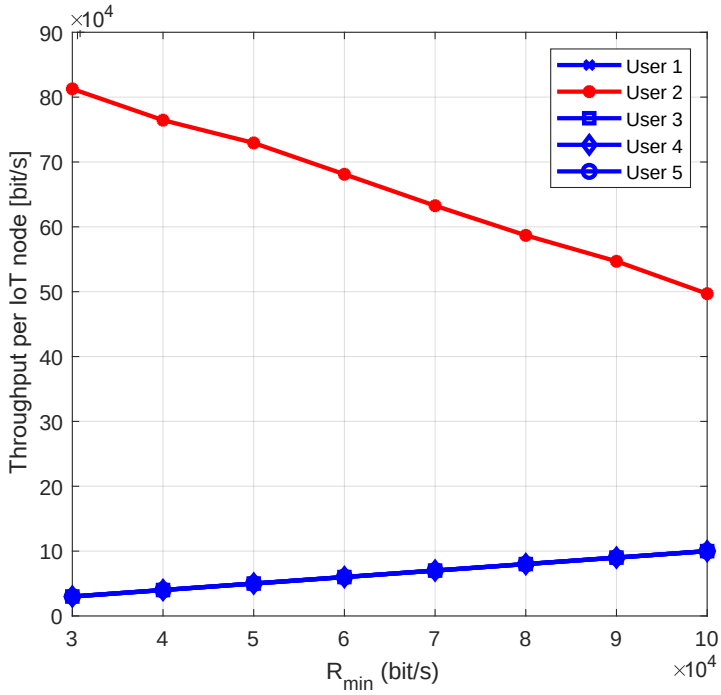

Fig. 10 Throughput versus minimum throughput requirement R_{min} ($\varphi = -30$ dB).

propagation loss difference between the fixed PB and the UAV is becoming small, which leads to this small EE gap.

5.5 Throughput Versus R_{min}

Fig. 10 illustrates the throughput of individual node versus R_{min}. It can found that the throughput of IoT node 2, node 3, node 4, node 5 is identical to the corresponding R_{min}, i.e., 3, 4, 5, 6, 7, 8 and 9×10^4 bits/s, respectively. However, the throughput of IoT node 2 is much higher than R_{min}. This is because that we aim to maximize the total EE of all the IoT nodes, most time is allocated to IoT node 2 since it can provide more EE than other IoT nodes do due to better channel condition from itself to the UAV and to the reader. This allows IoT node 2 to gain much more throughput. Meanwhile, the minimum throughput requirement of other IoT nodes needs to be met, thus, other IoT node's throughput only needs to equal to R_{min} for achieving maximum EE of all the IoT nodes. In addition, the throughput of IoT node 2 gradually decreases with higher R_{min}. Since more time is allocated to other IoT nodes for

meeting their minimum throughput requirement when increasing R_{min}, the throughput of IoT node 2 drops with less given transmit time.

6 Conclusions

In this paper, we have investigated the total EE maximization of all the IoT nodes in a UAV-enabled hybrid BackCom-HTT network. Since the optimization problem is non-convex, we have proposed a Dinkelbach based iterative algorithm to first transform the problem into a more tractable subtractive form, then use a BCD method to decompose the transformed problem into two sub-problems, where the communication resource allocation subproblem is solved by employing the Lagrangian dual method and the UAV trajectory optimization subproblem is solved by applying the SCP technique. Simulation results demonstrate that the total EE performance of our proposed algorithm is much better than the benchmark schemes, i.e., the UAV-enabled backscatter scheme, the UAV-enabled HTT scheme, the energy consumption minimization scheme, and the fixed PB based hybrid BackCom-HTT scheme. Moreover, our results show the total EE of all the ground IoT nodes increases for a lower throughput requirement, higher backscatter performance gap and higher UAV maximum speed under all the considered schemes. In addition, our proposed algorithm allocates more time for BackCom and/or active transmission to the IoT nodes with better channel conditions for improving the total EE of all the IoT nodes, while guaranteeing the other IoT nodes meeting their minimum throughput requirement.

In our future work, we will extend this work to the case with multiple UAVs serving a large number of IoT nodes distributed over a large area, where the interference mitigation during BackCom and the trajectory optimization for multiple UAVs will be the main challenges to tackle. It will also be interesting to extend the proposed system model to the case of fixed wing UAVs or for online operation.

Appendix A

Proof of Lemma 1

When P^u, $\mathbf{Z}$, $\boldsymbol{\tau}$, $\mathbf{t}$, $\mathbf{P}$ and $\mathbf{q}$ are given, the objective function in $\mathbf{P_1}$ monotonically increases with P^u since P^u only exists in the numerator of the objective function. Thus, the optimal UAV transmit power is obtained by its upper bound. Due to C4-C7 in $\mathbf{P_1}$, they are used to obtain the lower bound of P^u, the upper bound of P^u is given by P_{max}^{uav} and we have $P^{u*} = P_{max}^{uav}$. The proof is completed.

Appendix B

Proof of Lemma 2

Let us define two functions given by $f_1 = A\log_2\left(1+\frac{B}{C(H^2+F)}\right)$ and $f_2 = \frac{D}{H^2+F}$, where $A,B,C,D>0$ are constants, f_1 and f_2 are both convex with respect to F. Since the first-order Taylor expansion of a convex function is a global under-estimator of the function values, for any $F_0 \geq 0$ we can obtain

$$f_1 \geq A\log_2\left(1+\frac{B}{C(H^2+F_0)}\right) - \frac{A\log_2 e}{\left(1+\frac{C(H^2+F_0)}{B}\right)(H^2+F_0)}(F-F_0), \tag{B.1}$$

$$f_2 \geq \frac{D}{H^2+F_0} - \frac{D}{(H^2+F_0)^2}(F-F_0). \tag{B.2}$$

By substituting $A = W\tau_{i,n}$, $B = \varphi P_{\max}^{uav} h_i^r X_{i,n}\beta_0\mu$, $C = W\sigma^2\tau_{i,n}$ and $D = P_{\max}^{uav}\eta\beta_0\mu(\frac{\theta T}{N} - X_{i,n})$ into (B.1) and (B.2), then (36) and (37) are obtained. Also, the equalities in (B.1) and (B.2) hold when $F = F_0$, thus, the equalities in (36) and (37) hold when $\mathbf{q}^0 = \mathbf{q}^{l'}$. The proof is completed.

Appendix C

Benchmark Schemes

UAV-enabled backscatter scheme

In this scheme, we aim to maximize the EE of all the IoT nodes, where the overall time period T is allocated to the IoT nodes for wireless energy transfer and BackCom. Accordingly, the optimization problem of this scheme is formulated as

$$\mathbf{P_5}: \max_{\{\mathbf{Z}_n, \boldsymbol{\tau}_n, \mathbf{q}\}} \frac{\sum_{i=1}^{M}\sum_{n=1}^{N} W\tau_{i,n}\log_2\left(1+\frac{\varphi P_{\max}^{uav} h_{i,n}^{u} Z_{i,n} h_i^{r}}{W\sigma^2}\right)}{PC^B \sum_{i=1}^{M}\sum_{n=1}^{N}\tau_{i,n}}$$

s.t.

$$\begin{aligned}
&\mathrm{C7}, \mathrm{C8};\\
&\mathrm{C1}^{'}: \ 0 \le Z_{i,n} \le 1, \tau_{i,n} \ge 0, \forall i, \forall n;\\
&\mathrm{C2}^{'}: \ \sum_{i=1}^{M} \tau_{i,n} = \frac{T}{N}, \forall n;\\
&\mathrm{C3}^{'}: \ \sum_{n=1}^{N} R_{i,n}^{B} \ge R_{min}, \forall i;\\
&\mathrm{C4}^{'}: \ EH_i - \sum_{n=1}^{N} PC^B \tau_{i,n} \ge 0, \forall i;
\end{aligned} \tag{C.1}$$

UAV-enabled HTT scheme

In this scheme, we aim to maximize the EE of all the IoT nodes, where the IoT nodes only harvest energy from the UAV during the first time period and use the harvested energy to transmit information during the second time period. Accordingly, the optimization problem of

this scheme is formulated as

$$\begin{aligned}
\mathbf{P_6}: \quad & \max_{\{\theta,\mathbf{t},\mathbf{P},\mathbf{q}\}} \frac{\sum_{i=1}^{M} W t_i \log_2\left(1+\frac{P_i h_i^r}{W\sigma^2}\right)}{\sum_{i=1}^{M} t_i(P_i+PC^H)} \\
\text{s.t.} \quad & \\
& \text{C7, C8;} \\
& \text{C1}'': \ 0 \le \theta \le 1, 0 \le P_i \le P_{\max}^{node}, \forall i; \\
& \text{C2}'': \ \sum_{i=1}^{M} \tau_{i,n} = \frac{\theta T}{N}, \ \sum_{i=1}^{M} t_i = (1-\theta)T;, \forall n \\
& \text{C3}'': \ \sum_{i=1}^{M} R_i^H \ge R_{\min}, \\
& \text{C4}'': \ EH_i - \sum_{i=1}^{M} t_i(P_i + PC^H) \ge 0, \forall i.
\end{aligned} \tag{C.2}$$

Energy consumption minimization scheme

In this scheme, we aim to minimize the total energy consumption, where other constraints in $\mathbf{P_1}$ keep the same. Accordingly, the optimization problem of this scheme is formulated as

$$\begin{aligned}
\mathbf{P_7}: \quad & \min_{\{\theta,\mathbf{Z}_n,\boldsymbol{\tau}_n,\mathbf{t},\mathbf{P},\mathbf{q}\}} PC^B \sum_{i=1}^{M}\sum_{n=1}^{N} \tau_{i,n} + \sum_{i=1}^{M} t_i(P_i + PC^H) \\
\text{s.t.} \quad & \\
& \text{C1} - \text{C8}.
\end{aligned} \tag{C.3}$$

Fixed PB based backscattering with HTT scheme

In this scheme, we aim to maximize the EE of all the IoT nodes, where a fixed PB instead of the UAV is located outside the IoT node region. In particular, the first time period allocated to the BackCom is divided into M time slots with ith time slot allocated to ith IoT node by employing TDMA, which is the same as that in active transmission. Accordingly, the optimization problem

of this scheme is formulated as

$$\mathbf{P_8}: \quad \max_{\{\theta,\mathbf{Z}_n,\boldsymbol{\tau}_n,\mathbf{t},\mathbf{P}\}} \frac{\sum_{i=1}^{M}(R_i^B+R_i^H)}{EC_{sum}^{PB}}$$

s.t.

$$\begin{aligned}
&\text{C1};\\
&\text{C2}''': \ 0 \le P^B \le P_{\max}^B, 0 \le P_i \le P_{\max}^{node}, \forall i;\\
&\text{C3}''': \ \sum_{i=1}^{M}\tau_i = \theta T, \sum_{i=1}^{M} t_i = (1-\theta)T;\\
&\text{C4}''': \ R_i^B + R_i^H \ge R_{\min}, \forall i;\\
&\text{C5}''': \ EH_i^{PB} - EC_{sum}^{PB} \ge 0, \forall i,
\end{aligned} \tag{C.4}$$

where $R_i^B = W\tau_i \log_2\left(1+\frac{\varphi P_{\max}^B h_i^B Z_i h_i^r}{W\sigma^2}\right)$, $EH_i^{PB} = \sum_{n=1}^{N} P^u \eta h_i^u (\theta T - \tau_i Z_i)$ and $EC_{sum}^{PB} = \sum_{i=1}^{M}(PC^B\tau_i + t_i(PC^H + P_i))$, P_{max}^B and h_i^B denote the maximum PB transmit power and the channel power gain from the PB to the IoT nodes, respectively. P_{max}^B is set the same as P_{max}^{uav} for comparison. Based on the algorithms proposed to solve $\mathbf{P_1}$, we employ the same methods to solve $\mathbf{P_5}, \mathbf{P_6}$, $\mathbf{P_7}$ and $\mathbf{P_8}$, respectively. The optimization process for these four schemes is omitted for saving space.

References

[1] Q. Wu, W. Chen, D. W. K. Ng, and R. Schober, "Spectral and energy-efficient wireless powered IoT networks: NOMA or TDMA?," *IEEE Transactions on Vehicular Technology*, vol. 67, no. 7, pp. 6663–6667, 2018.

[2] S. Bi, Y. Zeng, and R. Zhang, "Wireless powered communication networks: an overview," *IEEE Wireless Communications*, vol. 23, no. 2, pp. 10–18, 2016.

[3] S. Bi, C. K. Ho, and R. Zhang, "Wireless powered communication: opportunities and challenges," *IEEE Communications Magazine*, vol. 53, no. 4, pp. 117–125, 2015.

[4] K. W. Choi, L. Ginting, A. A. Aziz, D. Setiawan, J. H. Park, S. I. Hwang, D. S. Kang, M. Y. Chung, and D. I. Kim, "Toward realization of long-range wireless-powered sensor networks," *IEEE Wireless Communications*, vol. 26, no. 4, pp. 184–192, 2019.

[5] B. Lyu, C. You, Z. Yang, and G. Gui, "The optimal control policy for RF-powered backscatter communication networks," *IEEE Transactions on Vehicular Technology*, vol. 67, no. 3, pp. 2804–2808, 2018.

[6] X. Kang, Y. Liang, and J. Yang, "Riding on the primary: A new spectrum sharing paradigm for wireless-powered IoT devices," *IEEE Transactions on Wireless Communications*, vol. 17, no. 9, pp. 6335–6347, 2018.

[7] H. Yang, Y. Ye, and X. Chu, "Max-min energy-efficient resource allocation for wireless powered backscatter networks," *IEEE Wireless Communications Letters*, pp. 1–1, 2020.

[8] Y. Ye, L. Shi, X. Chu, and G. Lu, "Throughput fairness guarantee in wireless powered backscatter communications with htt," *IEEE Wireless Communications Letters*, pp. 1–1, 2020.

[9] S. H. Kim and D. I. Kim, "Hybrid backscatter communication for wireless-powered heterogeneous networks," *IEEE Transactions on Wireless Communications*, vol. 16, no. 10, pp. 6557–6570, 2017.

[10] B. Lyu, H. Guo, Z. Yang, and G. Gui, "Throughput maximization for hybrid backscatter assisted cognitive wireless powered radio networks," *IEEE Internet of Things Journal*, vol. 5, no. 3, pp. 2015–2024, 2018.

[11] D. T. Hoang, D. Niyato, P. Wang, and D. I. Kim, "Optimal time sharing in RF-powered backscatter cognitive radio networks," in *2017 IEEE International Conference on Communications (ICC)*, pp. 1–6, 2017.

[12] L. Shi, R. Q. Hu, J. Gunther, Y. Ye, and H. Zhang, "Energy efficiency for rf-powered backscatter networks using htt protocol," *IEEE Transactions on Vehicular Technology*, vol. 69, no. 11, pp. 13932–13936, 2020.

[13] H. Ju and R. Zhang, "Throughput maximization in wireless powered communication networks," *IEEE Transactions on Wireless Communications*, vol. 13, no. 1, pp. 418–428, 2014.

[14] J. Xu, Y. Zeng, and R. Zhang, "UAV-enabled wireless power transfer: Trajectory design and energy optimization," *IEEE Transactions on Wireless Communications*, vol. 17, no. 8, pp. 5092–5106, 2018.

[15] L. Xie, J. Xu, and R. Zhang, "Throughput maximization for UAV-enabled wireless powered communication networks," *IEEE Internet of Things Journal*, vol. 6, no. 2, pp. 1690–1703, 2019.

[16] M. Hua, L. Yang, C. Li, Q. Wu, and A. L. Swindlehurst, "Throughput maximization for UAV-aided backscatter communication networks," *IEEE Transactions on Communications*, vol. 68, no. 2, pp. 1254–1270, 2020.

[17] L. Xie, J. Xu, and Y. Zeng, "Common throughput maximization for uav-enabled interference channel with wireless powered communications," *IEEE Transactions on Communications*, vol. 68, no. 5, pp. 3197–3212, 2020.

[18] C. Zhan, Y. Zeng, and R. Zhang, "Energy-efficient data collection in UAV enabled wireless sensor network," *IEEE Wireless Communications Letters*, vol. 7, no. 3, pp. 328–331, 2018.

[19] C. You and R. Zhang, "3d trajectory optimization in rician fading for uav-enabled data harvesting," *IEEE Transactions on Wireless Communications*, vol. 18, no. 6, pp. 3192–3207, 2019.

[20] J. Lyu, Y. Zeng, and R. Zhang, "Uav-aided offloading for cellular hotspot," *IEEE Transactions on Wireless Communications*, pp. 1–1,2018.

[21] Y. Zeng, Q. Wu, and R. Zhang, "Accessing from the sky: A tutorial on uav communications for 5g and beyond,"*Proceedings of the IEEE*, vol. 107, no. 12, pp. 2327–2375, 2019.

[22] M. Hua, Y. Wang, M. Lin, C. Li, Y. Huang, and L. Yang, "Joint CoMP transmission for UAV-aided cognitive satellite terrestrial networks,"*IEEE Access*, vol. 7, pp. 14959–14968, 2019.

[23] Q. Wu, Y. Zeng, and R. Zhang, "Joint trajectory and communication design for multi-UAV enabled wireless networks,"*IEEE Transactions on Wireless Communications*, vol. 17, no. 3, pp. 2109–2121, 2018.

[24] Y. Liang, R. Long, Q. Zhang, J. Chen, H. V. Cheng, and H. Guo, "Large intelligent surface/antennas (lisa): Making reflective radios smart," *Journal of Communications and Information Networks*, vol. 4, no. 2, pp. 40–50, 2019.

[25] N. Van Huynh, D. T. Hoang, X. Lu, D. Niyato, P. Wang, and D. I. Kim, "Ambient backscatter communications: A contemporary survey," *IEEE Communications Surveys Tutorials*, vol. 20, no. 4, pp. 2889–2922, 2018.

[26] B. Smida and S. Khaledian, "ReflectFX: In-band full-duplex wireless communication by means of reflected power," *IEEE Transactions on Communications*, vol. 65, no. 5, pp. 2207–2219, 2017.

[27] M. Ismail, W. Zhuang, E. Serpedin, and K. Qaraqe, "A survey on green mobile networking: From the perspectives of network operators and mobile users," *IEEE Communications Surveys Tutorials*, vol. 17, no. 3, pp. 1535–1556, 2015.

[28] W. Dinkelbach, "On nonlinear fractional programming," Management Science, vol. 13, pp. 492–498, March 1967,Available: http://www.jstor.org/stable/2627691.

[29] S. Boyd, Convex optimization. Cambridge, UK: Cambridge University Press, 2004.

[30] G. Yang, R. Dai, and Y. C. Liang, "Energy-efficient uav backscatter communication with joint trajectory design and resource optimization," *IEEE Transactions on Wireless Communications*, vol. 20, no. 2, pp. 926–941, 2021.

[31] H. Zhang, C. Jiang, N. C. Beaulieu, X. Chu, X. Wen, and M. Tao, "Resource allocation in spectrum-sharing OFDMA femtocells with heterogeneous services," *IEEE Transactions on Communications*, vol. 62, no. 7, pp. 2366–2377, 2014.

[32] J. Gondzio and T. Terlaky, "A computational view of interior point methods," JE Beasley. *Advances in Linear and Integer Programming. Oxford Lecture Series in Mathematics and its Applications*, vol. 4, pp. 103–144, 1996.

[33] F. Zhou, Y. Wu, R. Q. Hu, and Y. Qian, "Computation rate maximization in uav-enabled wireless-powered mobile-edge computing systems," *IEEE Journal on Selected Areas in Communications*, vol. 36, no. 9, pp. 1927–1941, 2018.

[34] Q. Wu, W. Chen, D. W. Kwan Ng, J. Li, and R. Schober, "User-centric energy efficiency maximization for wireless powered communications," *IEEE Transactions on Wireless Communications*, vol. 15, no. 10, pp. 6898–6912, 2016.

Chapter 8

Conclusions and Future Works

8.1 Conclusions

In this thesis, we have proposed four energy-efficient resource allocation schemes for solving EE related problems in different scenarios of WPCNs including a SWIPT-enabled D2D network, a UAV-enabled network, a SR network and the backscatter networks with multiple users.

In a SWIPT-enabled D2D network (Paper I), the proposed algorithms achieve a higher sum EE than some existing schemes. We also find that the sum EE is much higher with short D2D communication distance and more users. Furthermore, the number of SWIPT-enabled D2D links significantly reduces with long D2D communication distance due to the consideration of EH sensitivity in this paper. In the backscatter networks with multiple users working in the same frequency band and at the same time (Paper II), we propose an iterative algorithm to obtain the globally optimal solutions of the backscatter transmission power and the reflection coefficients of the backscatter devices for maximizing the minimum EE of a backscatter link. The EE gap between the best user and the worst user is much smaller when we employ max-min EE resource allocation scheme compared with system EE maximization scheme, and such EE gap is much smaller with higher throughput requirements for the backscatter links. We further find that this scheme is more effective when the throughput requirement of the BDs is lower and the channel power gain difference from the PB to each backscatter transmitter is smaller.

In a SR network with multiple BDs (Paper III), the system EE reduces with a longer PT-PR distance and a higher throughput requirement per backscatter link. Moreover, we find that the primary link dominates the system EE and the backscatter links only achieve the minimum throughput requirement in the PSR case. While in the CSR case, the maximum system EE is achieved when the BD that has the potential to obtained the highest throughput among all BDs is allocated the maximum allowed time for backscattering, while guaranteeing the throughput requirement of the other BDs. In a UAV-enabled network (Paper IV), the total EE of the IoT nodes is maximized, where the proposed UAV-enabled hybrid BackCom-HTT scheme achieves a higher EE than other benchmark schemes. Also, the total EE is maximized when the available time is used up and the IoT node that is closest to the reader achieves the highest throughput while guaranteeing the minimum throughput requirements of other IoT nodes. For the UAV trajectory optimization, the UAV tends to fly to the IoT nodes that are closer to the reader.

8.2 Future Works

For the future work, we propose the following future research directions for each paper included in this thesis. For Paper I, since we assume that there is only one D2D link sharing the RB with one CUE in this paper, an obvious future work is to consider multiple D2D links reusing the spectrum resource with one or multiple CUEs. Allowing multiple D2D links to work in the same channel can make the D2D receivers harvest more energy but also increases the co-channel interference, the optimization of the co-channel D2D transmission power is the main challenge to be addressed. Also, the optimization of the CUE transmission power can further help to improve the EE performance. This also brings more harvested energy and interference at the receiver, and such interference signal increases the difficulty for solving the EE maximization problem since the interference signal is constant in Paper I. For Paper II, the most significant challenge is to consider the number of co-channel backscatter links larger than two, this is extremely difficult to obtain the globally optimal solution of the PB transmission power since the analyzing conditions in Paper II is much more complex with higher number of co-channel backscatter links.

For Paper III, to extend the coverage of the SR network, multiple antennas deployed at the PT, BD and the receiver need to be considered. Such deployment of multiple antennas greatly increases the complexity of solving the EE maximization problem since the optimization process includes the matrix operation, and a new mathematical solution needs to be proposed. For Paper IV, a globally optimization of the UAV trajectory is expected even though this challenge is extremely difficult, and the existing works only find the globally optimal UAV trajectory in a 1-dimension network, where the UAV's trajectory is straight. Also, multi-UAV networks need to be studied for better system performance, e.g., wider network range, higher EE and throughput. However, such networks also bring some challenges including the trajectory design of multiple UAVs and the signal detection from different UAVs at the IoT nodes. Furthermore, other scenarios of WPCNs need to be classified, e.g., intelligent reflective surface (IRS) networks, satellite communication networks and relay networks, and the energy-efficient resource allocation scheme in these networks need to be further studied.